Elaboration and characterization of field-effect transistors based on organic molecular wires for chemical sensing applications

Peter Lienerth

UNIVERSITÉ DE STRASBOURG

Ecole Doctorale Mathématiques, Sciences de l'information et de l'Ingénieur

THÈSE présentée par :

Peter Lienerth

soutenue le : **31 Janvier 2014**

pour obtenir le grade de : **Docteur de l'université de Strasbourg**

Discipline : Sciences of engineering

Spécialité : Physics of organic semiconductors and devices

Elaboration and characterization of field-effect transistors based on organic molecular wires for chemical sensing applications

THÈSE dirigée par :

M. Thomas HEISER Professeur, Université de Strasbourg, France

CO-ENCADRANT :

M. Patrick LEVEQUE Maître de conférences, Université de Strasbourg, France

RAPPORTEURS :

M. Malliaras GEORGE Professeur, ENS des Mines de St. Etienne, France

M. Klaus LEIFER Professeur, University of Uppsala, Suède

AUTRES MEMBRES DU JURY :

Mme. Françoise SEREIN-SPIRAU Professeur, Université Montpellier, France

M. Bernard DOUDIN Professeur, Université de Strasbourg, France

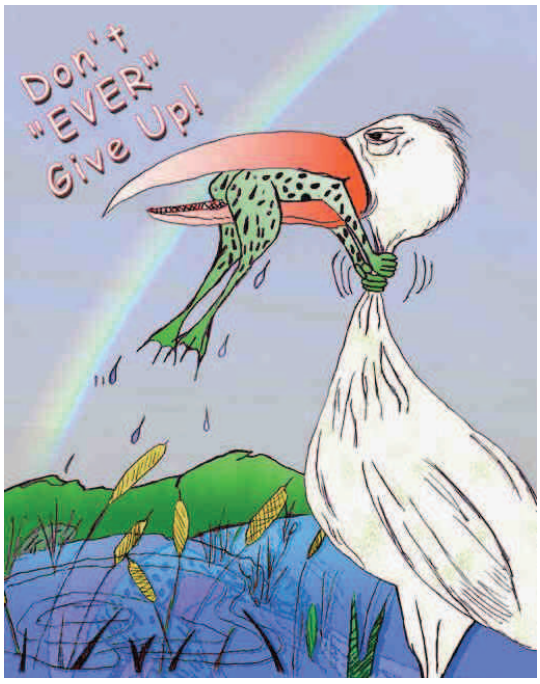

To my parents,
- for the provided opportunities

…my sister and her family
- for their inspiration and support

…my fiancée Annette
- beloved smile in hardships and joy

UNIVERSITÉ DE STRASBOURG

Peter Lienerth

Elaboration and characterization of field-effect transistors based on organic molecular wires for chemical sensing applications

Résumé

Il est reconnu que la structure des semi-conducteurs organiques influence la sensibilité et la sensitivité des capteurs des gaz. Pour améliorer la compréhension des mécanismes sous-jacents dans les capteurs à base des transistors d'effet de champ organique (OFETs) cette thèse a exploré trois pistes différentes :
L'utilisation de l'hystérésis des caractéristiques de transfert comme paramètre de détection des gaz est étudié. En ajoutant l'hystérésis aux paramètres standards, on améliore la sélectivité des OFETs à base de poly(3-hexylthiophène) aux gaz polaires. Des mesures transitoires de courant indiquent que la cinétique de piégeage et depiégeage des porteurs de charges est à l'origine de cette amélioration.
Pour comprendre l'influence qu'à la structure moléculaire sur la sensibilité aux vapeurs d'éthanol, des polymères avec des chaînes latérales alcoxyle dont on fait varier la polarité ainsi que l'encombrement stérique, ont été étudiés. L'intensité de la réponse est corrélée avec la quantité d'analyte absorbée et le moment dipolaire des chaînes latérales.
Pour permettre l'étude des mécanismes à l'échelle nanométrique, une partie de ce travail se concentre sur la fabrication de transistors avec une taille de canal réduite. En utilisant le nitrure de silicium comme couche diélectrique, on réduite les tensions de commande et les propriétés chimiques à l'interface.

Mots-clé : Transistors organique à effet de champ, Capteurs du gaz, Nano transistors, vapeur polaire, P3HT, réponse dynamique

Summary

The molecular structure of organic semiconductors which can be tailored by the chemical synthesis influences the sensitivity and selectivity of gas sensor devices. To improve the understanding of the ongoing mechanisms in sensors based on organic field effect transistors (OFETs) this thesis follows three different tracks:
The applicability of the hysteresis of the transfer characteristics as a gas sensing parameter is studied. As a complement to the standard transistor parameters the hysteresis improves the selectivity of poly(3-hexylthiophen-2,5-diyl) based OFETs to polar gases. Transient current measurements indicate the additional dependence on the detrapping kinetics as origin of the increased selectivity.
To understand the influence of the molecular structure on the gas sensing behavior, polymers with alkoxy side chains, varying in polarity and steric hindrance, are used as gas sensing layer for ethanol vapor. The response strength correlates with the amount of absorbed analyte and the dipole moment of the side chains.
To enable investigations of the mechanisms at the nanoscale, one part of this work focuses on the preparation of transistors with a reduced channel length. By using silicon nitride as dielectric layer, driving voltages decreased and interface properties could be improved.

Keywords: Organic field-effect transistors, Gas sensors, Nano transistors, polar vapors, P3HT, dynamic response

Contents

List of variables and abbreviations

a	Surface area of droplet (Hertz-Knudsen equation)
A	Active area of piezo crystal (QCM)
AC	Analyte chamber
AFM	Atomic force microscope
Al	Aluminum
ANR	Agence nationale de la recherche
Au	Gold
BSE	Bias stress effects
C	Capacitance per area (Charge transport in FET)
Ca	Calcium
DC	Detector chamber
DIBL	Drain induced barrier lowering
DMMP	Dimethyl methylphosphonate
DOS	Density of states
EBL	Electron beam lithography
FET	Field-effect transistor
f_0	Resonance frequency of quartz crystal (QCM)
G	Evaporation rate (Hertz-Knudsen equation)
HOMO	Highest occupied molecular orbital
IEEE	Institute of Electrical and Electronics Engineers
ITO	Indium tin oxide
I_d	Drain current
I_{on}	Current in the on regime of the OFET
I_{off}	Current in the off regime of the OFET
L	OFET channel length i.e. distance source-drain
LED	Light emitting diode
LUMO	Lowest unoccupied molecular orbital
MFC	Mass flow controller
Mg	Magnesium

MTR	Multiple trapping and release model
Neg end	Current 9 sec after more negative gate voltage is applied (Transient current measurements)
Neg start	Current at beginning of more negative gate voltage
OLED	Organic light emitting diode
OFET	Organic field-effect transistor
PECVD	Plasma enhanced chemical vapor deposition
Pos end	Current 9 sec after less negative gate voltage is applied (Transient current measurements)
Pos start	Current at beginning of less negative gate voltage
ppb	parts-per billion
ppm	parts-per million
ppq	parts-per quadrillion
Pt	Platin
p_q	Density of the quartz (QCM)
P3HT	Poly(3-hexylthiophene-2,5-diyl)
QCM	Quartz-crystal microbalance
SAW	Surface acoustic wave sensor
SCLC	Space-charge limited current
SMU	Source-measure unit
STM	Scanning tunneling microscopy
SiO_2	Silicon oxide
Si_xN_y	Non stoichiometric silicon nitride produced by PECVD
Si_3N_4	Stoichiometric silicon nitride
TNT	Trinitrotoluene
TPT	Collective name for poly(bithiophene-1,4dialkoxy-phenylene) based molecules
To39	Packaging used for Sensors (see 10.1)
t_{EOT}	Equivalent oxide thickness
VMU	Voltage measure unit
VRH	Variable range hopping

VSU	Voltage source unit
V_{GS}	Gate source voltage
V_{DS}	Drain source voltage
V_{th}	Threshold voltage
W	Width of OFET channel
XRD	X-ray diffraction
Δf	Frequency change of quartz
Δm	Mass change of quartz
ϵ_r	Dielectric constant
ϵ_{SiO_2}	Dielectric constant of silicon oxide
ρ_a	Partial pressure of analyte
ρ_{sat}	Saturated vapor pressure of analyte
μ	Charge carrier mobility
μ_q	Shear modulus of the quartz

1 Introduction

The groundbreaking work of Shirakawa, MacDiarmid and Heeger on doped and conjugated polymers at the end of the 1970s, initiated the exploration of the vast field of organic molecules for electronic applications. The facile processing and the promising performances have lead to their application in organic light emitting diodes (OLEDS), solar cells, integrated circuits and sensors. Though integrated circuits, have not yet left the status of laboratory investigation, OLEDS are already a serious competitor to inorganic LEDs for small scale displays. Also the first organic solar cells have recently appeared on the market, though their performance lacks far behind their inorganic counterparts. Commercially available gas sensors based on semiconducting organic molecules also show a very high performance by harvesting analyte induced changes of the electron configuration by optical means.

Despite this achievements, the theoretical understanding of charge transport at macro-, and especially at the nanoscale are still subjects of a continuing lively debate. For most of the applications named above, organic electronics are used in a bulk configuration, i.e. a high number of small molecules or polymers are used as the semiconductor. As a consequence charge transport in the semiconductor is not only governed by intramolecular conductance but rather by intermolecular hopping which is expected to result in inferior charge transport properties.

When the channel length of an organic field effect transistor is reduced, the number of intermolecular hopping steps, needed to traverse the organic semiconductor, decreases. The limit is reached, when individual molecules connect source and drain and the charge transport is governed by multistep hopping. In this regime, charges are injected into the molecular orbitals and drift along the molecular backbone by the applied electric field. Length dependent measurements, summarized in [65], have shown a transition from tunneling to hopping transport at channel lengths between 2 and 5 nm. However, most of these results were published 2008 or later and only few works have been published which connect the molecular architecture to the conduction properties on a molecular scale.

Downscaling of the transistor channel length is also of interest from an application

oriented point of view. The understanding gained from such experiments may help to improve the performances of the thin-film based devices, named above. Furthermore, a special interest arises from the application of single molecules in integrated circuits, as the success of information technology would not have been possible without the continuous miniaturization of electronic components, which lead to an increase of the computational speed and the integration density.

1.1 The project TRANSFILSEN

The framework of this thesis is given by the project TRANSFILSEN, which is funded by the French National Research Agency (Agence nationale de la recherche, ANR). The name TRANSFILSEN is an acronym of the words TRANSistor, FIL (french for "wire", i.e. nanowire) and SENsor and indicates the envisaged structure of an organic field effect transistor (OFET) whose conductive channel is made of several parallel aligned isolated nanowires which connect source and drain. While such a structure enables fundamental investigations on the charge transport mechanisms within conjugated molecules, the endeavored structure would be also very interesting for gas sensor applications. Figure 1.1 shows a scheme of the endeavored device structure.

To circumvent the critical electrode fabrication necessary at lengths of only a few nm, the chemistry group of the project focuses on the synthesis of elongated self-assembling molecular wires with a length of approximately 10 nm. Electron beam lithography (EBL) is employed for the fabrication of the nanoelectrodes. Though structures with a size of 10 nm are at the resolution limit of many EBL setups, this technique can enable well defined structures which are necessary to improve the reproducibility of the devices. In molecular junctions usually only very few molecules connect both electrodes. As this number can hardly be controlled, huge current density variations are observed. To cancel out these fluctuations, the project aims on the fabrication of electrodes with a relatively high width-to-length ratio. The large width of the electrodes is expected to lead generally to a high number of molecules bridging the gap and therefore to decrease the current variations between devices.

The molecular wires are designed to auto assemble between the gold electrodes by appropriate functionalization of the end-groups. Techniques like scanning tunneling microscopy (STM) and atomic force microscopy (AFM) allow to study the self-organization process. Furthermore the molecules incorporate side chains designed to hinder intermolecular charge transport by hopping and to confine the charge transport into the individual molecules.

From an application oriented point of view, the envisaged device geometry prospects

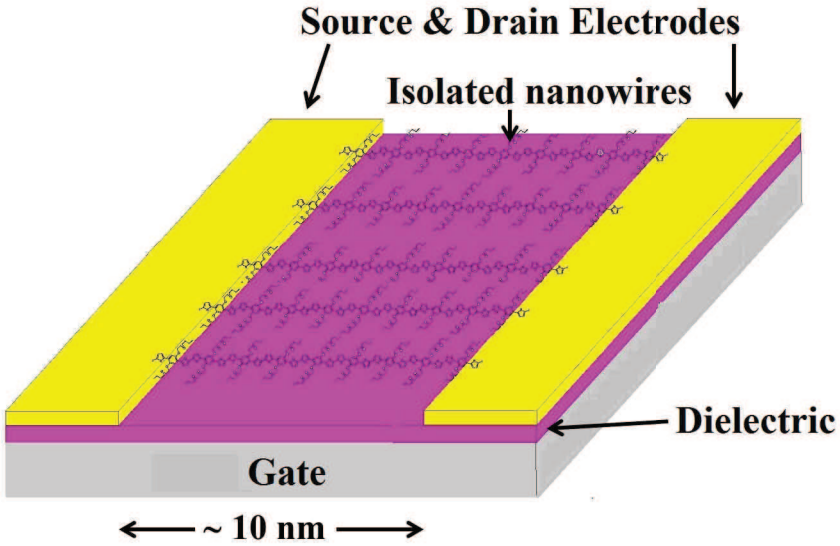

Figure 1.1: Scheme of the envisaged OFET structure.

significant improvements of OFET based gas sensors. While in conventional OFETs analyte molecules first need to diffuse through the semiconducting layer to reach the conducting channel, the proposed structure directly exposes the charge transporting molecules to the environment. Furthermore, single analyte-semiconductor interactions on one molecule could already cause a measurable response, as charge carrier can not circumvent the affected unit.

The TRANSFILSEN project was performed in collaboration with other groups specialized and experienced in different techniques vital for the project. The group of F. Serein-Spirau from the Ecole Nationale Supérieure de Chimie de Montpellier (ENSCM) and N. Leclerc from the Institut de Chimie et Procédés pour l'Énergie, l'Environnement et la Santé (ICPEES) in Strasbourg, designed and synthesized the π-conjugated isolated nanowires. L.Simon from the Institut de Science des Matéri-

aux de Mulhouse (IS2M) studied the conformation and the spectroscopic properties of the molecular nanowires by STM in ultra-high vacuum and the morphology in air by AFM. M. Hehn from the Institut Jean Lamour (IJL) in Nancy focused on the production of nanoelectrodes by electron beam lithography.
The group of Thomas Heiser at the Laboratoire des sciences de l'ingénieur, de l'informatique et de l'imagerie (ICube) in Strasbourg, is experienced in the investigation of charge transport in organic semiconductors by means of macroscopic organic field effect transistors. This background provided a solid basis for studies of the gas-analyte interactions. Furthermore, the experience in the optimization of macroscopic organic field effect transistors helped to reduce the transistor channel length to the nanoscale. Provided with the indicated background, this thesis followed several routes to contribute to the TRANSFILSEN project.
First of all, a gas test bench had to be build to allow a controlled exposure of the organic field effect transistors to various gases. To test the performance of the gas test bench, standard organic semiconductors have been characterized during gas exposure and compared to results reported in literature. In a next step, the electrical performances of molecules designed for the project TRANSFILSEN have been characterized during gas exposure and the influences of the molecular structure on the sensing performance was analyzed. Another major task of this work was the downscaling of the transistor channel length. Therefore the channel length was incrementally reduced and the devices were tested for short channel effects.

1.2 This thesis

Chapter 2 repeats the working principles of organic semiconductors with the focus on field effect transistors, before a detailed description of the utilization of organic molecules in gas sensor applications is presented.
Chapter 3 presents the molecules that have been used in this work. Particular emphasis is placed on the semiconducting molecules that have been designed especially for the project TRANSFILSEN and on the morphological characterizations of thin films that have been performed in collaboration with (AFM), or solely by project

(XRD) partners.

To enable device testing for sensor application a gas test bench has been established, presented in chapter 4. The method used to generate gas samples and to estimate the concentration will be explained. The last section covers the electrical configurations used for the device characterizations and the means of data acquisition and treatment.

In chapter 5 the procedure established for the sensor fabrication is explained and compared to the standard method established by former students at the ICube laboratory. Also a more detailed explanation of the automatized data treatment is given. Bias stress effects and potential issues arising from the gas test bench are discussed.

Chapter 6 presents the behavior of OFETs prepared from standard materials (P3HT) in the new build gas test bench in presence of ethanol. Though these test were initiated as a testing and training period, the results revealed new insights in comparison to literature. A unreported parameter, the hysteresis of the transfer characteristics, revealed a stable performance as parameter for the detection of polar gases. The performance of the hysteresis is compared to the conventional parameters used for the ethanol detection, on-current and mobility. The model system ethanol and acetone is used to test if the utilization of the hysteresis in combination with the conventional parameters, improves the ability to discriminate analyte gases. Measurements of the transient drain current are applied to investigate the origin of the hysteresis response. The last part discusses the potential measurements of the transient drain current show as a parameter for the gas detection.

Thin films of the polymers designed with the same backbone and side chains as the small molecules envisaged for the TRANSFILSEN project were characterized in terms of sensing performance to ethanol vapor in chapter 7. The different side chains attached to similar backbones gave rise to strong differences in the sensitivity. Measurements of the mass uptake and morphological studies were employed to investigate the origin of the different performances.

Chapter 8 describes the work performed on the elaboration of short channel transistors. Starting from standardized substrates with channel lengths between 20 and

2.5 μm on 200 nm SiO_2, this chapter compares the results obtained on SiO_2 at 3.5 μm to the performance on Si_xN_y. Latest results on OFETs with 350 and 500 nm channels are presented.

2 Scientifc background

2.1 Organic semiconductors

Organic solids in principle consist of carbon-based molecules. These molecules can be arranged in single crystals, polycrystals or amorphous glasses. Two major classes of organic molecules can be distinguished: low molecular weight oligomers, also referred to as small molecules, and polymers. On appropriate substrates, some small molecules form highly ordered thin films when deposited from the gas phase. Polymers are generally processed from solution by spin-coating for example, resulting in an amorphous or polycrystalline blend. In both cases, neighboring molecules are held together by dipole and Van der Waals forces.

2.1.1 Conductivity in organic semiconductors

Out of the large class of organic molecules, the ones with a conjugated π system are interesting for use in organic electronics. If a C atom is double bound to another C atom, two p and one s orbital form three degenerated and coplanar sp^2 hybridized orbitals, each occupied by one electron. The fourth valence electron of the C atom is in the residual p_z orbital, which is perpendicular to the plane of the sp^2 orbitals. This electron interacts with the electron in the p_z orbital of the other C atom and forms a π bond while the electrons in the sp2 orbitals form σ bonds. In a benzene ring, six C atoms are distributed on a hexagonal shape, each one bound to the two adjacent C atoms and one H atom. The six electrons in the p_z orbitals, one at each C atom, allow the formation of three π bonds which are delocalized over the benzene ring. Each atom contributes only one electron to the π bond, occupying only the energetically lower π orbitals in the ground state. These energy levels are also referred to as the highest occupied molecular orbital (HOMO) and contribute to the bonding of both atoms. The anti bonding $\pi^\star$ orbital is the lowest unoccupied molecular orbital (LUMO). In a planar molecule with several adjacent benzene rings, the p_z electrons are delocalised over the whole conjugated part of the molecule. As

the number of benzene rings increases, the conjugation length increases too. The higher number of binding and antibinding π orbitals reduces the band gap of the resulting molecule. While a single benzene ring has a band gap of ≈ 8 eV, tetracene, consisting of three benzene rings, has a band gap of ≈ 4 eV and pentacene ≈ 2 eV [81]. In semiconducting polymers conjugated units are connected by single carbon-carbon bonds which introduce high rotational freedom between neighboring units. As a consequence of the distorted planarity and the spatial alignment of the polymer, the conjugation can only extend over a couple of monomers leading to typical band gaps around 2 eV. However, also band gaps of 1.1 ev have been reported [118].
Due to the band gap between HOMO and LUMO, pure organic semiconductors are not conductive in the dark at low temperatures and low applied voltages. Only if excess charge carriers are created by injection through the electrodes, the internal photoeffect or by chemical doping, the organic semiconductor becomes conductive. Neighboring molecules interact only weakly through Van der Waals forces or dipole-dipole interactions, so the wave functions of excess charge carriers are localized at only a few or even one individual molecule, resulting in negative or positive charged ions. This polarizes the surrounding molecules. As the relaxation time of the polarized molecules is ≈ 100 times shorter than the transfer time needed for the electron or hole to tunnel with thermal assistance to the next molecule, the polarization follows the charged molecule. Therefore, electrons in the LUMO are also called negative polarons, while holes in the HOMO are called positive polarons. Ordered crystals exhibit a homogeneous polarization energy throughout the crystal and a larger overlap of adjacent π orbitals than disordered molecules. However, due to the weak delocalization of the π orbitals, the HOMO and LUMO energy levels have a bandwidth below 100 meV and the orbitals extend only over a few oligomers. As a consequence the highest charge carrier mobilities obtained for hole transport are around 35 cm^2/Vs at room temperature and up to 58 cm^2/Vs at 225 K, about one order of magnitude smaller compared to silicon whose hole mobility is around 450 cm^2/Vs at room temperature [43]. In amorphous organic semiconductors, locally different molecular environments change the polarization energy, which leads to a Gaussian distributed density of states within a range of 80 to 120 meV. Hopping

between adjacent states results in mobilities below 0.1 cm^2/Vs [66].
In inorganic devices the position of the Fermi level determines minority and majority charge carriers. While the position of the Fermi level can be tuned in the production process by doping of the inorganic semiconductor, organic semiconductors are rather classified as p or n-type material as a function of the energy of HOMO and LUMO levels with respect to the source and drain electrodes. Materials which are employed for the source and drain contacts have usually high workfunctions around 5 eV (Au, Pt, ITO) which impedes device degradation due to oxidation of the electrodes. If the HOMO level is close to the workfunction of the electrodes the device is a hole conductor. This is the case for most OFETs due to the position of the energy levels. The LUMO of most semiconductors is around 2 to 3 eV and an appropriate electrode material (Mg, Ca, Al) is not environmentally stable. A class of organic semiconductors with exceptionally high LUMO levels that can also be contacted with gold electrodes, are the fullerenes and their derivatives [115].

2.1.2 Organic field-effect transistors

Figure 2.1 presents the structure of the organic field effect transistors (OFETs) used in this thesis. The conductive gate electrode is separated by a dielectric layer from the active layer and the source and drain electrodes. Channel length and width are defined according to the image. Though this so called bottom-gate-bottom-contact structure does not reveal the highest mobilities, it offers several other advantages for OFETs: different organic semiconductors can easily be tested on standardized substrates which already incorporate gate, dielectric and source and drain electrodes, as the active layer just needs to be deposited by evaporation or wet deposition techniques. An additional advantage, especially for sensors, is the direct exposure of the active layer to the surrounding atmosphere as it facilitates the interaction between analyte vapor and the organic semiconductor.

In a field effect transistor the lateral current between source and drain is modulated by a voltage applied to the gate. Application of an appropriate gate voltage (negative for hole carriers, positive for electron carriers) causes the source electrode to inject charge carriers into the proximate semiconductor film where they accumulate at

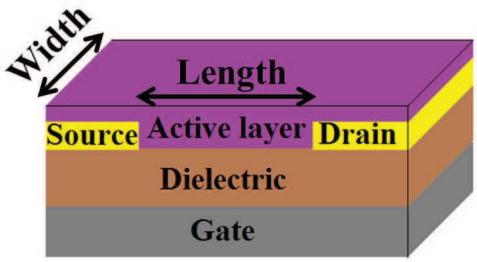

Figure 2.1: Scheme of organic field effect transistor indicating channel width and length

the dielectric/semiconductor interface [93] (see Figure 2.2 a) and b)). The voltage applied between source and drain causes the charge carriers to drift into the channel and generates a current transport between both electrodes (2.2 c) and d)).

To describe charge transport in organic field effect transistors the field induced

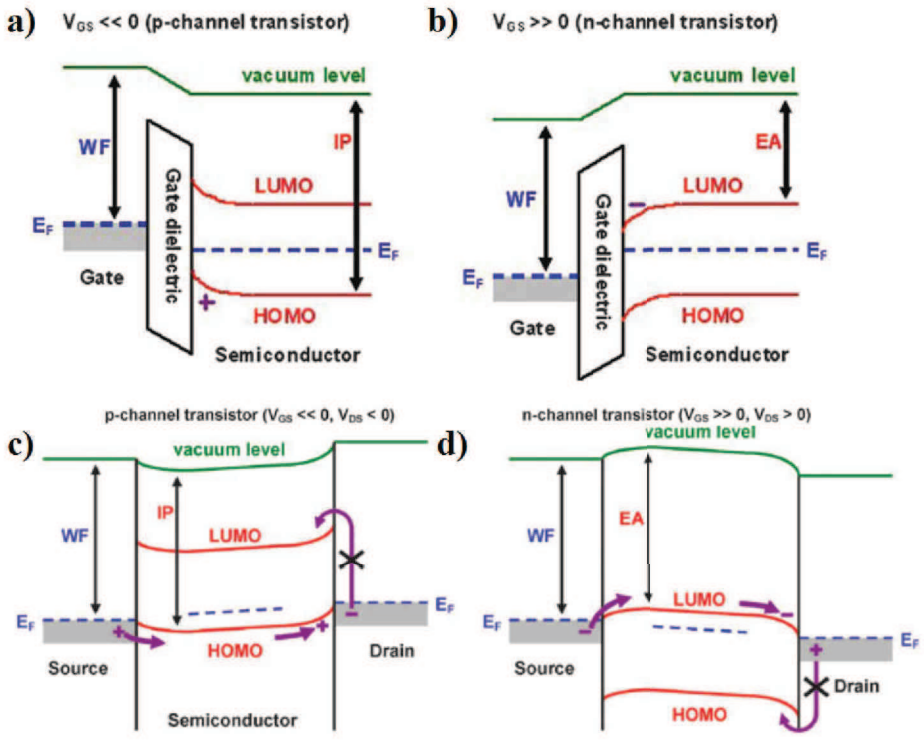

Figure 2.2: Energy-level diagrams perpendicular (a) and b)) and parallel to the dielectric surface (c) and d)). Electrode materials are chosen by their workfunction to enable injection into one energy level of the semiconductor and impede it into the other [47].

by the gate must be much larger than the field between source and drain. As a consequence of this gradual channel approximation charge transport is confined to the semiconductor/dielectric interface. For a constant mobility charge transport in

the conductive channel can be described as:

$$I_d = \frac{\mu CW}{L}\left((V_{GS} - V_{th}) - \frac{V_{DS}}{2}\right)V_{DS} \tag{2.1}$$

Where I_d is the source drain current, μ is the charge carrier mobility, C is the capacitance per area of the dielectric, W and L are width and length of the conductive channel, respectively. V_{GS} and V_{th} are the applied gate voltage and the threshold voltage, respectively, and V_{DS} is the source-drain voltage.
In the limit of $|V_{DS}| << |V_{GS} - V_{th}|$ the charge carrier density in the conductive channel can be approximated as constant, leading to:

$$I_d = \frac{\mu CW}{L}(V_{GS} - V_{th})V_{DS} \tag{2.2}$$

When the drain voltage equals the gate minus the threshold voltage the charge accumulated in the channel between source and drain does no longer connect both electrodes and the current becomes independent of the applied drain voltage:

$$I_d = \frac{\mu CW}{2L}(V_{GS} - V_{th})^2 \tag{2.3}$$

Figure 2.3 shows a scheme of current voltage characteristics of an OFET. In a) the current follows a linear dependence at low drain voltages and can be described by the equation 2.2. The gate voltage determines the slope of the current voltage characteristics in this linear region. At higher drain voltages I_d saturates and shows no more gate dependence. This happens above the pinch-off point where the longitudinal electric field becomes superior to the vertical field from the gate and creates a depletion region at the drain electrode. Here, in the saturation regime, charge transport follows equation 2.3.

The transfer characteristics in b) and c) allow to directly determine the charge carrier mobility as a function of the slope:
for the linear regime:

$$\mu = \frac{L}{WCV_d}\left(\frac{\partial I_d}{\partial V_g}\right) \tag{2.4}$$

and the saturation regime:

$$\mu = \frac{2L}{WC}\left(\frac{\partial \sqrt{I_d}}{\partial V_g}\right)^2 \tag{2.5}$$

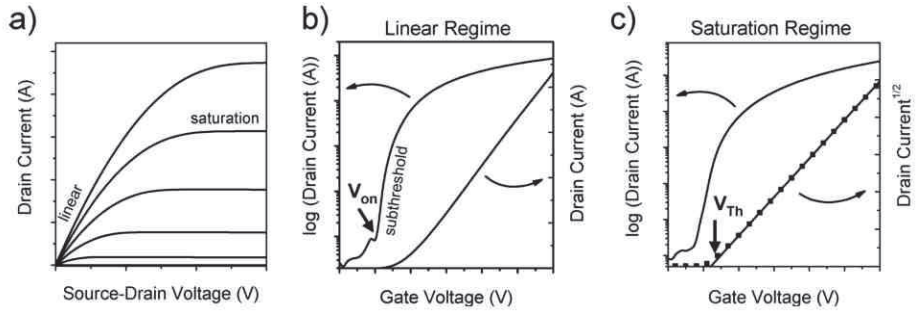

Figure 2.3: Ideal current voltage characteristics of an OFET. a) Output characteristics with linear and saturation regime. Transfer characteristics in linear b) and saturation regime c). b) V_{on} indicates onset voltage, and subthreshold slope. c) Indicates threshold voltage V_{th} [115]

Though these equations were derived for inorganic field effect transistors which work in inversion, OFETs which work in accumulation, show a relatively good correspondence, too. However, the assumption of a constant field effect mobility is not valid for organic semiconductors. Instead the mobility usually shows an increase with the applied voltages. As a consequence mobilities extracted from the saturation regime are higher compared to the linear regime.

2.1.3 Charge transport models for organic semiconductors

Due to the weak Van der Waals interactions molecular properties dominate over the crystalline ones in organic semiconductors and lead to localization of charge carriers onto single conjugated parts of the molecules. Therefore the mobility of charge carriers moving through the semiconductor is determined by the hopping transport between conjugated parts under the influence of an external field. The degree of localization determines the type of transport and depends strongly on the organization of the film. As a consequence mobilties ranging from 10^{-6} to almost 60 cm^2/Vs have been measured in organic semiconductors. Several models have been developed to explain charge transport in organic semiconductors out of which the multi trap and release and the variable range hopping model will be explained.
In the limit of high mobilities above 0.1 cm^2/Vs good agreement was found for the multiple trapping and release model (MTR) which was adapted from amorphous or

polycrystalline inorganic thin film transistors with high trap density. The assumption of the model is that most charge carriers in the semiconductor are trapped in localized shallow traps which are only a few k_BT shifted into the energy band gap. Such traps can be caused by structural or chemical defects and are immediately filled when encountered by charge carriers. Due to the low energy necessary for the charge carrier to be released from the traps, thermal activation can promote the charge carrier into an extended band where it moves to another state. As a consequence the mobility shows an exponential dependence on the temperature. The number of charge carriers available for transport depends on the energy difference between the trap levels and the extended band, temperature and the gate voltage. This model has found good agreement with results derived from organic semiconductors with a high degree of intermolecular orbital overlap, which is often observed in crystalline oligomer films. Though the existence of extended states is not clear yet in organic semiconductors, evidences for charge transport limited by phonon scattering were found by Jurchescu et al. for highly purified pentacene crystals [43]. From the start, the variable range hopping (VRH) model was considered for the charge transport in organic semiconductors and takes the isolated states of discrete molecules into account. As it is shown in figure 2.4, the states which can host charge carriers are distributed in space and energy. Charge carriers localized in one state can be thermally activated to move to another state either by tunneling over larger distances in space (a few nm) but only a small difference in energy or vice versa. As long as the gate voltage is small, charge carriers can get trapped in states at the band tail of the density of states. In these states the energy of the charge carrier is small and only few other states are accessible by thermal activation. As a consequence the time needed for the charge carrier to get released is long and the mobility decreases (figure 2.4 e)). For higher gate voltages charge carrier fill the low energy states and the high ratio of free charge carriers, contributing to the charge transport, increases the mobility. As it was shown by Vissenberg and Matters the probability for charge carriers to tunnel between two states depends strongly on the overlap of the orbitals and therefore the structural order of the organic films [105].

Though the approaches of both theories are different both models describe well the

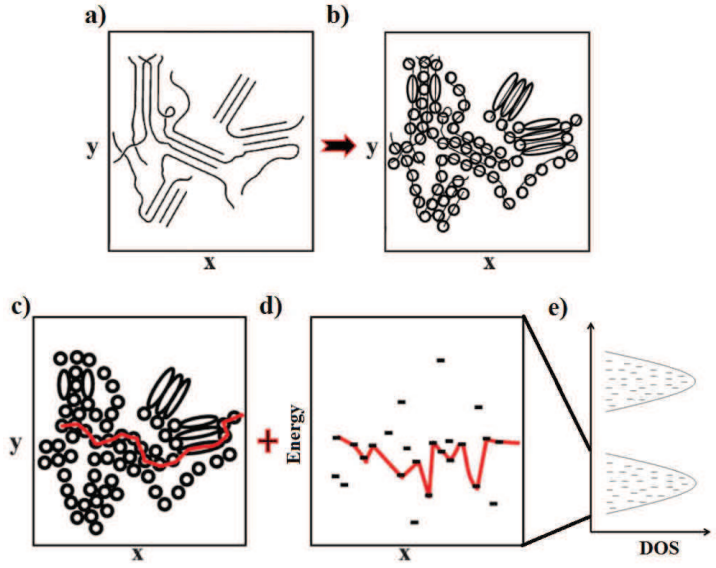

Figure 2.4: Scheme of polymer chains spatially arranged in films (a)) and according division into subunits. (b)). Possible charge transport path in space (c)) and energy (d)). Assuming hole transport in d), e) shows the energetic distribution of the density of states (DOS). Bottom: HOMO, top: LUMO. Adapted from [94]

characteristics of OFETs: the gradual turn-on caused by the filling of traps before a conductive channel is formed, thermally activated transport due to enhanced de-trapping at higher temperatures and the gate dependent mobility which is caused by Fermi-level dependence of the effective trap density.

The main difference of the models is how the density of states (DOS) is modeled. The VRH model assumes an exponential DOS where the tail extends into the energy band gap. This is a good approximation of the disorder induced Gaussian-like distribution of the DOS in amorphous semiconductors. In the MTR a defined energy separates the mobile states from the localized states which can be modeled by arbitrary distributions. Though VRH has been suggested for amorphous semiconductors and MTR for polycrystalline materials Salleo et al. used both to model temperature dependent measurements of polythiophenes. The temperature activated transport between 90 and 200°K was in good agreement with both models, making it difficult to distinguish purely based on the fit data. The MTR model was favored because of the polycrystalline nature of the investigated films and due to the unphysical parameter extraction for the VRH model [78].

An interpretation of the sensing behavior of organic semiconductors can be achieved by assuming variations of the width and shape of the trap density in the MTR model in presence of analytes. A reduction of the current could be due to a deeper energy level that may increase the residence time of charge carriers in the analyte induced trap states. In the VRH model the permittivity of the analyte could be expected to locally change the permittivity of the semiconductor and therefore also the hopping rate.

2.2 Organic semiconductors for gas sensor applications

The weak intermolecular interactions between organic molecules can be easily influenced by gas molecules. Shirakawa et al. reported an increase of the conductivity when polyacetylene films were exposed to the halogen vapors bromine, iodine and chlorine [83]. This observation of doping of organic polymers was rewarded by the Nobel Prize in 2000, and anticipated the application of conjugated organic molecules in gas sensors, as it was the prospect of Heiland and Laurs in 1987 when phthalocyanine films were exposed to oxygen, iodine and bromine [53]. Since then, the exploitation of polymers and oligomers in gas sensors has developed continuously and polymer based devices for the optical detection of explosives are already on the market [41].
This section will first motivate the need for organic semiconductors before the different interactions occurring between gases and the organic semiconductor will be discussed. The last part shows promising trends that have been reported and which may help to further improve the utilization of organic semiconductors in gas sensors.

2.2.1 Introduction to gas sensors

In todays society sensors have become an essential pillar of modern technology. From accelerometers in modern cell phones to oxygen level control in the ISS, sensors allow to convert an external stimuli into a signal which can be processed by electronic hardware. Therefore a sensor combines one element which is sensitive to the re-

spective stimuli and a second one which converts the interaction into a measurable electronic signal. Focusing only on the detection of gases, a vast number of techniques have developed in the last decades which imitate, and even outperfom, the olfactory sense of humans in individual tasks. However, the versatility of a human nose, for example is still very difficult to mimic, and canines remain the most reliable and accurate way to detect explosives and narcotics, yet. Additional interest for an artificial control of the environment, steams from industrial processes where toxic and dangerous gases have to be monitored. Table 2.5 gives a few examples for the threshold limit values at workspaces in Germany. Only for the few examples given, the hazardous concentrations vary over 8 orders of magnitude. Though a sensor does not have to monitor all of these components at the same time, the values indicate the demands which are imposed on gas sensing in general.

The concentrations of the gases (or analytes, as the gas of interest will be called

TLV	Some selected substances with the limit value given
5000 ppm	Carbon dioxide
1000 ppm	Refrigerants R11, R12, R13, R142b, Butane, Propane, i-Pentane, Sulfur hexafluoride
500 ppm	Acetone, Ethanol, Octane
200 ppm	Butanone (MEK), Methanol, i-Propanol
100 ppm	Butanol, Xylenes
50 ppm	Ammonia, n-Hexane, Toluene
20 ppm	Styrene
10 ppm	Hydrogen cyanide, Acetic acid, Carbon disulfide, Hydrogen sulfide
5 ppm	Butyl amine, Methyl acrylate, Nitrogen dioxide
1 ppm	Hydrogen peroxide
500 ppb	Chlorine, Sulfur dioxide
100 ppb	Bromine, Chlorine dioxide, Diboran, Fluorine, Hydrazine, Iodine, Ozone, Phosphine
50 ppb	Arsine
20 ppb	Phosgen
10 ppb	Methylisocyanate, Mercury vapour
5 ppb	Pentaborane
0.2 ppb	Osmium tetroxide

Figure 2.5: Threshold limit values for selected substances, published by the German Federal ministry of Labour and Social Affairs [24]

onwards) given in table 2.5 are expressed either in ppm (parts per million 10^{-6}) or ppb (parts per billion 10^{-9}). The parts-per notation expresses the molar concentration of analyte particles within the sample of gas being tested. For optical polymer based gas sensors detection limits of 1 part per quadrillion (10^{-15}) have

been reported [41].

The list above shows only a few examples of dangerous gases. The original document includes almost 400 different gases, each with its own threshold concentration. To meet such a demand, two properties are essential for the sensing unit.

The sensitivity of a sensor is an indicator for the minimum analyte concentration that will produce a detectable output change (response) [42]. It can also be expressed as the slope of the sensors response plotted over the analyte concentration in current or volt per ppm. Though modern electronics allow to compensate for deviations, an ideal sensor shows a linear dependence of the response on the concentration, at least in the concentration range of interest. Deviations from the linear behavior can also be caused by environmental factors like temperature, vibrations, pressure and humidity.

The selectivity of a sensor is the second parameter which is of major interest, as it indicates the ability of the sensor to distinguish the analyte of interest from possible interference gases. An interference gas can also modulate the sensors response to the analyte and cause unreliable responses. For some gases filters can be a convenient way to shield the sensor from the interference gas but allow the access of the desired analyte.

Organic semiconductors offer vast possibilities to tune the selectivity and sensitivity by covalently grafting functional groups to the conductive backbone which favor the interaction to specific analytes or by tuning the morphology of the sensing layer [98], [37], [64], [56]. A benchmark for the selectivity of gas detection was set by Torsi et al. by chiral discrimination of two terpenes at concentration of tens of ppm [99] (see also 2.2.5).

2.2.2 Sensors types based on organic molecules

To harvest the sensitivity of organic semiconductors to gaseous components for gas sensor applications several techniques have been developed. A recent detailed review can be found in [44].

Two of these techniques are classified as mechanical sensors and are based on piezoelectric crystals: quartz crystal microbalance (QCM) and surface acoustic wave

(SAW) sensors. Both use the fact that the resonance frequencies of piezoelectric crystals depend on its mass but they employ different type of oscillation to harvest this property. The QCM sensor is covered by a thin film of the sensing material and excited to shear vibrations by an AC voltage applied between electrodes on top and bottom of the quartz. Upon exposure, analyte molecules absorb and adsorb on the sensing material and change the mass of the vibrating unit and as a consequence also the resonance frequency. This technique has been employed in this thesis to improve the understanding of the side-chain influences on the sensor performances. A detailed explanation can therefore be found in section 7.1.1.1 or in literature: [12]. SAW sensors employ Rayleigh surface waves which propagate on the piezoelectric crystal between a transmitter and a receiver electrode (see figure 2.6 a)). Between both electrodes a film of the sensing material is deposited. As the resonance frequency of the surface waves is a function of the mass of the film, absorption or adsorption of analytes can be probed by a phase or frequency shift between the input and output voltages [12].

Appropriate manufacturing of the quartz crystals enables very sharp resonance frequencies which allow the detection of concentrations below 1 ppm. However, a drawback of these devices is the poor selectivity, as the response only reflects an increase of the mass. To tune the selectivity the sensing film needs to be tuned to selectively absorb only the desired analyte. While this techniques offer the possibility to use also nonconductive sensing materials to enhance the selectivity, analyte discrimination has been shown for combined application of a SAW structure with an incorporated chemiresistor for conductive polymers [71] [40].

Another class of gas sensors employ the optical properties of organic semiconductors to reflect changes of the electron configuration in presence of analytes. Doping or partial charge transfer changes the spectral absorbance of conductive polymers by formation of polarons or bipolarons [6]. Another optical property of some organic semiconductors is fluorescence. By absorption of light of the appropriate wavelength an exciton is generated. An exciton is a bound electron-hole pair which immediately decays into a free hole and electron in inorganic semiconductors due to the efficient screening of the Coulomb interaction by the high dielectric constant. In organic

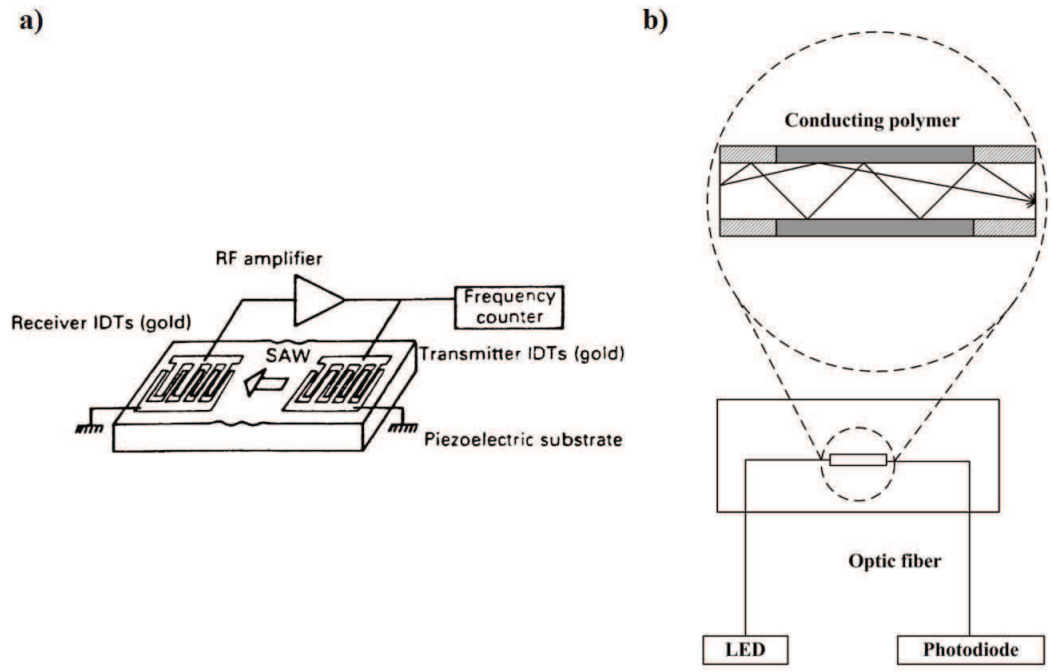

Figure 2.6: a) Schematic diagram of a SAW sensor. RF = radiofrequency, IDT = interdigitated transducer [12]. b) Optical fiber claded with polymers and reflection of the guided light [3]

semiconductors the dielectric constant is low, so the lifetime of the exciton is sufficiently long to diffuse along the polymer backbone and probe it for interactions with analyte gases, before it decays by radiative emission. Electronegative gases like nitro-aromatics, which occur in many explosives, have been shown to efficiently quench the fluorescence by offering non radiative paths for the exciton to decay [114]. To enhance the sensitivity of optical sensors, optical fibers can be claded with the gas sensitive material. Multiple reflections of the light inside the fiber probe the electron conditions of the film in various spots and allow a thorough scanning of the sensing film (See figure 2.6 b)). Such a waveguide claded with long interconnected fluorescent polymers has been shown to benefit from the thorough scanning of the film by the reflected light and from efficient scanning of the polymers by the diffusing exciton, at the same time. Commercially available explosive detectors combining these two advantages have been reported to show a detection limit of 1 ppq (10^{-15}) for the explosive TNT [41].

Figure 2.7 a) shows a basic scheme of the operation of an electrochemical cell.

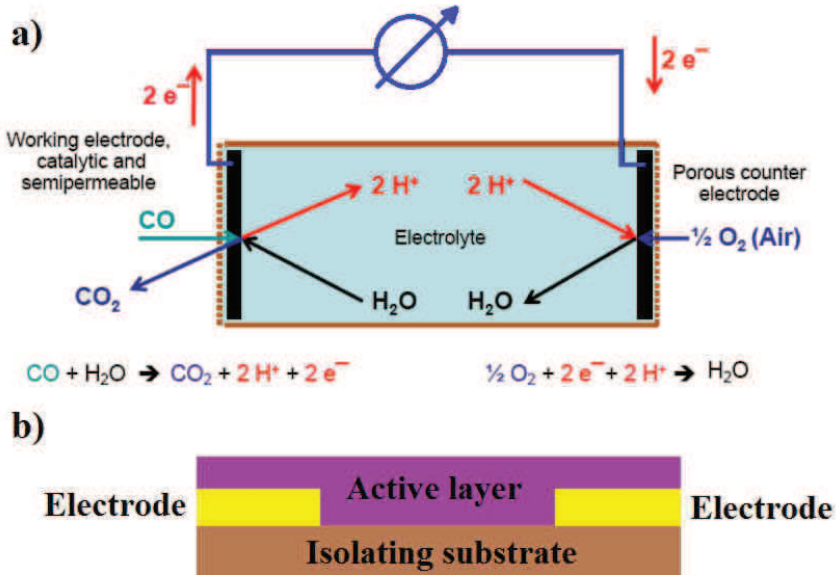

Figure 2.7: a) Schematic diagram of a electrolytic cell (adapted from [112]. b) Side view of chemiresistor.

The semipermeable working electrode is coated by the sensing material. Upon interaction with the oxidable analyte a catalyzed chemical redox reaction generates free electrons which generate a current flow to the counter electrode. The current between both electrodes is proportional to the concentration of the analyte at the working electrode. Inside the cell the oxidized H^+ ions diffuses to the counter electrode where the ambient oxygen is reduced and the circle is closed. While classical electrochemical cells employed liquid electrolytes, progress has been made towards solid state sensors based on polymer electrolytes [72].

In chemiresistors the sensing material is deposited between two electrodes on top of an insulating substrate (see figure 2.7 b)). To allow measurable currents, doped polymers are usually used. When the sensor is exposed to the analyte the resistance of the device is alternated either by interactions occurring in the active layer or due to contact effects. A major drawback of chemiresistors is that monitoring only the resistance does not allow to distinguish gases by the measured signal. It is impossible to distinguish if changes of this single parameter arise from concentration changes or changes of the analyte. However, good results can be obtained with this type of sensor too, if the sensitive material responds only to the desired analyte gases, i.e. the presence of interference gases is rather unlikely under the conditions of the

application.

In organic field effect transistors the active layer is directly exposed to the surrounding atmosphere (see figure 2.1). Interactions of the analyte with the semiconductor and the contacts are directly converted into changes of the current voltage characteristics. Due to the complexity of an OFET, the current voltage characteristics are described by several parameters (V_{th}, μ, I_{on}, I_{off} to recall only the most prominent) which can individually be influenced by analytes. Simultaneous monitoring of these parameters and a database with the mutual dependencies under the influence of different analytes, enables fingerprint-like identification of gases [95]. An additional advantage of the OFET structure arises from the current amplification by the gate potential, which has been shown to also amplify the response to analytes [3].

2.2.3 Gas detection with OFETs

Several mechanisms control the interaction of the organic semiconductor with the analyte gases in chemiresistors and OFETs. Figure 2.8 gives an overview of the steps leading to an interaction of the analyte with the active layer in an OFET. Analyte molecules adsorb on the surface of the film from where they can be absorbed into the film, depending on the film morphology. If an inorganic dielectric like SiO_2 is used, it works as a barrier for the diffusion and leads to an accumulation of the analyte molecules at the conductive channel of the OFET. Here analyte molecules can directly influence the charge transport through the sensor by chemical or physical interactions.

While Dudhe et al. showed that the response of polymer composites films to explosives can be enhanced by increasing the porosity and therefore the diffusion of the analyte to the sensing channel, Zhang et al. reported that changing the porosity and therefore the nanostructure of the film can completely alter its sensing behavior depending on the analyte-semiconductor interaction [21], [57].

Someya et al. have investigated the response of crystalline DHα4T films to 1-pentanol to identify the spatial origin of the interaction. Systematic variation of the size of the polymer grains and the channel length of the transistors has revealed grain boundaries as origin of the vapor sensing [87]. Torsi et al. have found similar

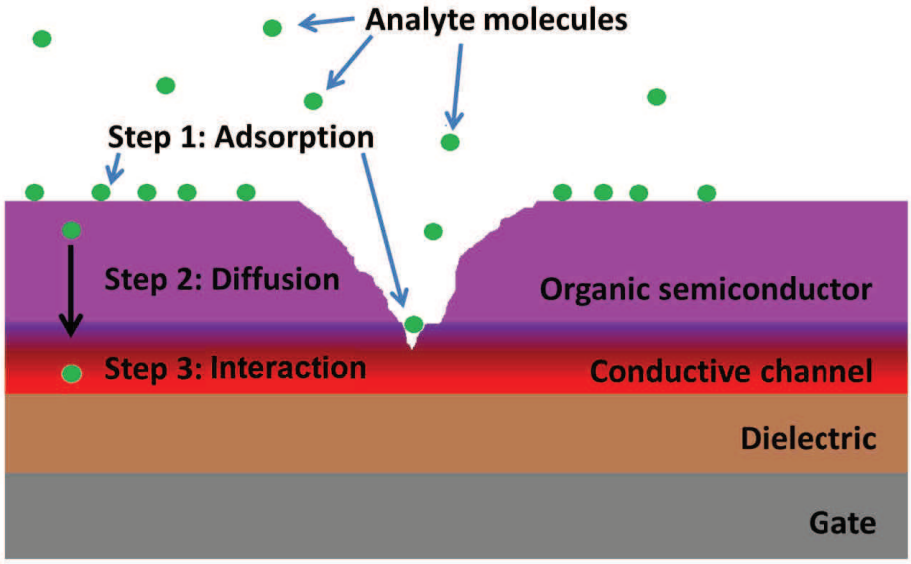

Figure 2.8: Scheme of analyte-OFET interaction. The void in the organic film should indicate grain boundaries.

results with the same materials and added that no swelling of the film was observable by ellipsometry [96]. As a consequence the analyte would be mostly adsorbed on the surface of the grains. Liao et al. investigated the absorption of butylamine and acetone in polythiophene films by measuring the thickness with X-ray reflectivity scans [63]. In contrast to the crystalline DHα4T films, the absence of Bragg-peaks in the depicted X-ray scans indicates an amorphous structure for these polymers. During exposure the Kiessig fringes clearly indicate a reversible increase of the film thickness. The swelling was found to be independent of the film thickness indicating an interface effect where the analyte accumulates at the semiconductor/dielectric interface. Due to this results the report of Liao questions the reliability of the ellipsometry measurements of Torsi but no comparative study was performed with polycrystalline materials to further the understanding of these effects. Summarizing these results, amorphous films seem to allow the analyte molecules to diffuse in the bulk of the film and to the conductive channel where they directly interact with the charge carriers. In crystalline films interactions seem to occur between charge carriers and analyte molecules at grain boundaries.

2.2.4 Semiconductor-analyte interactions

The location of the interaction between the analyte and the semiconductor is most important for the dipole interactions of polar molecules. While the gate voltages typically applied to OFETs are in the order of 10 to 100 V, the perturbation in the electric potential by a polar molecule is only a few tenths of a volt at a distance of 10 Åfrom the molecule. Someya et al. argue that the potential from the gate drops already across the gate dielectric and 80-90 % of the gate potential arriving at the film, drops very close to the surface [86] [34]. The polar methanol molecule has been reported to cause a Fermi level shift by 200 mV in α-sexithiophene which is in the range of typical trap states in organic semiconductors. However, as the free charge carriers inside the semiconductor will screen the electric field of the polar analyte, the analyte molecules need to be at, or close to the conductive channel to significantly influence the charge transport.

Torsi et al. compared the influences of alky (nonpolar) and alkoxy (polar) side chains on the sensing behavior of polythiophenes for ethanol vapor. While the nonpolar type showed no response the current of the device with the polar side chains decreased upon exposure, probably due to the dipole-dipole interactions [98]. Higher responses compared to the ones obtained with polythiophene based devices have been reported for pentacene [67]. Though pentacene is a nonpolar molecule, polar analyte molecules at grain boundaries can increase the disorder and enhance trapping. An explanation for the enhanced response of the unfunctionalized, but highly ordered molecule pentacene, could be based on a report of Bora et al. where a high energetic disorder of OFET based sensors was suggested to possibly obscure the response to the analyte [5]. The high structural order in pentacene films results in a smaller energetic disorder in comparison to semicrystalline polythiophene films. Further indications for trapping induced current decrease upon exposure to polar vapors was given by Duarte et al. [20]. Upon exposure to ethanol pentacene revealed an increase of the activation energy for hopping, which is consistent with an increase in the number of traps [86].

The formation of hydrogen bonds is another mechanism that has been reported to account for current decrease in organic semiconductors. In doped and undoped

polyaniline, methanol has been reported to form hydrogen bonds. These hydrogen bonds can cause a twisting of the polyaniline molecules which decreases the conjugation length and therefore the conductance [89]. The conductance decrease in doped and undoped polypyrrole was also assigned to hydrogen bonding based on the observation of a weakened C=O bond in the acetone upon adsorption [77].

Doping of the semiconductor can occur by redox reactions or acid-base reactions. The influence of redox gases on the charge carrier concentration in the organic semiconductor depends on the position of the Fermi level relative to the Mulliken electronegativity of the redox gas. If the electron affinity of the analyte is lower than the Fermi level of the organic semiconductor an electron is transfered to the semiconductor and vice versa [13]. Gases like NO_2 and I_2 are relatively strong electron acceptors which remove weakly bound electrons from the aromatic rings of the semiconductor. For p-type organic semiconductors this results in an increase of the charge transport while a decrease can be observed for n-type semiconductors [16] [70]. The electron donor ammonia on the other hand reduces the conduction in hole transporting materials [1].

Ammonia showed also another mechanism which allows to change the charge carrier concentration of the organic semiconductor. Exposure of polyaniline to ammonia causes a current decrease due to deprotonation by acid-base reactions. The used form of polyaniline is doped (protonated) and has therefore an acid character. The free electron pair in the nitrogen atom of the ammonia molecules makes it a base which deprotonates the polyaniline: $NH_3 \rightarrow NH_4$. The dedoped form of polyaniline can now be doped again by acidic gases like HCl, H_2S and CO_2. It should be noted that the reversible acid/base doping process of aniline is a rather unique property and not representative for all organic semiconductors.

If the analyte vapor diffuses inside the organic semiconductor the charge transport can also be influenced without any specific interactions. Vercelli et al. have shown that the response of polythiophenes and polypyrroles follows the relative variation of the dielectric constant. If the dielectric constant ϵ_p of the polymer is larger compared to the analyte ϵ_a conductivity decreased and vice versa [102]. Variable range hopping (VRH) was shown to explain this behavior. VRH can also result in

a decrease of the current due to an increased interchain distance. This effect was amplified by Ruangchuay et al. by exposing a blend of isolating PMMA and doped polypyrrole to acetone. During exposure the acetone absorption was stronger for PMMA which increased the isolating gaps between the conductive polypyrrole and caused a decrease of the current [76]. Such behavior is especially interesting as the enhanced absorbing part does not have to show semiconducting properties which leaves more possibilities to find composites with a high inherent selectivity.

2.2.5 Current trends

One concept to circumvent the low selectivity of gas sensors in general, is inspired from the olfactory system of mammals. The human nose, for example, incorporates more than 100 different receptors which allow to distinguish up to 10000 different odors [112]. Instead of using one receptor for each odor, the combination of different response patterns enables analyte specific recognition. The electronic replica of the human nose can be made out of several sensors which can even rely on different principles (electrical, optical, mechanical). Due to fabrication techniques like printing, organic electronics are a very interesting candidate for such sensor arrays as they would allow a very cheap manufacturing process. Printed OFET arrays based on 5 different types of P3HT, functionalized by acidic and basic groups, showed unique response patterns for 12 different chemicals [10]. Also discrimination within one class of analytes (amine vapors) was achieved only by variation of the side chain lengths in OFETs [64]. More complex gas-mixtures were investigated and successfully recognized by Guadarrama et al. Chemiresistor arrays of 16 conducting polymers were used to distinguish 15 olive oils as a function of the used olives and the region of their growth [30]. As these artificial noses can be made of other types of sensors, too, products based on metal-oxide semiconductors, SAW and QCM are already on the market [112].

Bilayer devices are composed of a functionalized outer layer on top of an organic semiconducting film. This structure can be used when the functionalizing side chains, which are attached to the semiconducting molecule, make the initially semiconducting molecule insulating. Huang et al. employed hydroxy-functionalized

derivatives of 6PTTP6 on top of 6PTTP6 for dimethyl methylphosphonate (DMMP, to simulate nerve agents) detection. In comparison to the unfunctionalized 6PTTP6 device a faster and higher response was observed which was explained by the the formation of hydrogen bonds between DMMP and the OH group in the functionalized molecules [39]. A bilayer structure was also employed by Torsi et al. to allow functionalization of oligomers with enantioselective side chains as the steric hindrance of the functional groups impeded gate modulated charge transport. The resulting selectivity to both enantiomers of citronellol at a tens-of-ppm level is especially interesting, as their discrimination is generally very difficult even with chromatographic techniques [99].

Zhang et al. showed that the electrical response of the same polymer (P3HT) to analytes can be contrary, depending on the nanostructure of the film [57]. While some analytes only varied the strength of the response as a function of porosity, others changed the polarity of the conductance change, depending on the dominant underlying sensing mechanisms. Liqiang et al. addressed the fact that the conductive channel in an OFET is typically covered by a several tens of nm thick layer of the film which the analyte has to pass to interact with the charge carriers in the channel. By growing dendritic microstripes with 4-6 molecular layers, the analyte molecules could directly access the conducting channel at the semiconductor/dielectric interface. Comparing the results to conventional 20 nm thick films of the same molecules the sensitivity to NH_3 increased by almost one order of magnitude. Additionally response- and recovery time after removal where also significantly improved [61].

A better understanding of the ongoing sensing mechanisms was provided by Wang et al. by investigating the sensing behavior of a series of channel lengths between 300 μm and 10 nm. During exposure to 1-pentanol P3HT and pentacene devices showed a decrease of the current for large channel lengths due to an increase of the charge carrier trapping at grain boundaries. When the channel length became lower, the number of grain boundaries decreased and a different mechanism became dominant which manifested as an increase of the source-drain current. While the resistance of the channel in an OFET decreases with its length, the contact resistance can

be considered to stay constant. At channel lengths of only a few nm the device is dominated by the contact resistances. When charge carriers are injected into the organic semiconductor, they accumulate in the vicinity of the electrode and induce an image charge in the electrode, creating an interface dipole. Analyte molecules can diffuse between the injected charge carriers and the electrode and screen the electric field, resulting in an enhanced charge carrier injection [109], [109].

2.3 Thesis in context

To further the application of organic semiconductors in gas sensors the project TRANSFILSEN (explained more detailed in 1.1) combines the two last points presented. Based on the results reported by Liqiang et al, the envisaged structure, which directly exposes the conducting channel of the OFET to the surrounding environment, can be expected to enhance the sensitivity and the response time of the sensor, as it eliminates any delay or attenuation caused by diffusion of the analyte through the bulk [61]. The more fundamental oriented work of Wang, revealed unconsidered effects which appear at short channel lengths, but which may also be important to understand the behavior of long channel devices.

Though the exploration of nanoscale devices was not possible in the course of this thesis, other important aspects could be covered.

As explained in section 2.2.2, the identification of the analyte is one of the most important properties of a gas sensor. The higher number of parameters that can be extracted from OFETs make these device structures favorable for many applications, in comparison to chemiresistors. The simultaneous monitoring of on- and off current, mobility and threshold voltage allows to use analyte-specific response patterns for the identification of the analyte. In this work the hysteresis of the transfer characteristics is suggested as an additional parameter for the detection of polar vapors. It is shown that the hysteresis provides additional information which can not be received from the conventional parameters, and that it therefore improves the selectivity of an OFET to polar vapors. Furthermore, measurements of the transient

drain current were performed, which allow to indicate different dynamics of trapping and detrapping as origin of the selectivity enhancement by the hysteresis.

The dependence of the sensitivity of gas sensors on the side chains of the used molecules is shown for a new class of polymers, designed for the project TRANSFILSEN. Measurements of the ethanol mass uptake revealed direct correlations between the sensitivity and the absorption of the films for side chains with similar polarity. As morphological studies indicate, a higher crystalline fraction in the rather amorphous films decreases the mass uptake and therefore also the sensors responses. More polar side chains revealed a lower mass uptake but a high response. Though the mechanism of the enhanced interaction of ethanol with the strongly polar side chains was not revealed, the obtained results indicate a very high sensitivity to ethanol for polymer based devices.

3 Used organic semiconductors

This chapter introduces the organic semiconductors used in the course of this thesis.
P3HT is a standard material which is well understood and can be purchased from various manufacturers. It has been used to test the performance of the new installed gas-test bench where it revealed interesting new properties that have not been published yet, and therefore motivated deeper investigations.
Poly(bithiophene-1,4dialkoxy-phenylene) (TPT) are a new designed class of molecules that were synthesized by the group of professor Serein-Spirau in Montpellier for the project TRANSFILSEN. Different side-chains were attached to the same conjugated backbone to study the influences of the side-chains on the sensor performance.

3.1 Poly(3-hexylthiophene-2,5-diyl)

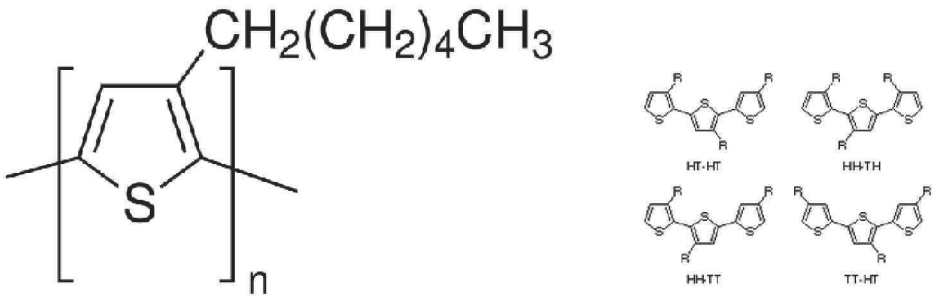

Figure 3.1: Chemical structure of P3HT and possible configurations of the side chains

Poly(3-hexylthiophene 2,5 diyl) (P3HT) is among the most studied semiconducting polymers and has been used in various electronic devices from organic solar cells over OLEDs to OFETs. Good solubility and film forming ability allow usage of low-cost deposition techniques while a low glass-transition temperature and suitable solid-state supramolecular organization enable hole mobility values of 0.18 cm^2/Vs, comparable to those of amorphous silicon [84] [107].

With a HOMO level position of -5.2 eV below the vacuum level, gold (-5,1 eV) is the most appropriate element for hole injection and extraction. The LUMO of P3HT is at -3.5 eV.

P3HT is a polythiophene based conjugated polymer whose structure can be seen on the left in figure 3.1. Depending on the location of the coupling between the thiophene ring and the hexyl side-chain four different configurations are possible (right in figure 3.1). If the configuration HT-HT is repeated for all monomers of the polymer it is called regioregular and shows well ordered thin films. The three other variations can not be controlled and lead to random positions of the coupling throughout the polymer. This type of P3HT is called regiorandom and shows only amorphous structures. Regioregular P3HT always contains also a fraction of regiorandom P3HT. Fell et al. [23] showed that films with a low content of regioregular P3HT (81 %) form unfavorably oriented lamellaes embedded in an amorphous matrix which is expected to be the reason for the low mobilities observed in regiorandom P3HT. On SiO_2, films with a high content of regioregular P3HT ($>$ 91 %) show a favorable organization in lammellar-like 2 dimensional conjugated sheets, separated by disordered zones (see figure 3.2). Adjacent sheets are held together by π-stacking between neighboring P3HT molecules and are oriented perpendicular to the SiO_2 substrate. These two points are very favorable for charge transport in a transistor geometry as they enable intra-chain transport along the molecular axis and enhance inter-chain hopping between adjacent sheets. As a consequence mobilities up to 0.18 cm^2/Vs were measured.

Kline et al. have shown a clear correlation between the field-effect mobility of regioregular P3HT and its molecular weight [49]. By varying the molecular weight between 3200 and 36500 g/mol a proportional increase of the hole mobility from 1.7 x 10^{-6} to 9.4 x 10^{-3} cm^2/Vs was observed for transistor structures. This improvement of the mobility could not be explained by an improved organization, as structural studies by X-ray diffraction and AFM revealed a higher cristallinity for the lower molecular weight P3HT. However, the morphology of the AFM images showed better defined grain boundaries in the case of low molecular weight P3HT. Based on the observation that grain boundaries limit the mobility in organic semi-

conductors [35], the interpretation given by Kline hypothesizes that long polymer chains connected to two adjacent ordered domains can provide pathways for charge transport between crystalline domains.

All P3HTs used in the course of this thesis were purchased from BASF or Rieke Metals and have molecular masses higher than 32000 g/mol. Regioregularity of the polymers was always higher than 91 %.

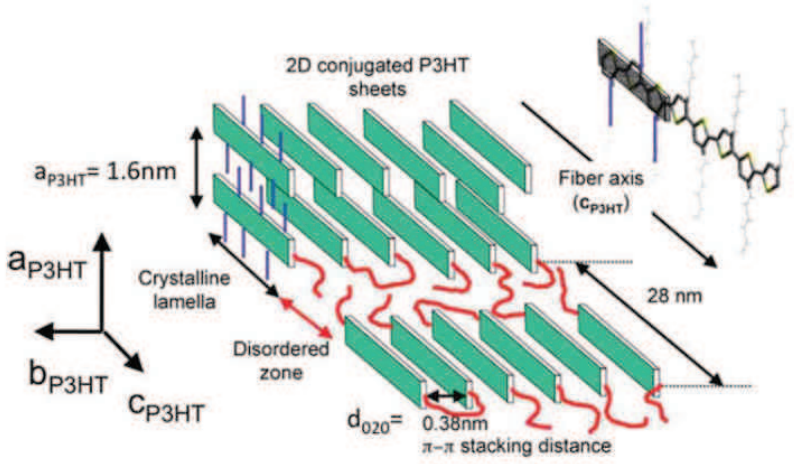

Figure 3.2: Semicrystalline structure of P3HT. Red segments represent disordered P3HT in the amorphous zones. [7].

3.2 Poly(bithiophene-1,4dialkoxy-phenylene)

Selectivity and sensitivity of organic semiconductor-based gas sensors are crucially dependent on the side chains of the conjugated molecule [64] [98] [97]. Comparing alkyl and alkoxy-substituted polythiophenes Torsi et al. found an enhanced sensitivity for alkoxy substituted polymers to polar vapors [98]. Enhanced dipole interactions with the more polar alkoxy chains were considered to be the underlying reason.

To further the understanding of the influence of alkoxy-side chains on the sensor performance the chemistry group of professor Serein-Spirau from the University of Montpellier synthesized a group of new semi conducting polymers with the same conjugated backbone but different side chains.

3.2.1 Molecular structure

3.2.1.1 Molecular backbone

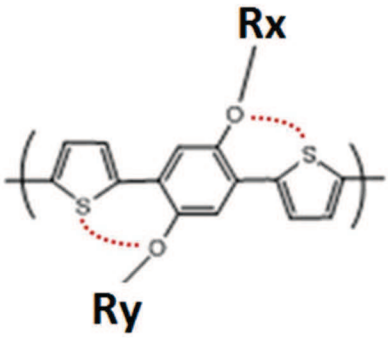

Figure 3.3: Conjugated backbone of the bithiophene-phenylene polymers. The red dotted lines indicate the planarizing sulfur-oxygen bonds.

The backbone of the Poly(bithiophene-1,4dialkoxy-phenlylene) polymers (TPTs) consists of a fully conjugated thiophene-phenylene-thiophene group, as shown in figure 3.3. Different sets of alkoxy side chains, which will be presented in the next section, are attached to the phenyl group. The vicinity of the electron-rich oxygen atom in the alkoxy side chains to the sulfur of the neighboring thiophene rings leads to an attractive intramolecular interaction between these two moieties. As a consequence, the rotational freedom of the thiophene rings and the phenyl group is expected to be reduced and the molecule should be stabilized in a planar configuration. A planar structure enlarges the delocalization of the molecular orbitals and increases intermolecular interactions, both of which are favorable for charge transport and lead to an increase of the charge carrier mobility. On the other hand, between neighboring monomers two unsubstituted thiophene rings are located next to each other. Such a configuration has high rotational freedom and reduces the effective π-conjugation length. While this is unfavorable for the mobility, unsubstituted thiophenes are often used to increase the air stability, as they are known to lower the energy level of the highest occupied molecular orbital (HOMO) [73]. The LUMO and HOMO of the TPT based molecules were measured by the chemistry group for oligomers with different numbers of repetitive units. It has been found that the energy levels remain constant for oligomers or polymers consisting of more

than four repeating units, indicating that the average conjugation length does not exceed the length of four TPT repeating units. The LUMO and HOMO of the used polymers were found to be approximately -2,3 eV and -4,7 eV.

3.2.1.2 Side-chain properties

Cheap manufacturing of organic electronics by wet coating techniques, like drop casting, spin coating, inkjet printing or screen printing is an enormous advantage compared to inorganic semiconductors but it also puts restrictions on the used polymers. To make polymers soluble in organic solvents, soluble side chains (usually alkyl or alkoxy groups) have to be covalently grafted to the polymer backbone. The longer the side chains are and the higher their density, the better is the solubility of the final polymer. On the other hand, side chains have a huge impact on the molecular structure and the organization of the polymer backbone in thin films [4] [98]. Sterical strains imposed on the aromatic units by the configuration of the side chains in thin films can twist the conjugated backbone and reduce the effective conjugation length. As a consequence a trade-off between the solubility of the molecule and the organization in thin films has often to be found.

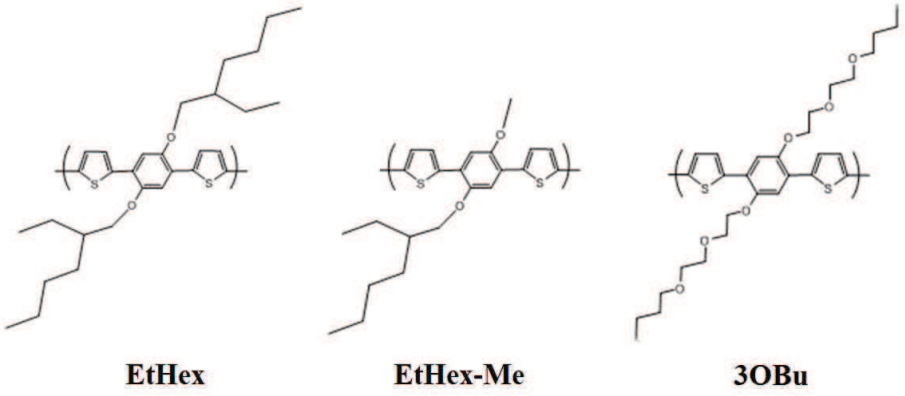

Figure 3.4: Molecular structure of bithiophene-phenylene polymers with respective side chains

To study the influences of the side chains on the sensitivity of organic semiconductor-based gas sensors the chemistry group of professor Serein-Spirau synthesized polymers with three different side chains grafted to the bithiophene-

	EtHex	EtHex-Me	3OBu
Molecular weight [g/mol]	21900	17500	30176
Repeating units	44	44	53

Table 3.1: Molecular weight and corresponding number of repetitive units in PTPT polymers

phenylene backbone, presented in the previous section. The structure of the three resulting polymers can be seen in figure 3.4. The ethyl-hexyl side chains of the EtHex polymer are favorable for a good solubility in organic solvents but can be unfavorable in thin films due to the pronounced steric hindrance. A decreased steric hindrance is expected if the ethyl-hexyl side chains are replaced by shorter methyl chains, as it was done for the EtHex-Me polymer. However, to keep the polymer soluble, only one of the ethyl-hexyl side chains could be exchanged for a methyl chain. The ethyl-hexyl and the methyl side chains are both based on non-polar carbon-hydrogen units which give the molecule only a very small dipole moment [98]. A higher dipole moment is achieved for the 3OBu molecule by providing oxygen-enriched octane chains. Table 3.1 displays the molecular weight of the three different polymers. The analytes weights were measured by the group of Serein-Spirau by gel permeation chromatography. The second line shows the number of repeating units corresponding to the respective molecular weight. As it can be seen all three polymers have comparable lengths.

3.2.2 Film morphology

X-ray diffraction and AFM are important tools to investigate structure and ordering of organic semiconductors in thin films. Understanding these fundamental properties does not only help to understand the charge carrier mobility. The sensitivity of organic semiconductors to gaseous components is also strongly dependent on the nanostructure of the material [57].

Xray-measurements were performed by Jean-Pierre Lere Porte, member of the group of professor Serein-Spirau from the Institute Charles-Gerhardt at the University of Montpellier. Films were deposited by spin coating from 10 mg/ml tetrahydrofuran

solution on glass substrates. The measurements were performed with a powder X-ray diffractometer in Bragg Brentano configuration operated at 40 kV and 35 mA. A wavelength of 1.54 Å was generated by the k_α transition of the Cu anode.
Figure 3.5 shows the reflectivity scans for all three polymers. 3OBu and EtHex-Me show an almost featureless shape with only minor peaks of the first order. This indicates a very amorphous structure for both molecules with EtHex-Me showing a slightly higher order than 3OBu. The peaks around 10,5 and 7,3 Å for 3OBu and 9,7 and 6,2 Å for EtHex-Me, indicate a very weak lamellar-like organization perpendicular to the substrate, driven by the side-chains of the molecules. EtHex shows a more ordered structure with Bragg-peaks up to the fourth order. The Bragg-peak corresponds to an interlayer spacing of 12,8 Å and marks the dominant spacing between two adjacent planes of the EtHex molecules.
It is important to note that none of the three films showed π-stacking, which is usually marked by peaks at low spacing distances around 3 to 4 Å.

AFM measurements in tapping mode were performed in collaboration with Wael Hourani, postdoc at the group of Laurent Simon from the Institute de Science des Materiaux de Mulhouse. Samples were prepared on the same substrates and under similar conditions like the transistors used for the detector studies (See chapter 5.1.1). The transistors have shown thicknesses below 10 nm by profilometer measurements. No annealing was performed prior to the measurement. Images were taken close to the center of the sample, in vicinity to source and drain electrodes. This way, the obtained morphology should also be representative for the film in the channel between source and drain.
Figure 3.6 shows the surface morphology of all three polymers. The two amorphous molecules 3OBu and EtHex-Me show an isotropic nodule structure while the more ordered EtHex molecule shows no distinctive features. Even though the films are cohesive on a macroscopic scale AFM images reveal microscopic holes in all films that reach down to the SiO_2 substrate. This is indicated by the phase shift observed in the highly resolved images shown in figure 3.7. An additional indication that the holes reach down to the substrate is given by the profile images in the same figure.

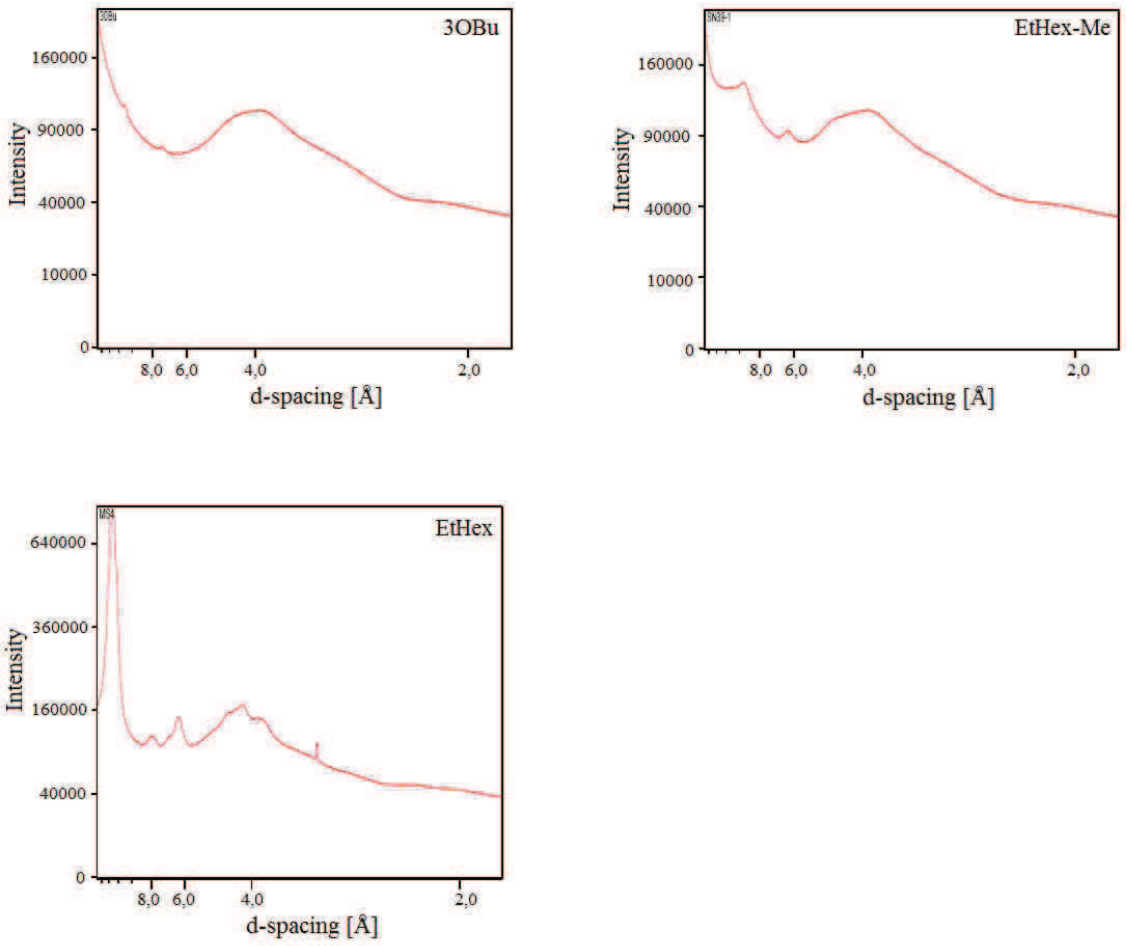

Figure 3.5: X-ray reflectivity scans of bithiophene-phenylene polymers

The deepest spots of every sample are always at the same height while the rest of the film shows no other repetitive heights which would mark a terrace-like structure. For amorphous films, as it was indicated by the X-ray results, the presence of a lower limit for the height distribution supports the assumption that the holes reach down to the underlying substrate.

Image d) in figure 3.6 shows the height distribution of all three polymers for the 1×1 μm images with 0 nm height corresponding to the level of the SiO_2 substrate. Each sample shows several points that reach down to the substrate. As it can be seen all three films have comparable thicknesses in the range of the results obtained by the profilometer measurements 5.1.1. 3OBu and EtHex have a comparable gaussian-like height distributions. The EtHex film is approximately 3 nm thicker than the 3OBu film, shown by the shift of the height distribution towards higher values and from

	EtHex	EtHex-Me	3OBu
RMS roughness [nm]	1,7	1,2	1,4
Average height [nm]	8,1	6,3	5,5
Overall surface area [μm ^{2}]	1,017	1,011	1,010

Table 3.2: Roughness, film height and ironed surface area extracted from 1x1 μm AFM images

the average heights in table 3.2. The height distribution of EtHex-Me is more narrow compared to the other two molecules, which indicates a slightly lower roughness (see also table 3.2). A shoulder at lower heights broadens the height distribution towards lower thicknesses. This can improve the accessibility of the sensing channel at the dielectric/semiconductor interface for gas molecules.

The last line in table 3.2 compares the overall surface area of the three PTPT molecules in the 1x1 μm scans. For a gas sensor, the overall surface area describes the area where gas molecules can adsorb on the sensing layer. A higher roughness usually goes with an increased surface area and can be beneficial for the sensitivity. Even though the PTBT molecules show significant differences for the roughness values, the variations of the overall surface area are below 1 %.

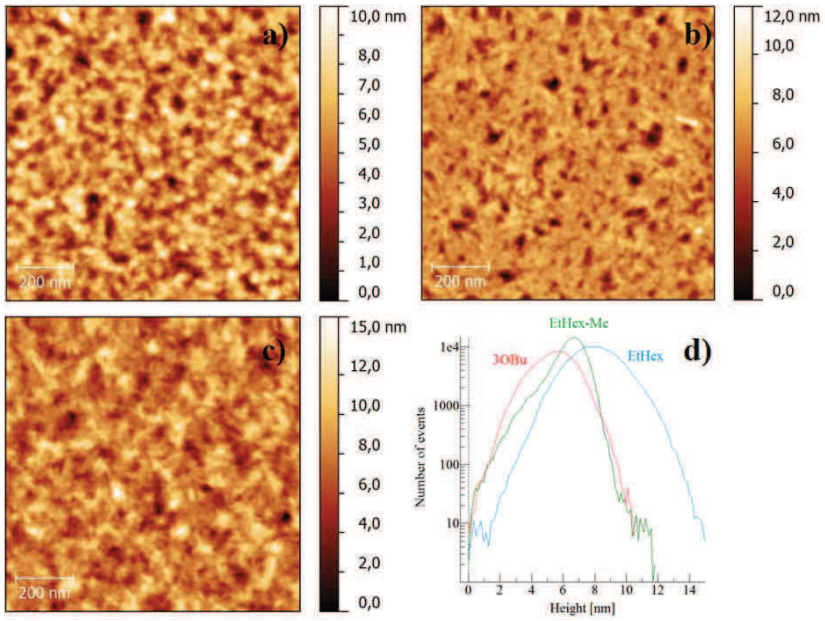

Figure 3.6: AFM topography images of a) 3OBu b) EtHex-Me c) EtHex. Image d) shows the height distribution of the three PTPT molecules. Height 0 corresponds to the level of the SiO_2 substrate.

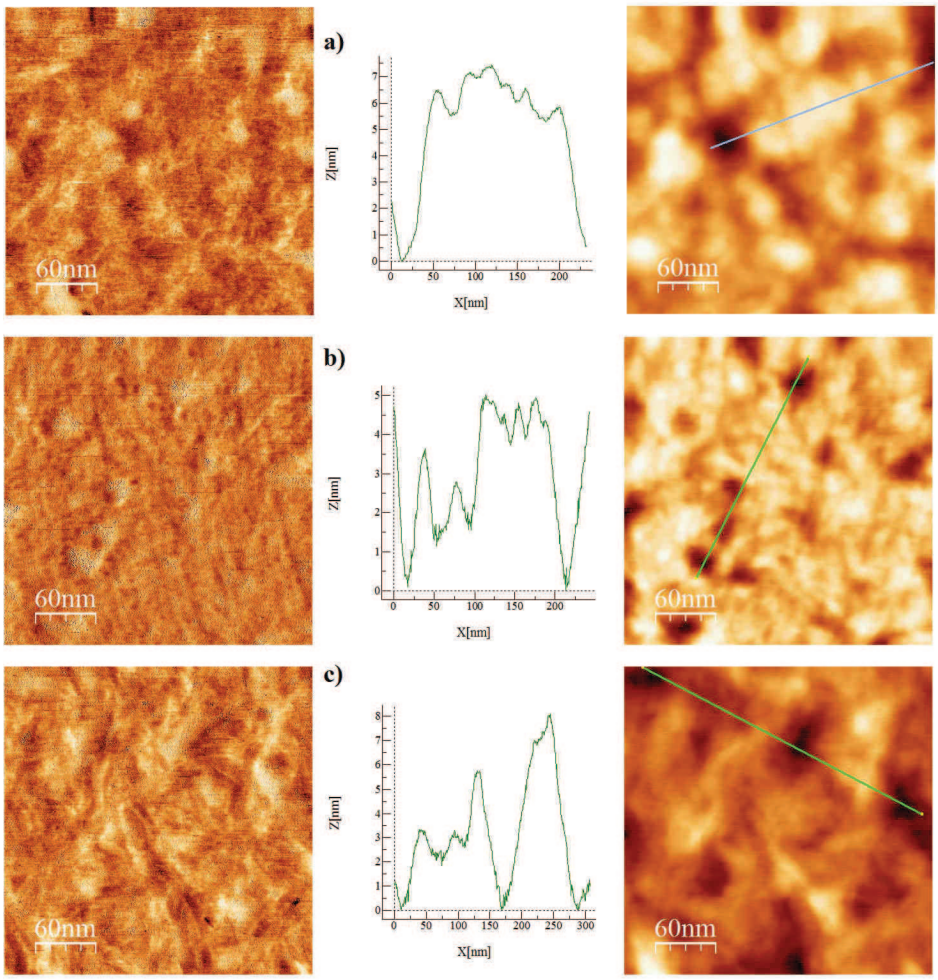

Figure 3.7: Phase (left), profile (middle) and topography (right) images of a) 3OBu b) EtHex-Me c) EtHex. Straight lines in c) show where the height profiles were taken.

4 Establishing a gas-test-bench for OFET sensors

In order to allow a controlled exposure of organic semiconductors to analyte gases a gas test bench had to be established in the course of this work. Several requirements had to be fulfilled to enable proper operation:

- sensors needed to be exchangeable inside a glove box to avoid degradation by air exposure
- a nitrogen atmosphere should be maintained inside the gas test bench
- several sensors should be tested at once to ensure comparable conditions
- resolution of electrical measurements should be sufficient for low currents inherent to organic semiconductors
- various gases should be available for testing

This chapter presents the experimental apparatus before the different measurement configurations are presented which were employed in this thesis.

4.1 Experimental apparatus

Figure 4.1 shows the gas test bench build and modified during this thesis with the help of the technical staff at ICube. It basically consists of three main components: AC denotes the analyte chamber where arbitrary volatile analyte sources can be inserted to create samples of the respective vapor. The second set of components is responsible for the delivery of the analyte samples to the sensor: mass flow controllers (MFCs) control the flows of nitrogen (pureness $>$ 99,99 %, purchased from Air Liquide) which is used as a carrier gas for the analyte samples or to purge the sensors in the detector chamber (DC). The last part includes the electrical connections and the measurement apparatus used to characterize the sensors electrically.

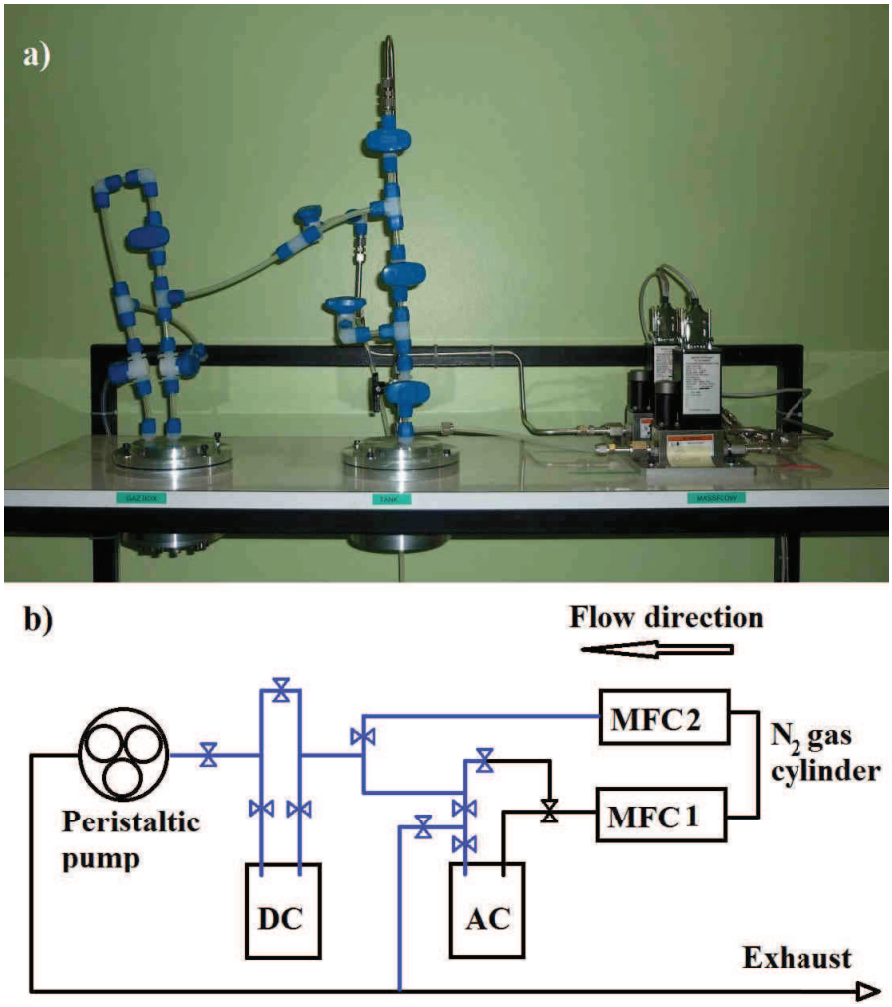

Figure 4.1: Image a) and b) scheme of the gas test bench established in this thesis. PFA tubings are displayed blue in the scheme of the setup. DC and AC denote detector and analyte chamber, respectively.

Two different materials are used for the tubings, valves and fittings of the gas test bench which were all purchased from Swagelok. PFA tubes were used for all tubings in contact with the analyte gas between the AC and the DC. PFA tubing offers several advantages as it shows properties similar to PTFE which is used as lining inside the DC. Both materials are very non-reactive which ensures chemical resistance to most chemicals and reduces adsorption of analyte molecules on the inner side of the tubing. Analyte molecules adsorbed on the inside of the tubings can desorb after the exposure has finished and lead to uncontrolled exposure of the sensor. Additionally PFA has low vapor transmission rates compared to most other plastic tubings and effectively reduces contamination of the gas samples by air. For

the tubings between the gas cylinder and the MFC stainless steal was used as these parts are not in contact with analytes.

The AC and DC chambers are made from aluminum and host the analyte source and sensors during the measurement. While the AC is simply an empty cylindrical chamber with gas inlet and outlet, the DC is divided into two hermetically separated parts. In the bottom of the DC BNC bulkhead fittings allow to electrically contact the sensors in the DC with BNC cables to reduce noise and enable low current measurements. Individual BNC connectors are provided for every terminal of the sensors. As the body of the DC consists of aluminum which is grounded by the outer shield of the BNC cables, it serves as a Faraday cage. As also no high frequency measurements are performed, unshielded cables are used inside the DC to connect the BNC feedthroughs to the sensors. Centered in the top part of the DC three sockets are mounted to connect the sensors via To39 electrical supports. The inside of the top part is either lined with pure PTFE or coated with a sprayed PTFE layer. To ensure a homogeneous delivery of the analyte to all samples the flow of the incoming gas is widened and distributed by a shower head-like cap mounted below the gas inlet and above the sensors. The size of the DC was chosen according to the dimensions of the air locks of the glovebox at the ICube laboratory to enable the exchange of the sensors in a nitrogen atmosphere.

The calibrated MFCs used to control the flow of nitrogen to the AC or DC were purchased from BROOKS. Both allow flow rates between 0 and 24 l/h with a resolution of 0.1 l/h and can be controlled by a purchased computer program. A MFC is a passive device which can only be used to limit the flux of a gas or liquid to a determined value. To ensure a pressure gradient the valve at the outlet of the nitrogen cylinder is set to deliver an overpressure between 0.5 and 1 bar during operation.

To test tubings and chambers for leakage both MFC are opened to 24 l/h while the last valve before the exhaust remains closed. The smallest detectable leak that can be measured by the MFC is 0.1 l/h and corresponds to a loss of 1.6 sccm (square cubic centimeter per minute). Variation of the delivered pressure from the nitrogen cylinder improve the accuracy of this testing method.

For purging the gas test bench can be evacuated by a peristaltic pump.

4.1.1 Gas samples generation

To create gas samples two different methods can be employed with the installed test bench. The analyte gas can be bought with a certificated concentration in a gas cylinder which can be connected to the MFCs and diluted with additional N_2 by the second MFC to vary the concentration. For the second possibility a source of the analyte is placed inside the AC and left to evaporate. A stream of nitrogen is then used to carry the analyte vapor to the sensor.

Though the first solution offers a convenient and precise possibility to expose the sensors to analytes, it suffers from a lack of versatility as every analyte needs to be purchased separately and the range of available concentrations is strictly limited by the concentration of the purchased gas cylinder and the range of the MFCs. The second option offers a very versatile solution as gas samples can be created of almost any volatile compound which is solid or liquid at ambient conditions. As the selectivity and sensitivity of organic semiconductors to analyte vapors are not completely understood and rather determined by experimental results, the higher versatility of the latter solution was used in this thesis.

To create analyte samples in the AC, the volatile source is placed inside the chamber and the chamber is locked. Under a constant stream of nitrogen, typically 3 or 6 l/h, an equilibrium between the evaporating analyte and the flushing nitrogen is established over time. For the highly volatile compounds like ethanol and acetone, which were used in this thesis, an equilibrium was expected to be established after 30 minutes. At this point the concentration of the analyte which leaves the AC carried by the nitrogen flow, is considered to be constant. As the sensors are usually under operation while the equilibrium is established, the outlet of the AC is directed directly to the exhaust without passing at the DC. To expose the sensor to the equilibrated analyte flow from the AC the flow is directed to the DC. To ensure a constant flow rate at the sensor the pure nitrogen flow from MFC 2 is reduced by the flow rate of MFC 1. If the concentration of the analyte sample has to be decreased a higher flow rate for MFC2 was chosen in the beginning. This allows to dilute the analyte by adding additional nitrogen.

The measurements reported in this thesis are either analyzing the variations of

transistor parameters which are recorded within a single measurement (chapter 6), or they are comparing the responses of different materials upon simultaneous exposure to the same atmosphere (chapter 7). The results of these comparative approaches do not depend on the reliability of the concentration of the analyte but on the reproducibility of the experimental conditions.

To estimate the order of the analyte concentration it was approximated from the weight loss of the analyte source during a constant flow of nitrogen (3 or 6 l/h). The weight loss of the analyte and the volume of the nitrogen used for purging were converted to mole and the fraction of analyte per nitrogen was calculated under the assumption of an ideal gas (24 l were used as volume for one mole of gas). To reduce the error of this method, induced by the time needed to establish an equilibrium, the AC was left for at least 12 hours under the constant nitrogen flow. As the concentration values derived by this procedure are only an approximation they will be given with only a one digit precision for the according power of 10.

The Hertz-Knudsen equation describes the evaporation rate G in kg/s from a liquid drop with the surface area a, the partial pressure p_a and the saturated vapor pressure p_{sat}:

$$G \propto a \times (p_{sat} - p_a) \tag{4.1}$$

Though the description of a droplet and the geometrical restrictions are not valid for the analyte sources used in this context, the dependence on the surface area of the liquid and on the difference between the actual partial pressure and the saturated vapor pressure can be assumed to hold as well for the evaporation in the AC. As a consequence the concentration of the analyte coming from the AC can also be changed by varying the interface area between the analyte source and the surrounding atmosphere. Table 4.1 lists the measured approximated concentrations of ethanol at the outlet of the AC at 6 l/h N_2 flow rate for vessels with various diameters.

The measurements listed in table 4.1 were performed under a constant flow of 6 l/h N_2 from MFC 1 through the AC, while MFC 2 was off (see also figure 4.1). For a given vessel in the AC, the analyte concentration can be decreased by adding additional nitrogen via MFC 2 which will dilute the analyte concentration. To test

Interface area [mm^2]	concentration in 6 l/h N_2 [ppm]
1519	30000
21	4000
7	800
1	200

Table 4.1: Approximated ethanol concentration available from the AC for a nitrogen flow of 6 l/h. The diameter of the ethanol containing vessel is varied to change the interface area between liquid ethanol and the surrounding atmosphere inside the AC.

if the pressure increase in the gas test bench, induced by the additional nitrogen from MFC 2, influences the evaporation dynamics in the AC, a flow of 22 l/h was added from MFC 2 to the 6 l/h flow through the AC. Averaged over 27 hours the concentration at the outlet of the AC was found to be 700 ppm (while it was 800 ppm when MFC 2 was off). As the flow rate used from MFC 2 during sensor operation is usually limited to values smaller than 22 l/h, due to the occurrence of noise from the sensor, the variation of the concentration by 13 % can be assumed to be an upper limit to the flow induced error.

As the temperature of the gas test bench was not regulated, variations of the ambient temperature are an additional error source. Temperature induced changes of the saturated vapor pressure will affect the evaporation speed according to the Hertz-Knudsen equation 4.1. The laboratory where the bench is located is windowless in the middle of the institute. This limits the temperature fluctuations during a day to less than one degree. Between summer (27°C) and winter (20°C) the changes are up to 7°. Figure 4.2 plots experimental data and theoretical values of the saturated vapor pressure as a function of temperature. Though the differences of up to 7°C between summer and winter can shift the absolute values of the concentration by up to 50 %, the variation within a single measurement sequence which is performed on the timescale of a day should be less than 7 %.

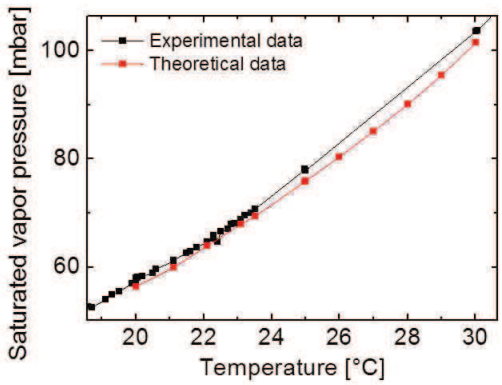

Figure 4.2: Vapor pressure of ethanol as a function of temperature. Experimental values were provided by the Dortmund Data Bank [19]. Theoretical values calculated online from Bronkhorst [8].

4.2 Electrical measurements

The electrical connection from the DC to the sensor is established by To39 supports which are explained detailed in the next chapter 5.1.1. BNC connectors on the bottom of the DC allow the connection to most instruments for the electrical characterization of the sensors. Inside the DC unshielded cables are used to connect the BNC feedthroughs to the sockets as the grounded aluminum chamber provides a Faraday cage for the internal wiring and no high-frequency measurements are planned. Figure 4.3 a) presents the off current of 10 sequenced measurements of one transistor, performed with a short integration time of 640 μs. The integration time determines the time period over which measurements samples are averaged and can be chosen between 80μs and 2 s with the analyzer used. Part b) of the figure plots the standard deviation from the average value of the 10 measurements as a function of the measured current. Reliable measurements with an error of less than 4 % can be performed for currents in the range of 10 pA.

4.2.1 Measurement modes

The characterization method for the transistor based sensors which was primarily used during this work are measurements of the transfer characteristics. The measure-

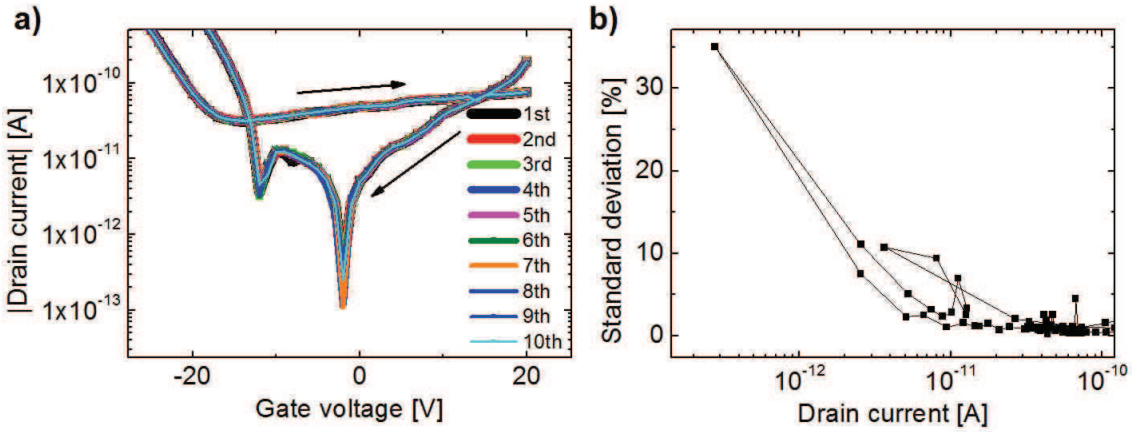

Figure 4.3: a) Ten successive transfer characteristics measurements in the off regime of a transistor, measured in the gas test bench to indicate the resolution of the setup. Arrows indicate the direction of the voltage sweep. b) Shows the relative variation of the measured currents as a function of the magnitude of the current.

ment was performed with a 4156C Agilent semiconductor parameter analyzer. This instruments offers 4 source measure units (SMUs), 2 voltage source units (VSUs) and 2 voltage measure units (VMUs). To enable simultaneous characterization of up to three sensors, one VSU port was set to 0 V and connected to the sources of all sensors. SMU4 was connected to all gates in parallel and performed the determined gate voltage sweep while SMU1 to 3 where kept at a constant potential and used to measure the drain current of each sensor. Between successive measurements of the transfer characteristics the instrument automatically grounds all terminals.

Measurements of the transient current are a second type of electrical measurements which is reported in this work. The aim of this measurement is to analyze the trapping and detrapping of charge carriers in the sensors by switching the gate voltage between two values in the on regime of the transistor. To cancel out additional trapping and detrapping by automatic grounding of the terminals by the 4156C, a different configuration is needed which ensures continuous control of the potential of all terminals. Therefore a constant positive voltage was applied continuously to the sources of the sensors by an Agilent E3631A Triple Output DC Power Supply. The drains of the sensors were set to 0V by the SMUs of the Agilent 4156C which was also used to measure the individual drain currents. A 33210A Function/Arbitrary

Waveform Generator connected to the gate provided a square wave voltage which abruptly changed the potential between two determined values within the instruments range of ±5 V. All instruments were connected to the same ground. Figure 4.4 shows a scheme of the configuration.

Applying a positive bias to the source and keeping drain and gate around 0 V is

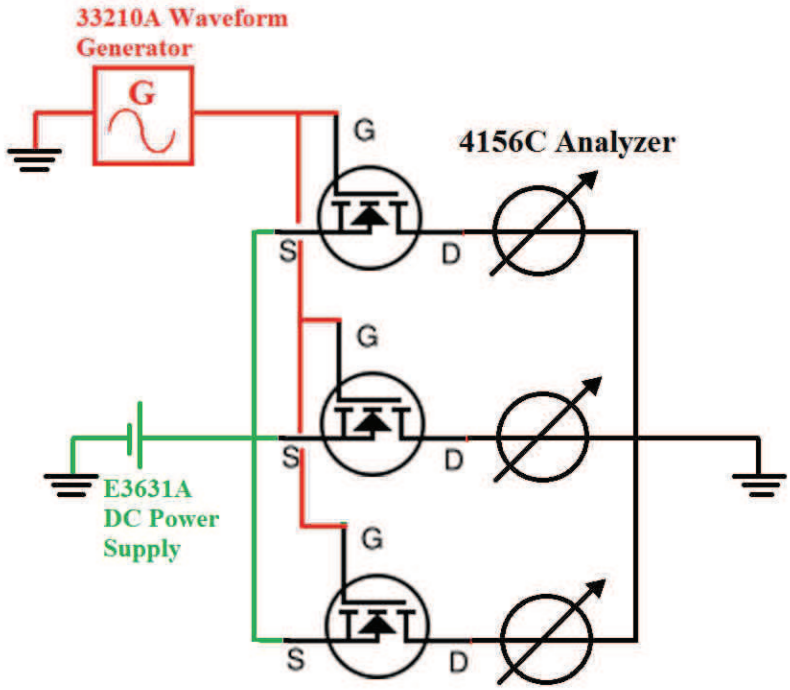

Figure 4.4: Instruments and sensor connections used for transient current measurements. All instruments are connected to the same ground.

equal to applying the same negative potential to drain and gate. The advantage of this method is the continuous control of the potential of all terminals of the OFET sensors which is not possible by the usage of the 4156C only.

4.2.2 Instrument control and data acquisition

As it is explained in chapter 5.2.2 organic semiconductors show pronounced changes of their electrical characteristics over time which risk to undermine the response to the analyte. To establish a stable behavior and therefore a baseline for the measurements, the devices have to be measured in a similar manner and within constant time intervals, until bias stress and recovery between succeeding measurements equi-

librate. To enable a reproducible measurement procedure during a complete measurement sequence and to facilitate storage of the vast amount of data produced, LabVIEW programs were created for the different measurement modes used in this thesis. User friendly interfaces for the LabVIEW programs were established by Thibault Desbordes during his master I internship, under the supervision of the author of this manuscript.

5 Elaboration and characterization of gas sensors

Bottom gate bottom contact OFETs offer the most appropriate configuration for the elaboration of gas sensors as the sensitive layer is directly exposed to the surrounding atmosphere. Pre-patterned substrates incorporating gate, dielectric and source and drain electrodes, facilitate manufacturing as only the respective organic semiconductor needs to be deposited. To deposit the organic semiconductors spin coating was used in this work, as it results in relatively homogeneous and reproducible films.
To enable characterization of the OFET sensors in the gas test bench a solution had to be found to electrically contact the devices without the need for micromanipulators. Commercially available semiconductor packages are plugged in the corresponding socket and facilitate electrical contacting. Wire bonding or conductive paste can be used to contact the sensors to the package. This chapter will present the procedure established to manufacture the sensors for the gas test bench and discuss the main points that have to be taken into account to enable reproducible measurements.

5.1 Device production

The standard OFET fabrication was established at the ICube laboratory before this work by former PhD students of professor Thomas Heiser. This procedure, quickly summarized in the first subsection, enables the reproducible characterization of organic semiconductors in the glove box system by the use of a conventional probe station. the second section explains the device fabrication for sensing in the gas test bench.

5.1.1 Standard OFET fabrication

All transistors and sensors, except the ones discussed in chapter 8, are fabricated on commercially available bottom gate bottom contact substrates purchased from Fraunhofer Institut Photonische Mikrosyteme offering the following specifications:

- unpatterned gate composed of n doped silicon with 10^{17} cm^{-3} doping on wafer surface
- 230±10 nm SiO_2 grown by thermal oxidation as dielectric layer
- 30 nm gold on 10 nm ITO with high workfunction, as adhesion layer for source and drain electrodes
- channel lengths of 2.5, 5, 10 and 20 μm with a constant width of 1 cm

Figure 5.1 shows a scheme of a 1.5×1.5 cm substrate from Fraunhofer incorporating four interdigitated source and drain electrodes of every channel length.

Upon delivery all samples were covered by a protective resist to protect the structures and the SiO_2 from contamination. To remove the resist and possible contamination on the surface the samples where cleaned by 15 minutes ultrasonic baths in the following order: soap and distilled water, acetone and isopropanol. A subsequent UV/ozone treatment during 15 minutes ensured removal of various contaminants. After this procedure the substrates were inserted into the nitrogen atmosphere of

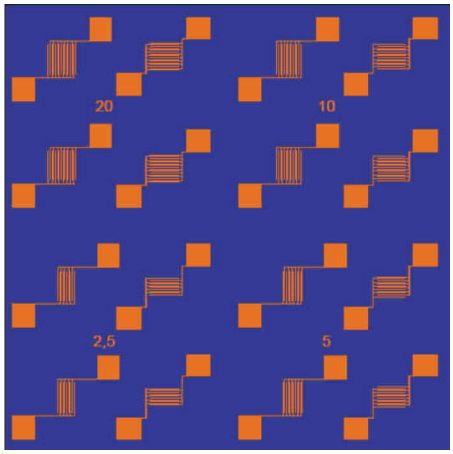

Figure 5.1: Scheme of source and drain electrodes of the employed bottom gate bottom contact substrates

the glove box and the organic films were deposited by spin coating. In the last step the devices were stored in the evaporator at pressures below 10^{-6} mbar for 2 hours at least, to remove remaining traces of the used solvents.

5.1.2 Sensor fabrication

As the utilization of micromanipulators was not possible inside the gas test bench an alternative way had to be found to electrically contact the devices. To39 packages offer three pins to establish electrical contacts to the body of the package and to two isolated contacts channeled through the body (packages were purchased from SCHOTT, datasheet see Appendix 10.1). To mount the Fraunhofer transistor substrates on the To39, single transistors were separated by cleaving and glued on the packages with H20E electrically conductive epoxy from EPO-TEK. The conductive epoxy ensures proper electrical contact to the gate of the transistor. For curing of the epoxy the device was either put into an oven for 3 hours at 80° C or for 30 minutes at 120°. No difference in performance was observable after these treatments.
After curing, several layers of the isolating epoxy H70E were deposited around the substrate to cover the sides of the gate of the transistor and on the body of the To39 between the substrate and the two contacts on top of the To39 body (see image c) in 5.2). After every layer the devices had to be cured similar to the conductive epoxy.

Up to this point the protective raisin remained on the substrates to reduce contamination of the surface. As the used epoxies show good compatibility to many chemicals the complete devices were immersed during the cleaning process with soap and distilled water, acetone and isopropanol. Similar to the standard substrates the devices were exposed to an UV/ozone treatment for 15 minutes before the organic films were spin coated in the glovebox. Subsequently samples were dried in the evaporator for two hours at least. After drying an electrical contact was established by connecting the To39 electrodes to the source and drain pads with a stripe of conductive epoxy.

Though wire bonding is a more convenient way to contact the electrodes on top of the substrates the devices prepared with this method showed a yield below 10 %. Wedge and ball bonding were tested at ICube and IPCMS but the dielectric layer

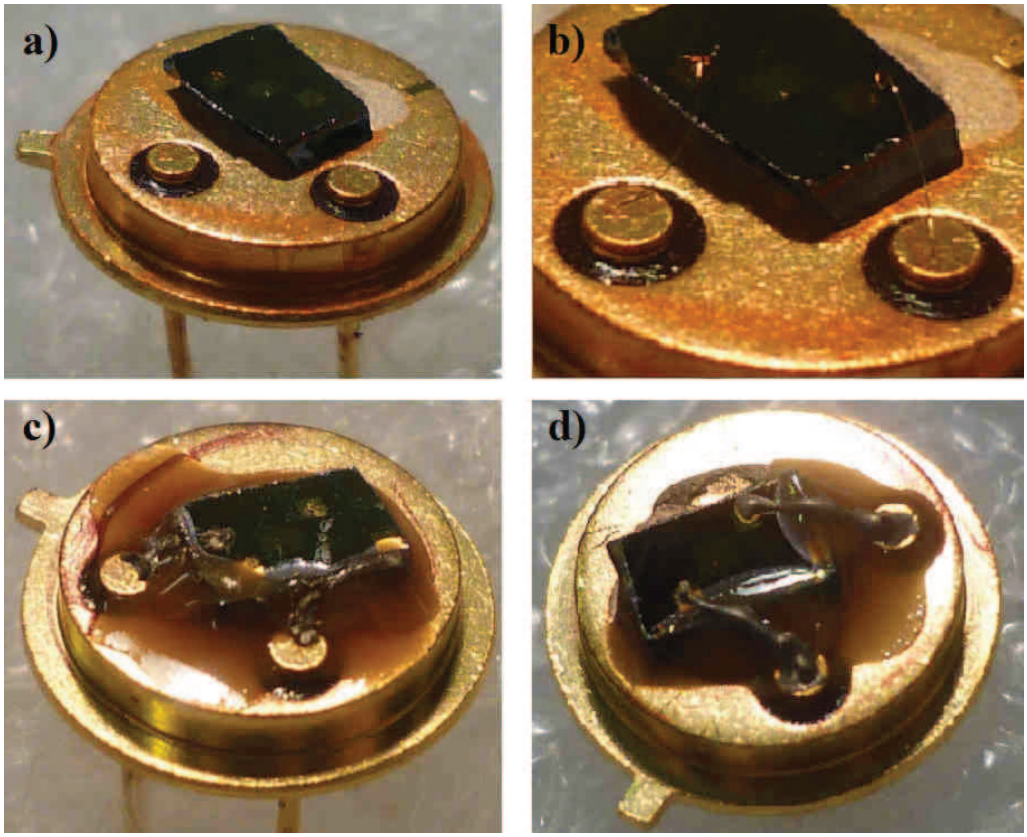

Figure 5.2: a) Transistor substrate mounted on To39. Only gate is contacted by conductive epoxy. b) Same device with bonded source and drain contacts. c) Sensor with isolating epoxy around the transistor substrate. d) Sensor contacted with conductive epoxy.

of the OFETs was pierced for most of the devices, creating irreversible short circuits between source or drain and the gate. To weld the gold or aluminum wire both techniques apply a combination of heat and pressure which destroys the 200 nm dielectric layer underneath. Though more complex substrate structures with patterned gates or locally thicker SiO_2 for the contact pads could impede short circuits, these possibilities were not tested in this work.

Table 5.1 compares the mobilities of the PTPT molecules extracted from devices made according to the procedure established in this work and the standard device fabrication method. While the standard device fabrication method was only used for a maximum of two devices per molecule type, at least 5 different samples were prepared on the To39 supports

	μ(To39) [cm^2/Vs]	μ(Standard) [cm^2/Vs]
EtHex	$3.7\pm1.6\times10^{-6}$	$1{,}9\pm0.2\times10^{-6}$
EtHex-Me	$3.3\pm0{,}8\times10^{-5}$	$4{,}8\pm0.3\times10^{-5}$
3OBu	$1.8\pm0.3\times10^{-5}$	$1{,}5\pm0.8\times10^{-5}$

Table 5.1: Mobilities of PTPs extracted from fresh devices. Left column shows mobilities extracted from To5 sensors, right column from standard devices.

5.2 Basic device performances

This section first describes the transistors parameters that have been used during this thesis and briefly explains how they were extracted automatically by MATLAB scripts. The influences of the measurement itself on the organic semiconductor based sensors and of external parameters like flow rate changes, pressure changes and temperature will be briefly discussed.

5.2.1 Parameter extraction

To analyze the data several MATLAB scripts have been written during this thesis which automatize the extraction of mobility, on current and hysteresis from the transfer characteristics. User friendly interfaces have been programmed by the internship student Thibault Desbordes. Figure 5.3 shows how the individual parameters are extracted and plots the according evolution during a measurement sequence. While for the on current a stable performance was obtained by following simply the current at the largest applied gate voltage, the slope of several data points had to be averaged to obtain stable values for the mobility. The number of points was a function of the stability of the device at the according measurement parameter and the gate voltage step size. The hysteresis was extracted by subtracting the current in the reverse sweep from the current in the forward sweep for every gate voltage step and by multiplication of the result with the gate voltage step size.

To quantify the response of the sensors to an analyte the relative variation of the

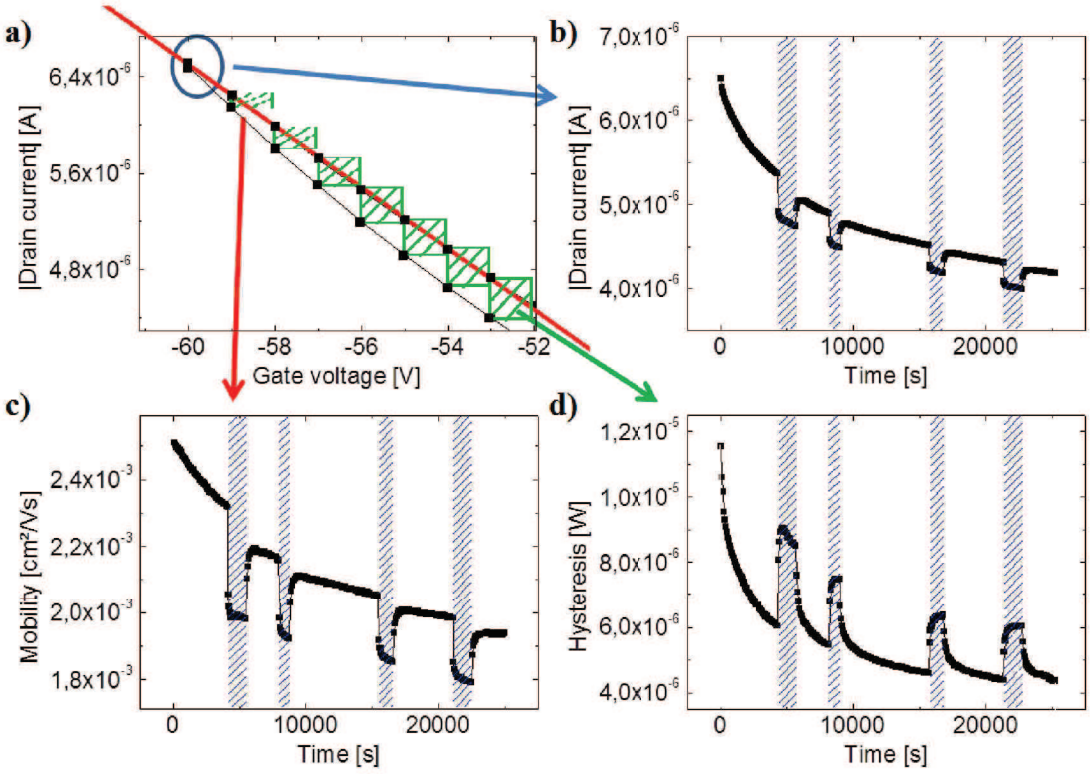

Figure 5.3: a) zoom into transfer characteristics of P3HT based OFET sensor with 20 μm channel length to display parameter extraction. b) on current: current measured at -60 V gate voltage. c) Mobility extracted from the average slope of the highest applied voltage. d) hysteresis: approximation of the area enclosed by forward and reverse sweep. Blue background indicates exposure to 1600 ppm ethanol

respective parameter X was considered:

$$Response = |\frac{X_2 - X_1}{X_1} \times 100| \tag{5.1}$$

Here X_1 is the respective parameter before exposure and X_2 is the same parameter during exposure. To make the results comparable, the best trade of between signal response and drift of the characteristics was chosen to define the point X_2.

5.2.2 Bias stress effect (BSE)

As it can be seen in figure 5.3 b), c) and d) the different parameters extracted from the transfer characteristics are subjected to drift, which is especially pronounced at the onset of the measurement sequence. Such a behavior not only complicates the determination of a baseline reference but also affects the reliability of the ex-

Exposure	Current		Mobility		Hysteresis	
	$\times 10^{-7}$ [A]	[%]	$\times 10^{-4}$ [cm^2/Vs]	[%]	$\times 10^{-6}$ [W]	[%]
I	5.5	10.3	3.3	14.4	3	49
II	3.9	7.9	2.2	10.5	1.9	34
III	3.0	6.5	1.8	8.7	1.5	32
IV	2.8	6.4	1.8	8.5	1.4	33

Table 5.2: Responses of P3HT to ethanol exposures from figure 5.3.

tracted response. The blue backgrounds in figure 5.3 indicate four exposures to the same concentration of ethanol. Table 5.2 compares the relative responses measured 5 minutes after the onset of the exposures. Though the relative variation of the parameters are used, the fourth response is only 50 % of the first response due to the drift of the baseline.

Drift of the electrical characteristics are a typical characteristic of most organic semiconductors and has been observed in polymers and oligomers [28] [25] [82]. While most publications report the origin as a shift of the threshold voltage, some of the samples used in this thesis revealed threshold voltage shifts as well as mobility degradation depending on the used organic semiconductor (see also 7.1.3).

The observed drift and especially the shift of the threshold voltage are generally referred to as bias stress effect (BSE). The origin of BSE is expected to be trapping in deep traps at the semiconductor/dielectric interface [82]. However, Chang et al. have shown an acceleration of the V_{th} shift with an increase of the semiconductor thickness, indicating additional contribution from the bulk of the film to the BSE [11].

To reduce the influences of BSE on the performance of OFETs, IEEE (Institute of Electrical and Electronics Engineers) suggested to ground devices for at least 10 minutes before any measurement [26]. Figure 5.4 compares the influences of the waiting time between measurements on the transistor parameters on current, mobility and hysteresis. The 5 min waiting time measurement sequence was performed first and the device was left for a night to recover, before the 1 min waiting time experiment was performed. Between the 1 min and the 3 sec experiment the device

was left grounded for 90 minutes. As it can be seen, the device recovers well from the BSE between two measurement sequences.

As figure 5.4 shows the behavior of all three parameters during a measurement

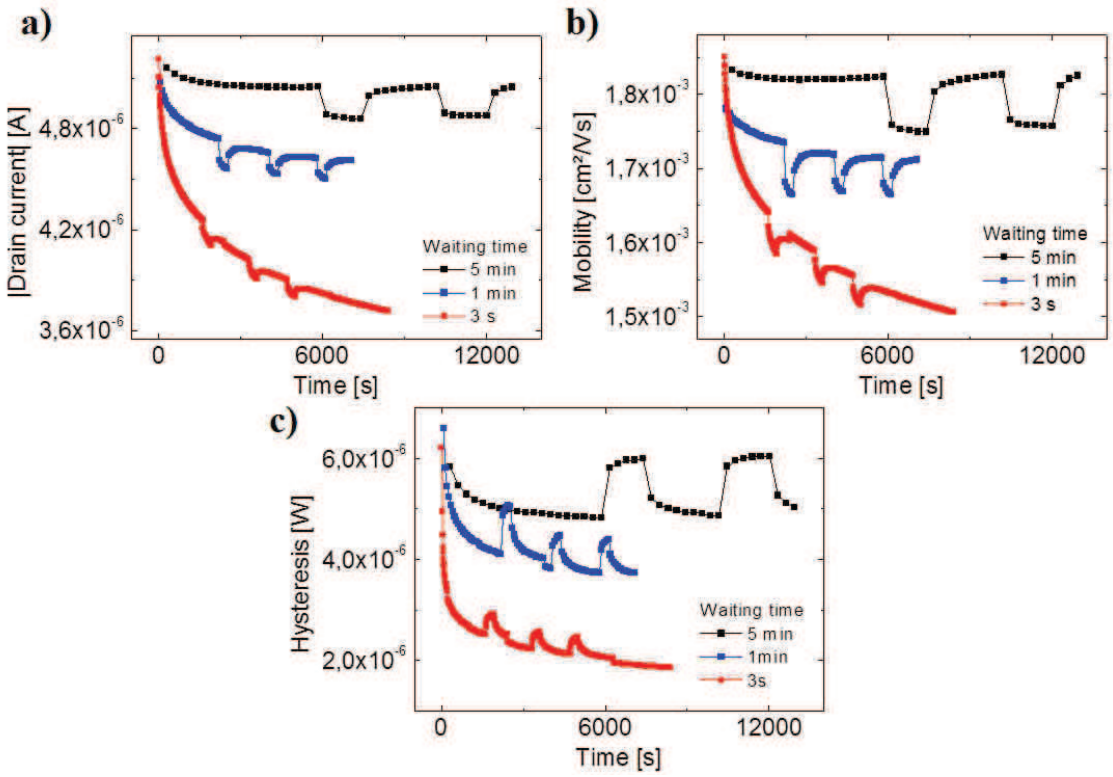

Figure 5.4: Behavior of a) on-current, b) mobility and c) hysteresis for similar measurement parameter but different waiting times between measurements.

sequence depends strongly on the time the device is left grounded between two successive measurements. This observation corresponds well to the trapping induced BSE effects. The longer the device is left grounded during the waiting time, the more charge carriers can be released from traps. As a consequence, the equilibrium between trapping during the measurement and detrapping in between, shifts more towards detrapping for long waiting times and therefore causes only minor decreases of the current and vice versa. As the same behavior can also be observed for the mobility, trapping can be assumed as origin of the mobility decrease too, though it was not reported as BSE.

Trapping as origin of BSE can also explain the drift of the hysteresis which is a measure for the current difference between forward and reverse sweep. If only few traps are filled, in the beginning of a sequence or for long waiting times, the number

	5 min	1 min	3 s
Current [%]	3.5±0.2	2.5±0.1	1.5±0.1
Mobility [%]	3.8±0.3	2.8±0.2	2.4±0.1
Hysteresis [%]	23.7±0.2	16.0±0.1	10.0±0.2

Table 5.3: Responses of P3HT to ethanol exposures from figure 5.3.

of additionally filled traps within one gate voltage sweep (i.e. one measurement) is high, leading to a huge hysteresis. If most traps are already filled at the onset of an individual measurement, i.e. for a short waiting time after the device has settled, the number of traps additionally filled between the forward and reverse sweep is rather small and leads only to a small hysteresis.

Table 5.3 summarizes the responses from figure 5.4. All three parameters show a decrease of the relative response with an increase of the bias stress, i.e. a decrease of the waiting time between measurements. The response of a unfunctionalized polymer like P3HT to ethanol is expected to be caused by an increase of the trapping [20]. As table 5.3 indicates the higher number of unoccupied traps in long waiting time measurements, enhances the trapping effect of the ethanol. This indicates that similar trap states are responsible for the BSE and the response to polar vapors.

Though the longer waiting time results in higher responses, waiting times between 10 seconds and 1 minute were typically employed during this work as waiting times of 5 or 10 minutes increase the time necessary for the characterization of devices to several days. Additionally the experiments discussed in this thesis are comparative studies which did not aim for the highest possible response.

The BSE induced decrease of the parameters follows typically an exponential decay. To ensure stable responses devices were measured in pure nitrogen for approximately one hour and cross-checked with several exposures at the same concentration, before the actual experiments were performed.

Though it was not used in this work, pulsed measurements are an alternative route for some molecules to reduce the BSE [64].

5.2.3 Possible origins of parasitic responses

The established gas test bench (see figure 4.1) should allow to probe the sensitivity of organic semiconductors to gaseous analytes. Therefore it had to be ensured that the bench and the test-procedure itself, do not cause parasitic signals that falsify the measured responses.

At the onset of an exposure the flow of nitrogen is changed manually during the waiting time between two adjacent measurements. This includes reduction of the flow rate from MFC2 which is used to purge the DC with pure nitrogen and redirecting the flow from MFC1 over the AC to the DC. These changes give raise to two possible falsifications of the sensor signal.

The first one is the change of the pressure inside the system due to the change of the flow rates and the additional amount of the analyte which adds to the nitrogen. The amount of analyte typically used is below 3000 ppm which corresponds to an increase of the total flow by 0.3 %. To change the concentration of a given analyte source the flow rates were changed by up to 12 l/h without affecting the baseline of the sensors contacted by conductive epoxy. Wire bonded sensors however, showed a strong increase of the noise for flow rates above approximately 15 l/h. Probably due to mechanical influences of the flow on the bonding wire.

A second point that can be a possible origin of parasitic signals is the temperature of the nitrogen. When the N_2 leaves the gas cylinder over a pressure-reducing valve the gas undergoes an expansion. In an ideally insulated valve the expansion is an isenthalpic process and described by the Joule-Thomson effect. For an expansion from 200 bar to 1 bar the theoretical decrease of the temperature of the gas is approximately 30°C. However, valve and tubings between the nitrogen gas cylinder are at room temperature and heat the nitrogen before it reaches the DC. To ensure the longer retention period in the AC chamber and the therefore increased temperature does not influence the sensor response, the empty AC was annealed to 36°. Before the sensor was purged with the nitrogen from the AC the nitrogen was stored inside for 4 minutes to ensure a higher temperature than the N_2 coming directly from the gas cylinder via MFC2. To expose the sensor to the nitrogen from the AC the flow of MFC2 was set to 0 l/h and completely replaced by 6 l/h N2 from the AC. No

influences on the baseline were observable.
As a consequence of these two points it has been shown that no parasitic signals deteriorate the response from the analyte vapor generated in the AC.

5.3 Conclusions

The last two chapters introduced the gas test bench that was established during this thesis and explained the applied measurement configurations. A very versatile method to generate gas samples was applied and the way to approximate the order of magnitude of the concentration was introduced. The manufacturing of the OFET sensors was presented and the performances of the transistors were compared to devices made according to the standard procedure. Both type of devices showed comparable charge carrier mobilities.
The methods of OFET parameter extraction were briefly introduced and factors, which could degenerate the devices performances were discussed.

6 OFET response to polar analytes

Excluding or identifying unwanted, parasitic responses is an important challenge for gas sensors. To reduce this cross-sensitivity, organic semiconductors offer the possibility to functionalize the semiconducting molecule by introducing analyte-specific receptors on the conjugated backbone or to assemble different semiconductors in sensor arrays where the patterns of the individual responses allow to identify various analytes. A more basic approach was introduced by Torsi [95] by showing how the different parameters of a field effect transistor can be used to provide a fingerprint for individual analytes with unfunctionalized organic semiconductors.
This chapter discusses the application of the hysteresis of the transfer characteristics as an additional parameter for the detection of polar vapors. Acquired in the same measurement as the reported OFET parameters, I_{on}, I_{off} V_{th} and μ, direct comparison of their suitability is performed. The model system ethanol and acetone vapor is used to show that the hysteresis allows to extract additional information that helps to distinguish gases which can hardly be distinguished by using the conventional parameters. In the second part of this chapter it is shown how measurements of the transient drain current can help to understand the underlying mechanism. The results indicate enhanced trapping in the presence of polar analytes as origin of the hysteresis increase and suggest different trapping dynamics as origin for the analyte selective hysteresis variation.

6.1 Transfer characteristics response to polar vapors - state of the art

OFETs based on unfunctionalized organic semiconductors like P3HT and pentacene have been shown to undergo changes of the current voltage characteristics when they are exposed to polar analyte gases [62]. Additional information can be extracted when the organic semiconductor is applied in a field-effect transistor structure. The transistor parameters I_{on}, I_{off} V_{th} and μ can be influenced individually when the

transistor is exposed to a non-inert gas atmosphere providing a fingerprint of the respective gas [95] [17].

Alcohols are an interesting class of analytes which can be found in many applications for environmental or product monitoring. Many organic semiconductors show a repeatable and reversible response to various alcohols which makes them especially interesting for gas sensing applications as many inorganic gas sensors, such as metal oxide sensors, are poisoned by alcohols [17] [97] [57] [20]. Li reported an increase of the conductance for P3HT based chemiresistors during exposure to ethanol vapor [57] . On the other hand, in field-effect transistors, P3HT and various other polymers and small molecules have shown a decrease in current when they were exposed to polar vapors. Liao et al. showed by X-ray measurements that swelling occurs when polythiophenes are exposed to butylamine vapor but that it can not completely account for the observed changes of the electrical characteristics [63]. Additional insights were given by temperature dependent measurements of pentacene transistors during exposure to ethanol vapor. While the mobility followed an Arrhenius like dependency on the temperature, it showed a concentration dependent decrease during exposure to ethanol. It was suggested that ethanol diffuses to the grain boundaries of the crystalline pentacene film where it interacts with the organic semiconductor by modulating the local electronic environment due to its polar nature. This increases the number and depth of traps at the grain boundaries and as a consequence the activation energy for hopping transport [20] [86].

Figure 6.1 shows the forward sweep of the transfer characteristics in the linear regime of a P3HT gas sensor before, during and after exposure to ethanol vapor. The experiment was performed under a constant flow of nitrogen (3 l/h) and ethanol vapor was added during the exposure. The device was fabricated according to the procedure established in section 5. The drain voltage was kept at -15 V while the gate was swept from 20 to -60 V in 2 V steps. Between adjacent measurements all terminals were set to 0 V for 10 seconds to reduce the bias stress of the device and achieve a more stable electrical performance. Channel length and width of the transistor are 20 μm and 1 cm, respectively.

In this section the discussion is limited to the forward sweep only, as this is the part

of the transfer characteristics which is used to extract the transistor parameters I_{on}, I_{off}, V_{th} and μ and has been the focus of all cited publications.
Under exposure to ethanol vapor the device in figure 6.1 a) shows a decrease in current in the on regime (see also magnification in graph b)). Besides the current decrease, the device exhibits also a decrease of the slope of the current voltage characteristics. In the linear regime the charge carrier mobility of a transistor is directly proportional to the slope of the ID-VG curve and therefore also shows a decrease under ethanol exposure (see part c) of the same figure). After withdrawal of the analyte current and slope recover back to their initial values, showing the reversibility of the response.
The graph in d) shows the relative changes of current and mobility during exposure. Around 0 V, the device works like a chemiresistor and the current shows an increase of 5 %. However at 0 V the transistor is still turned off and the absolute value of the current change is only 0,5 pA, which is below the noise level of many of the transistors examined during this thesis. For the mobility change only the on regime of the transistor is shown as the curve is dominated by noise at lower gate voltages. Similar to the observations of Tanese et al. the response of mobility and current increase with the gate voltage. Even though the applied voltages were limited to -60 V in the used setup, it can be seen that the responses are amplified by the gate voltage allowing OFET based sensors to outperform chemiresistors [91].

6.2 Hysteresis response

The response of polymer-based sensors to ethanol has mostly been reported as changes of the on-current or mobility. Both of these parameters are extracted from the forward sweep of the transfer characteristics. In this section it is shown that the hysteresis of the transfer characteristics shows a performance comparable to the other parameters and enriches the information about the analyzed gas by also taking into account the behavior of the reverse sweep.

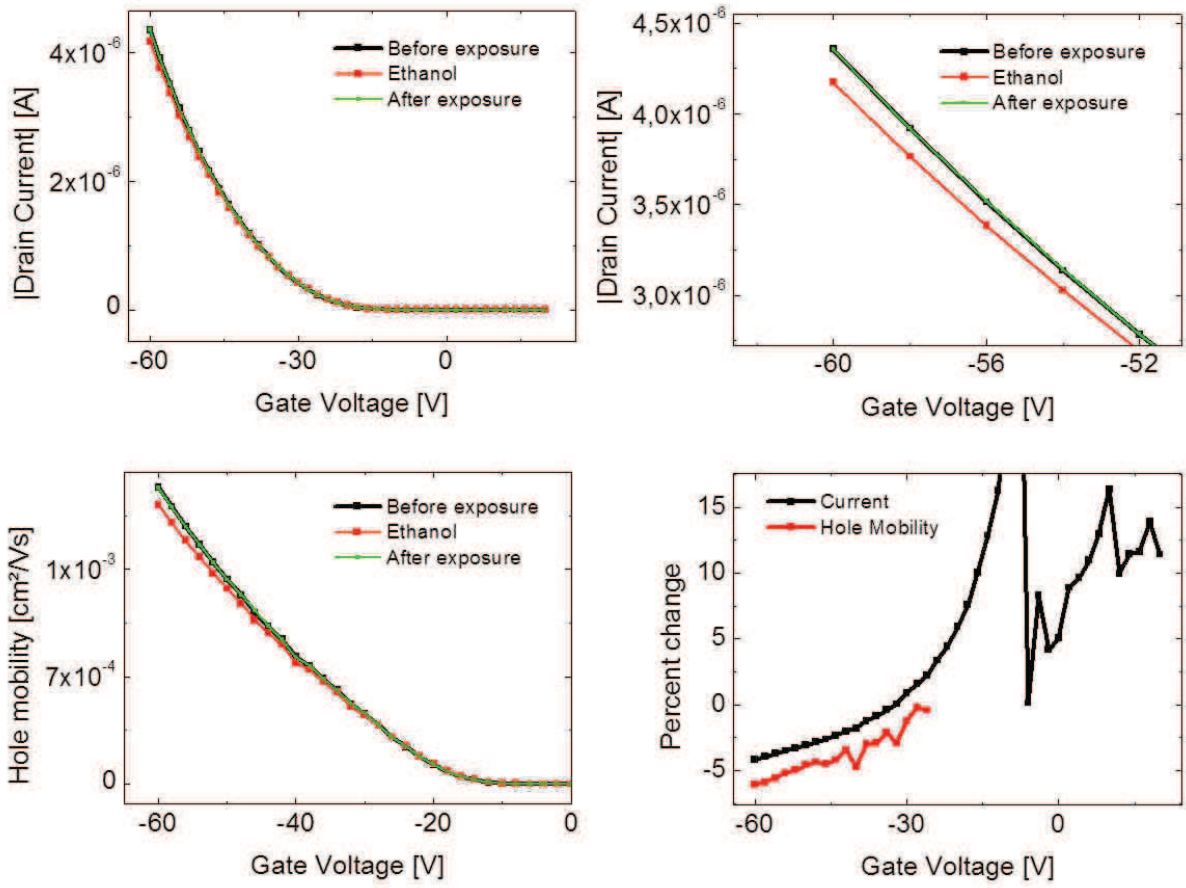

Figure 6.1: Response of P3HT sensor to ethanol exposure. a) ID-VG characteristics of a P3HT transistor measured in the linear regime. Before, during and after exposure to ethanol vapor. b) Magnification of I-V characteristics at high Vg. c) Mobility behavior. d) Relative change of current and mobility during exposure.

6.2.1 Response enhancement by application of complete transfer characteristics cycle

To measure the transfer characteristics of a transistor the drain and source voltage are kept constant while the gate voltage sweeps from the off regime to the on regime of the transistor and back to the off regime. For a hole carrier semiconductor like P3HT the drain is kept at a negative potential while the applied gate voltage increases from 0 V or a positive value to a negative voltage higher than the threshold voltage. This part is called the forward sweep and has been the focus of most of the publications about gas sensors. The previous section discussed this part of the transfer characteristics and compared the behavior of the P3HT transistors used in

this study to the behavior reported in literature. For the reverse sweep the applied gate voltage sweeps from the negative value back to the start voltage. In an ideal transistor the resulting source-drain current is not affected by the direction of the gate voltage sweep and forward and reverse current match with each other. However, in organic transistors exist several mechanisms that can change the reverse current compared to the forward current. A brief description was given by Egginger et al. in [22].

Figure 6.2 shows forward and reverse sweeps of the P3HT sensor discussed in the previous section. For better visibility a magnification of the IV characteristics in the on-regime is shown on the right side of the figure. In pure nitrogen (before and after exposure) and also during the exposure to ethanol forward and reverse current are not similar. Independent of the ambient atmosphere, the current is always higher in the forward sweep and lower in the reverse sweep, as it is indicated by the black arrows in the graph.

One measurement artifact which can be responsible for the presence of hysteresis

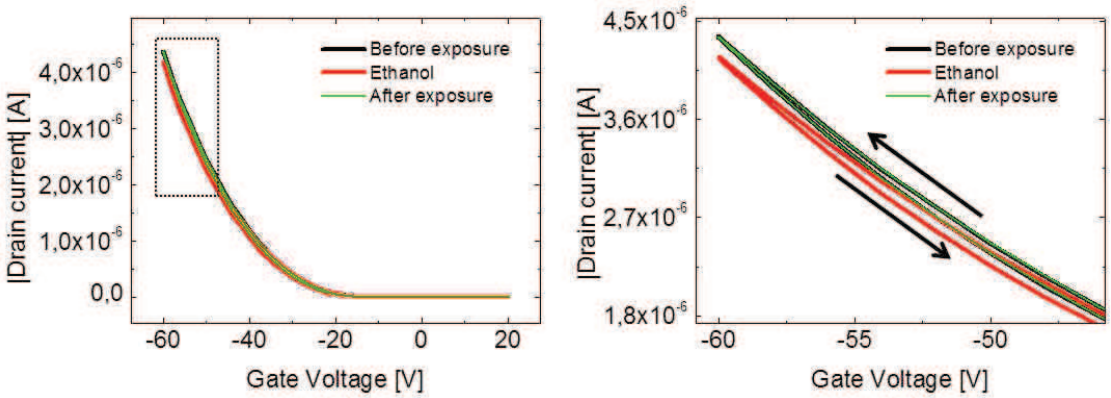

Figure 6.2: Forward and reverse transfer characteristics of a P3HT transistor measured in the saturation regime. Before, during and after exposure to ethanol vapor. Right: magnification of framed area shows hysteresis in the on regime. Hysteresis shows a lower back sweep current in all atmospheres as indicated by the arrows.

is charging and discharging of a capacitor. If a capacitor with the capacitance C is charged through a resistor R the time required for an external voltage change ΔV to change the potential of the capacitor by $\Delta V/e$ is defined by the RC time constant: $\tau = RC$. An OFET works like a capacitor. When a voltage is applied to the gate,

charge carriers are getting injected from the source into the semiconductor to balance the electric field from the gate. If the delay time of a measurement is shorter than 5 times the time constant τ the capacitor has not finished charging before the measurement is performed. As a consequence, the measured drain current would be higher or lower than the drain current which corresponds to the respective gate voltage. The deviation towards higher or lower values is a function of the sweep direction, showing lower currents in the forward sweep and higher currents in the reverse sweep. Egginger suggested to call such a kind of hysteresis higher back sweep current (higher BSC) hysteresis. As it can be seen in figure 6.2 the hysteresis in the devices examined during this thesis show a lower BSC hysteresis, indicating that the observed behavior is not a capacitive artifact.

The left graph in figure 6.3 shows a magnification of the transfer characteristics in the on-regime of the device. As discussed in the previous section the slope of the I-V characteristics decreases under ethanol exposure which indicates a decrease of the mobility. Additionally it can be seen that the difference of the currents in the forward and reverse sweep is higher during ethanol exposure. To better visualize this behavior the graph in the right part in figure 6.3 shows the difference between the current in the forward and in the reverse sweep, calculated for every applied gate voltage step. The response to ethanol vapor is marked by a pronounced increase of the hysteresis and an almost complete recovery after withdrawal of the analyte.

Table 6.1 summarizes the three parameters current, mobility and hysteresis and

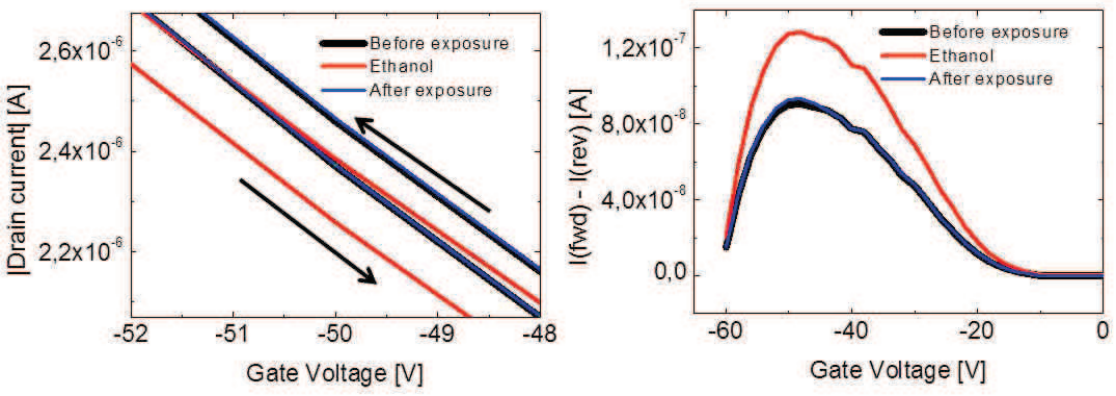

Figure 6.3: Left: Zoom into the transfer characteristics presented in 6.2. Right: Difference between current in forward and reverse sweep plotted over gate voltage.

	Before	Ethanol	After
Current [10^{-6} A]	4,36	4,18	4,36
Current change [%]	-	-4,13	-
Mobility [10^{-3} cm^2/Vs]	1,94	1,82	1,93
Mobility change [%]	-	-7,7	-
Hysteresis [10^{-6} W]	1,24	1,79	1,26
Hysteresis change [%]	-	43,7	-

Table 6.1: Absolute values and relative changes of current, mobility and hysteresis before, during and after exposure to ethanol.

their respective percentual changes during exposure to ethanol vapor. For current and mobility the values at the maximum applied gate voltage in the on-regime (-60 V) were used. To quantify the response of the hysteresis and make it comparable to the reported parameters current and mobility, the areas under the curves of the right graph in figure 6.3 are calculated. It has to be pointed out that every set of the three parameters under the respective conditions was extracted from the same measurement of the transfer characteristics. As it can be seen the hysteresis shows a more than 6 times higher response to ethanol than the mobility and almost 10 times higher than the current.

To examine the applicability of the hysteresis as a parameter for gas detection, repeatability and concentration dependence of the hysteresis response to ethanol vapor was tested. A P3HT based sensor with a 5 μm channel was exposed to different ethanol concentrations ranging from approximately 500 ppm to 2800 ppm. The drain voltage was fixed at -15 V while the gate performed a sweep from 20 to -60 V and back in 5 V steps. Between two measurements the device was grounded for 10 sec to reduce bias stress. The period of the measurements, including the recovery time, was 24 sec.

Figure 6.4 compares the behavior of mobility, hysteresis and current. Upon exposure to ethanol vapor all three parameters show a pronounced and immediate change. After removal of ethanol with pure nitrogen all three parameters gradually recover to their previous values. In terms of response speed and repeatability the hysteresis

	ΔI	$\Delta I/Noise$	$\Delta\mu$	$\Delta\mu/Noise$	$\Delta Hyst$	$\Delta Hyst/Noise$
Noise [%]	0,017		0,10		0,48	
500 ppm	0,84	47	1	9	9,3	19
1000 ppm	1,26	72	2	19	16,5	34
2000 ppm	2,06	117	3,2	32	24,1	50
2800 ppm	2,59	147	4,1	40	31,1	64

Table 6.2: Percentual changes of current, mobility and hysteresis during exposure to different ethanol concentrations. The second columns compare the response to the average noise in N_2 which is reported in the second row for each parameter.

shows a behavior which is comparable to the two reported parameters current and mobility. Table 6.2 compares the responses of all three parameters 8 minutes after the exposure to ethanol vapor has started. The trend of the hysteresis to show a stronger response than current or mobility is observed again (compare to table 6.1). One of the key features of a sensor is the sensitivity which determines the strength of the response when an analyte is detected. To test if the higher response of the hysteresis indicates a higher sensitivity, table 6.2 compares the responses to the average noise for every parameter. While this representative example shows the lowest response for the current it is also the parameter which suffers least from noise and therefore shows the highest sensitivity. The hysteresis shows a more than 10 times higher response but suffers also from the strongest noise. As a result the signal to noise ratio of the hysteresis is inferior to the current but still significantly better compared to the mobility.

Even though complex pattern recognition techniques are able to compensate a non-linear dependence of the sensor response on the analyte concentration, a linear response is still more favorable as it facilitates calibration and quantification of the response. Figure 6.5 shows the results obtained during two consecutive exposures to ethanol concentrations between 500 and 2800 ppm. The error bars indicate the divergence of the two responses at the respective concentration. Das [17] and Mori [67] reported a linear response of the OFET current to ethanol vapor for methoxy-substituted poly(triaryl amine) and pentacene, respectively. Figure 6.5 shows also a

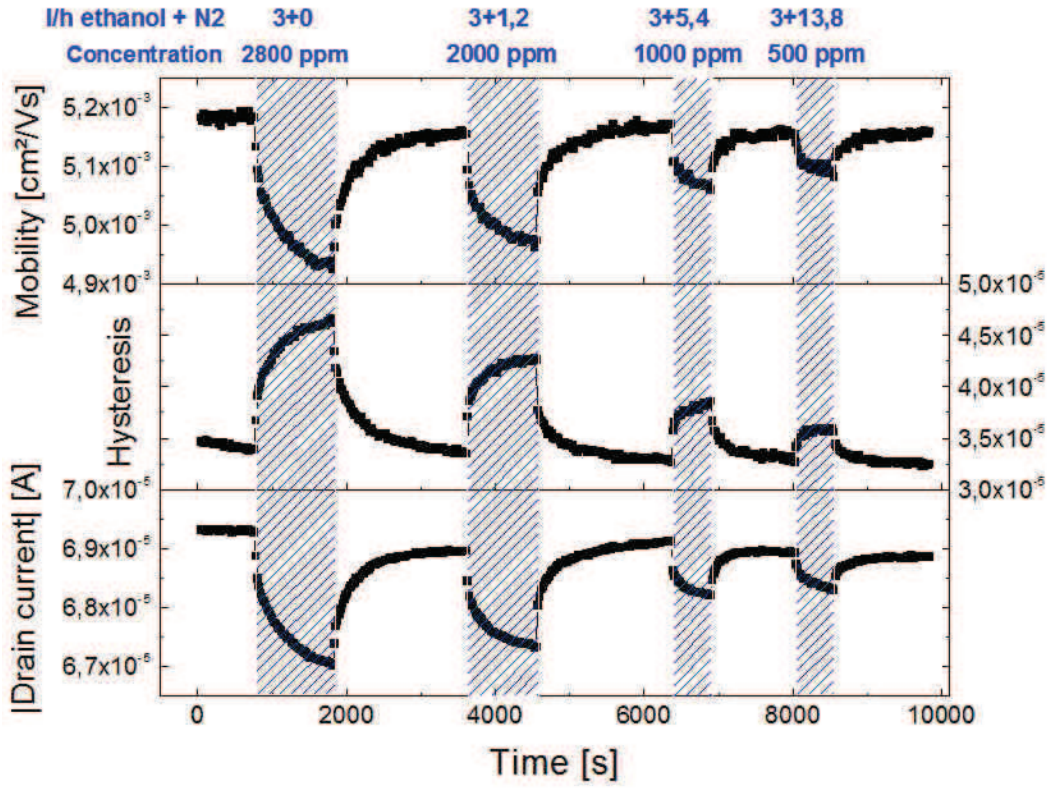

Figure 6.4: Behavior of mobility, hysteresis and drain current during exposure to ethanol vapor (exposure is indicated by blue background). Between exposures device was purged with pure nitrogen. Exposure to 2800 and 2000 ppm lasted 15 min and only 8 min for 1000 and 500 ppm. Blue description on top describes the flow rate used through the chamber with ethanol (first value, always stable at 3 l/h) and the flow rate of pure N_2 added to change the concentration. Below the approximate concentration of ethanol in nitrogen is shown.

linear dependence of the current and mobility response on the ethanol concentration. Additionally, also the hysteresis response shows a linear dependence on the concentration. Similar results were also obtained for methanol and isopropanol vapors.

In Figure 6.4 the time to reach a stable response changes as a function of the analyte concentration. This can be either due to a decreased diffusion of ethanol into the semiconductor at high ethanol concentrations or due to a delayed increase of the ethanol concentration in the measurement chamber. A delay of the concentration increase would be more pronounced at low flow rates, as they are used in the depicted measurement to enable high concentrations of ethanol vapor. The re-

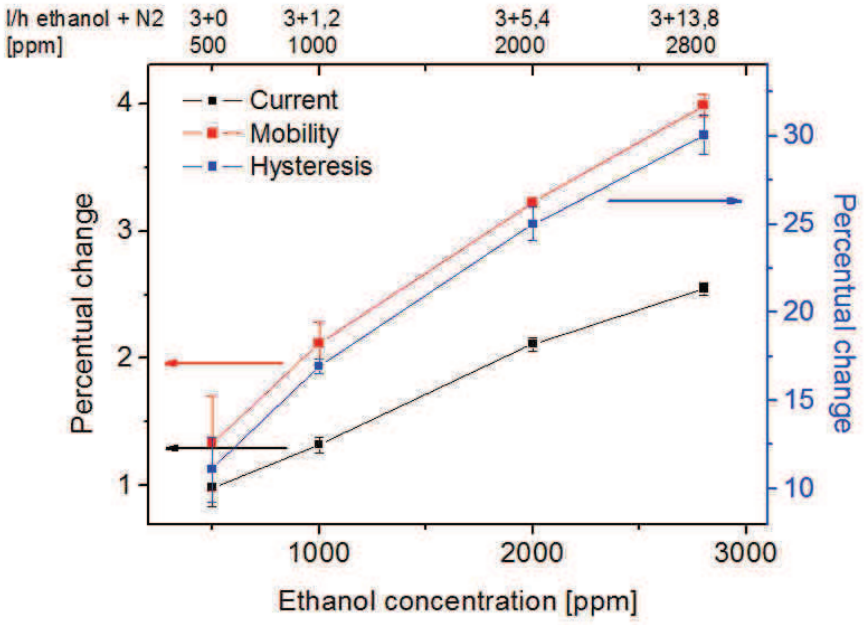

Figure 6.5: Comparison of current, mobility and hysteresis response to different ethanol concentrations.

sponse saturated faster in measurements where high concentrations and high flow rates were used, indicating the concentration increase in the chamber to be the underlying reason. However, as the object of this section is the comparison of the hysteresis response to the mobility and current response a possible inaccuracy of the concentration would affect all parameters in the same way.

6.2.2 Analyte discrimination by hysteresis application

One of the most important properties of a sensor is its ability to selectively detect a given analyte without interference from other components. One step towards a higher selectivity is the utilization of a transistor structure instead of a chemiresistor. By measuring several parameters simultaneously OFET-based sensors have been shown to be able to discriminate analytes [95] [18]. However, the ability to discriminate is often limited only to a few analytes. In order to evaluate if the hysteresis enriches the information extracted about the analyte-semiconductor interaction and increases the recognition ability of the sensor, P3HT based sensors were alternately exposed to different concentrations of ethanol and acetone. Most

publications suggest that the response of unfunctionalized organic semiconductors is driven by an increase of the energetic disorder implemented by the polar moment of the analyte. The polar moment of acetone (2,91 Debye) is almost two times higher than for ethanol (1,69 Debye). Additionally both molecules have a comparable size and atomic composition which should reduce variations of the diffusion into the sensing layer. Furthermore the high vapor pressure of acetone facilitates the generation of gas samples of various concentrations.

Figure 6.6 shows the transfer characteristics of a 5 μm channel device. For a better visibility only the forward sweep is plotted. The device was measured in the same way as the transistor in the previous section: Vd was fixed at -15 V while the gate voltage was swept from 20 to -60 and back to 20 V in 5 V steps. To compensate for the drift of the threshold voltage that occurred in between the two exposures the I-V characteristics of the second set of data (N_2 and acetone exposure) was shifted by 0,2 V. In this way the I-V curves under nitrogen matched to each other for both measurements as it can be seen in the magnification of the transfer characteristics.

In the chosen example the forward I-V characteristics show also a comparable re-

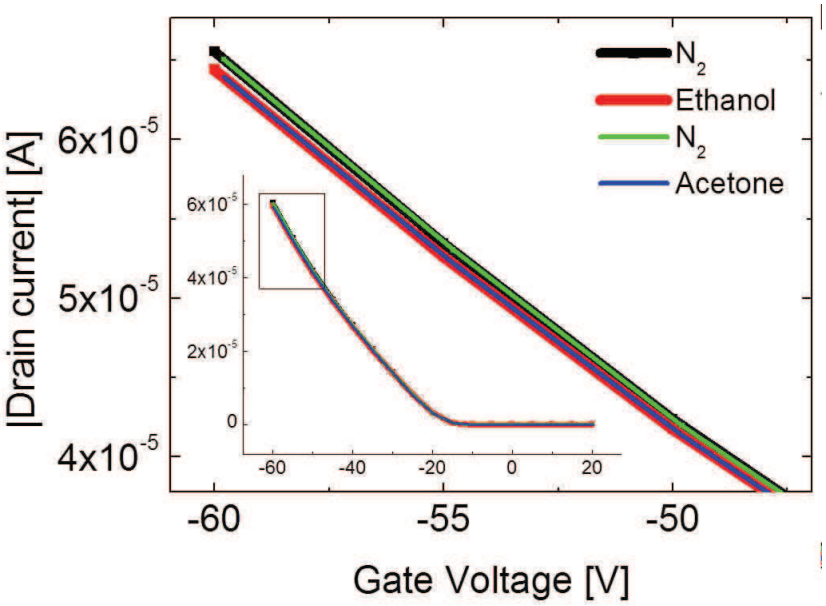

Figure 6.6: Zoom into transfer characteristics before and during exposure to ethanol and acetone. Inset shows complete transfer characteristics. Frame indicates magnified area.

sponse to acetone and ethanol vapor exposure. As it can be seen in figure 6.7 also

the mobilities shows a comparable behavior, independent of the analyte. As the matching I-V and mobility curves also lead to a similar threshold voltage change it can be said that, for the presented system, no determination of the present analyte is possible with the parameters typically used in literature. Publications showing a discrimination of ethanol and acetone vapor typically employ sensor arrays consisting of various organic semiconductors [17], [111].

The right side of figure 6.7 shows the hysteresis recorded in the same measurements. While only minor differences can be seen for the two measurements performed in nitrogen, a significant difference is visible in presence of the analytes. Ethanol vapor causes an increase of the hysteresis by 16 % while acetone vapor increases the hysteresis by only 7 %. As a consequence this shows that the simultaneous utilization of the on-current or mobility response with the hysteresis response allows to discriminate the two analytes ethanol and acetone.

Figure 6.8 compares the response patterns of mobility versus on-current to hys-

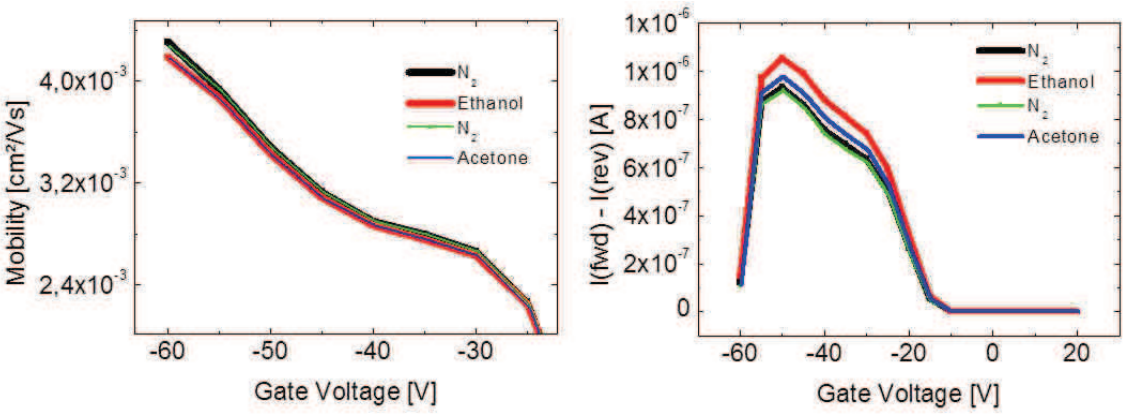

Figure 6.7: Mobility (left) and hysteresis (right) over gate voltage before and during exposure to ethanol and acetone.

teresis versus on-current for acetone and ethanol vapors at several concentrations. Ethanol was varied between 1000 and 3000 ppm and acetone between 1000 and 7000 ppm. To ensure the variations of the responses are not related to drift only, the analyte was repeatedly changed from ethanol to acetone and vice-versa. The left graph shows that the mobility response varies as a function of the current response for both analytes with almost the same slope. Only at higher responses a deviation can be seen, making a discriminative detection of ethanol and acetone vapor difficult or

even impossible. The right side shows the hysteresis response as a function of the current response. As a function of the used analyte two distinctive slopes of the responses can be distinguished. For comparable current responses ethanol shows a two times higher hysteresis response than acetone allowing the identification of the measured analyte over the whole measured concentration range.

Considering only the dipole moment of both molecules the weaker response of

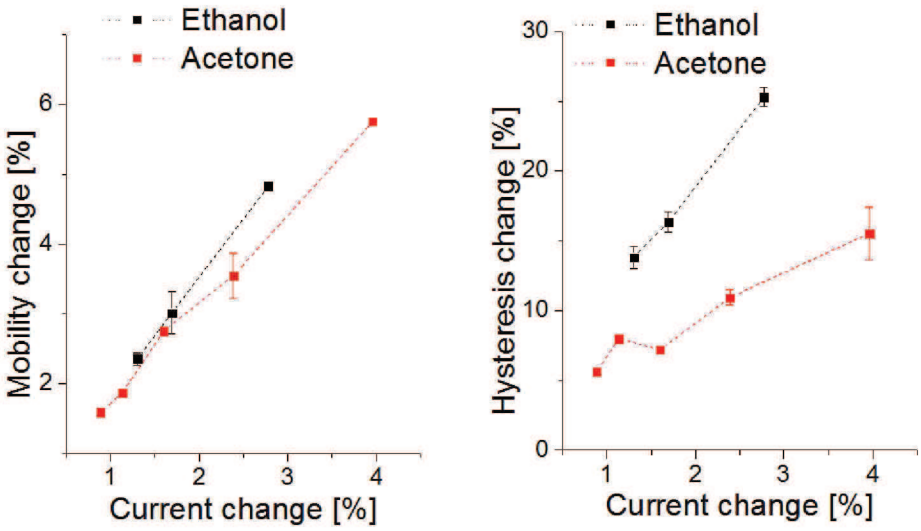

Figure 6.8: Left: Response of mobility as a function of on-current response. Right: Hysteresis response versus on-current response. Each point indicates a different concentration.

acetone seems unexpected. However, Li et al. also reported the current response of P3HT to acetone and ethanol and found similar results [57]. Additional mechanisms influencing adsorption and absorption of the vapors could give rise to this behavior.

6.2.3 Understanding hysteresis origin by measurements of the transient current

While there are a considerable number of publications studying the origin of hysteresis in organic field effect transistors, only the paper of Tang et al. mentions the influence of gas exposure on the hysteresis of the transfer characteristics [92]. During exposure of a dendrimer-based OFET to para-nitrotoluene, a chemically similar compound to the explosive 2,4,6-trinitrotoluene (TNT), Tang observed an increase of the hysteresis which was not completely reversible after withdrawal of

the analyte. Long-living trap states due to bias stress were suggested as origin of the irreversibility. For pentacene transistors Gu [29] and Kim [45] reported an increase of the hysteresis due to moisture-induced trapping.

For the measurements performed in the previous sections residual water inside the analyte source is rather unlikely to be the reason for the observed hysteresis increase as freshly opened ethanol with a pureness higher than 99,9 % showed similar responses as the normally used ethanol which was stored in the chemistry cabinet. Examining pentacene transistors on a SiO_2 dielectric, Gu reported electron trapping as origin of the observed hysteresis. During off bias initially neutral acceptor-like traps are occupied. Some of these traps have a sufficiently long lifetime to induce extra holes in the channel while the device is biased from the off to the on state resulting in an increase of the measured drain current during the forward sweep. At high negative gate voltages many of the trapped electrons are released and the number of extra holes needed to compensate the trapped electrons decreases thereby reducing the drain current in the on to off sweep.

In order to understand if electron traps contribute to the hysteresis increase observed in polar vapors the gate sweep range was limited to negative biases and compared to responses observed for a sweep range from 20 to -40 V. A 10 μm channel P3HT sensor was first measured only at negative gate biases between 0 and -40 V in 1 V steps before the sweep range was changed to 20 to -40 V. To cancel out possible contributions from the drift, the device was measured afterwards again in the range 0 to -40 V. To reduce bias stress the device was left for 1 minute grounded between two measurements resulting in a total period of 85 and 102 seconds for the 0 to -40 and the 20 to -40 sweep, respectively. Figure 6.9 shows the behavior of the hystersis and on-current at -40 V during repeated exposures to similar ethanol concentrations. While the baseline of the current is not affected by the change of the gate voltage range, the hysteresis shows a small increase, probably due to enhanced detrapping of holes during application of a positive bias. The responses of hystersis and current are almost not altered upon exposure. Table 6.3 shows that the differences are within the error margins of the parameters. This results indicate that electron traps do not significantly contribute to the response of the hysteresis to polar vapors.

Sweep range [V]	Current response [%]	Hysteresis response [%]
0 to -40	2,4 ± 0,2	15,6 ± 0,9
+20 to -40	2,4 ± 0,1	14,6 ± 0,4

Table 6.3: Responses of on-current and hysteresis to 800 ppm ethanol at different gate sweep ranges.

Ucurum et al. investigated the hysteresis of pentacene field effect transistors with

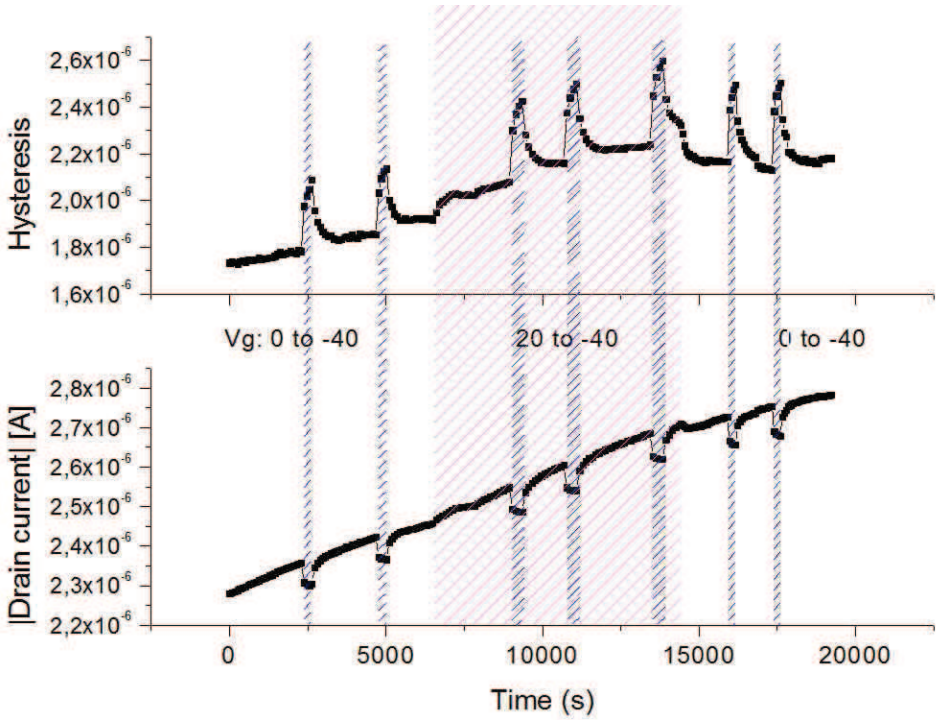

Figure 6.9: Influence of gate sweep range on behavior of on-current and hysteresis during exposures to 800 ppm ethanol. Gate voltage range are given in the graph. Magenta colored background highlights extension of the sweep range to positive bias. Blue background indicates exposure.

SiO_2 as gate dielectric in a nitrogen atmosphere [100]. Results obtained from transient measurements provide evidence for hole trapping in the bulk as origin of the observed lower back sweep current hysteresis. Figure 6.10 shows the explanation given for the hysteresis in the same publication. At the start of the off to on sweep the hole traps in the semiconductor are still empty (t_0). When the gate voltage increases charge carriers are getting injected into the channel which causes a huge current increase first (t_1). The free charge carriers start to fill the traps in the chan-

nel and therefore reduce the available number of free charge carriers and the drain current. This continues at every step of the forward sweep until a maximum number of traps are filled at the highest applied gate voltage (t_4). Charge carrier traps can have sufficiently long lifetimes to remain filled during the on to off sweep. Therefore the electric field of the gate is screened by more immobile charge carriers in the reverse sweep (t_6) compared to the forward sweep and the drain current becomes lower in the reverse sweep.

To probe trapping in OFETs Ucurum employed measurements of the transient cur-

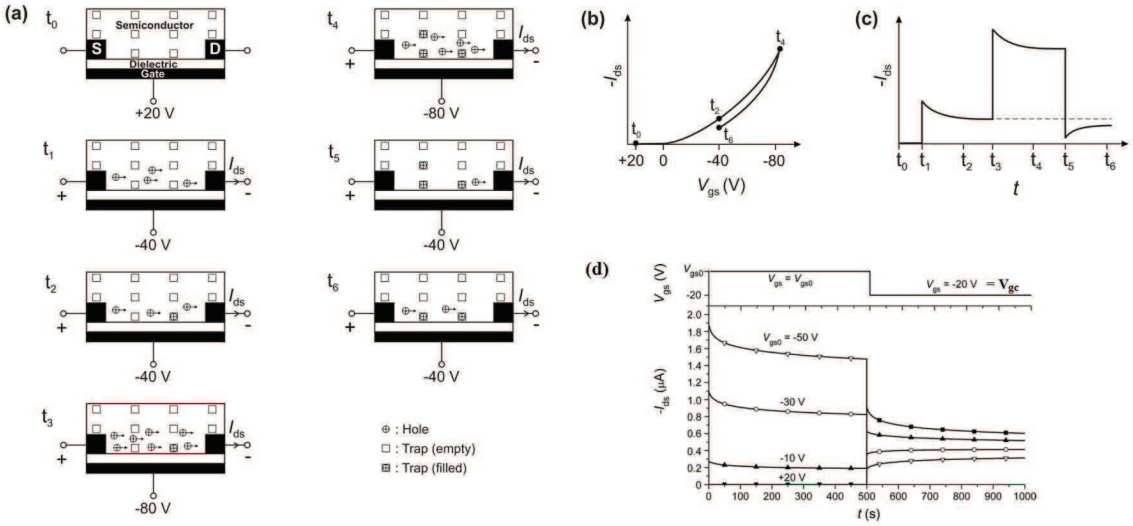

Figure 6.10: Model suggested by Ucurum et al. to explain the influence of hole traps on the hysteresis in field effect transistors (extracted from [100]). a) Schematic cross-sectional view of bottom gate contact FET showing charge carrier and hole traps distribution in the active layer during the gate voltage sweep. b) Resulting behavior of the transfer characteristics. c) Transient current behavior of the FET during gate-voltage sweeps. d) Gate voltage applied for the transient measurements (top) and measured currents (bottom).

rent. During this measurement a constant voltage is applied to the drain. The gate is kept at an constant initial voltage for a given time before it is abruptly switched to a different voltage V_{gc} in the on regime of the transistor (see figure 6.10 d)). While V_{gc} is the same for all measurements the initially applied voltage is varied to more positive or negative values. The drain current measured at V_{gc} shows an increase or decrease over time, as a function of the initially applied gate voltage. If the device was first stressed at more negative values (deeper in the on regime) the number of

filled traps is above the equilibrium concentration for V_{gc}, resulting in an increase of the drain current over time due to detrapping of holes. If the device was first stressed at a more positive gate voltage the current is high in the beginning but decays with time due to trapping.

Even though the suggested method gives interesting insight into the trapping

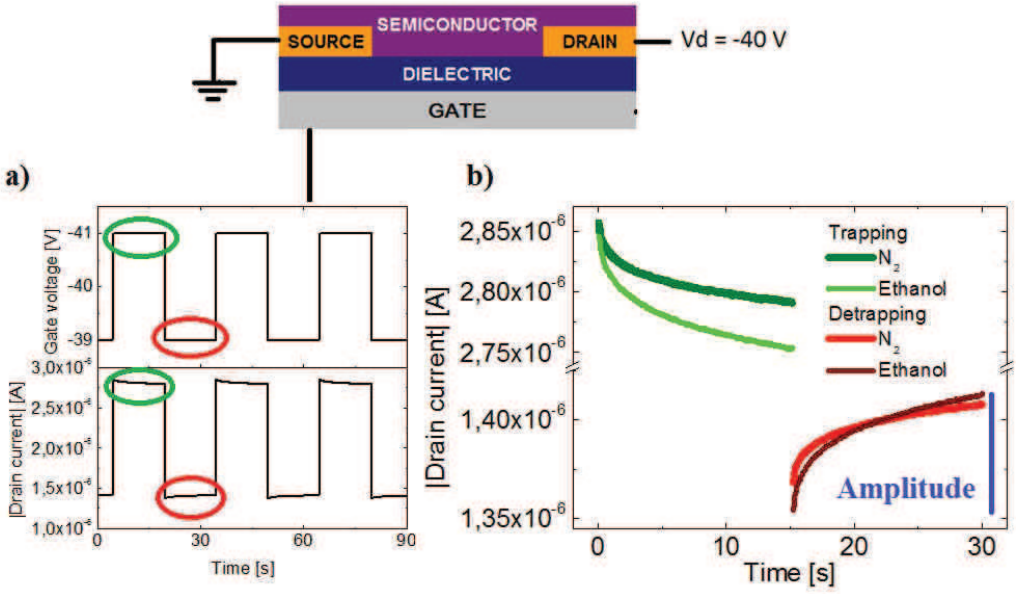

Figure 6.11: Side view of transistor structure and applied voltages during measurement of the transient current applied in this work. The measurement interval of the current is 50 ms. a) depicts the applied gate voltage and the resulting transient drain current. b) magnifies the transient responses in nitrogen and at 2500 ppm ethanol. The red circles mark low gate voltages where detrapping occurs, the green one marks the trapping during higher gate voltages. The amplitude of the trapping and detrapping is indicated as example for the detrapping in ethanol.

dynamics of a field effect transistor it demands very long time spans for a single measurement. Additionally a comparison of succeeding measurements can be difficult if no equilibrium state is reached, as an ongoing measurement can be influenced by sustained effects of a former measurement [101]. As it was shown in chapter 5.2.2 the used OFET devices can need up to several hours to reach an equilibrium state which is very important for sensor devices where changes of only a few percent have to be detected. In order to probe hole trapping as origin of the hysteresis change

found in P3HT based gas sensors, the transient current was measured following a slightly different procedure. The drain voltage was fixed at a potential of -40 V to the source, while the gate voltage was alternated with a period of 30 seconds between two values in the on regime of the transistor. This method allows to accumulate charge carriers in the channel at higher on voltages (will be called trapping regime onwards) which populate the hole traps (corresponding to t_3 and t_4 in 6.10 a)). If the gate voltage decreases to a lower on voltage the number of occupied traps is higher than the equilibrium and trapped charge carriers get released leading to an increase of the drain current (t_5 and t_2) (detrapping regime). This method cycles the device permanently between trapping and detrapping of charge carriers and allows to reach a dynamic equilibrium between these two processes. Figure 6.11 shows a side view of the used transistor structure and indicates the applied voltages. In a) the alternating gate voltage is shown on top and the resulting transient current in nitrogen at the bottom. As it can be seen in the magnification of the transient current in b), the current decreases in the trapping regime at high gate voltages (marked green in a)) due to trapping and increases in the detrapping regime at low gate voltages due to detrapping (marked red). b) Compares the transient current in nitrogen with the transient current measured in ethanol vapor. The transient currents decrease and increase over a larger current range, when the device is exposed to ethanol. This increase of the amplitude indicates enhanced trapping and detrapping in ethanol which is expected to be the origin of the observed hysteresis increase.
This observation is also in agreement with Duarte et al. who showed an increase of the activation energy for hopping in the presence of ethanol and suggested that the carrier trapping energies are altered upon vapor exposure [20].

6.2.4 Understanding the discriminative behavior of the hysteresis

The previous sections introduced the hysteresis of the transfer characteristics as a parameter for the gas detection with non functionalized OFET sensors. A linear dependency of the response on the ethanol concentration has been shown, as well

as a sensitivity intermediate to the generally used on-current and the charge carrier mobility. Transient measurements indicated enhanced trapping during the exposure as origin of the observed effect. For the model system ethanol and acetone vapor the additional information gained by using the hysteresis in combination with the on current, allowed to distinguish these two components, which were shown to be almost impossible to distinguish with the conventional transistor parameters.

In order to understand the selective behavior of the hysteresis, the transient current was measured during repeated exposures to ethanol and acetone vapor. While the amplitudes of the transient current increased in the presence of both vapors, no analyte specific difference was found for the amplitudes of the transient currents in the trapping and detrapping regime. However, the time resolution of the measurement is limited to 50 ms. Though this is fast enough to measure long-lifetime traps it is too slow for fast traps. An indication for the existence of such fast traps in the investigated P3HT devices is the difference of the transient current amplitudes in the trapping and detrapping regime. The amplitude in the trapping regime in figure 6.11 b) is about 1,5 times higher than the amplitude in the detrapping regime. As the graph in a) shows, the device has almost reached equilibrium and does not show a constant decrease of the current, as it would be expected if more charge carriers are getting trapped than released. Detrapping on a time scale below the resolution of the measurement can help to explain this behavior.

To follow the population and depopulation of the fast charge carrier traps, figure 6.12 b) and c) plot the first values of the transient current after the gate voltage has changed (start) and the last current values before the next gate voltage change (end). Graph b) shows the start and end values in the trapping regime. In nitrogen the amplitude in the detrapping regime is only 30 % of the amplitude in the trapping regime. Even though the device is not completely settled and still shows a pronounced drift to lower currents, the differences of the start or end values between adjacent measurements is much lower than 70 % of the amplitude in the trapping regime, indicating the existence of traps which release trapped charge carriers faster than the resolution of the measurement.

The start values during ethanol (green) and acetone exposure (blue) show a general

difference in the trapping regime. Upon exposure to ethanol the start values show an increase of the current, compared to the results obtained in nitrogen. However, enhanced trapping decreases the current and leads to lower end values. On the other hand, exposures to acetone decrease the start current. As a consequence the end current is lower compared to ethanol exposures for a comparable amplitude of the transient current. In the detrapping regime, depicted in c), exposures to both analytes show a comparable behavior, indicating that most of the additional traps, filled in the trapping regime during acetone exposure, were released faster than the resolution of the measurement.

To investigate if the difference of the hysteresis response in the transfer character-

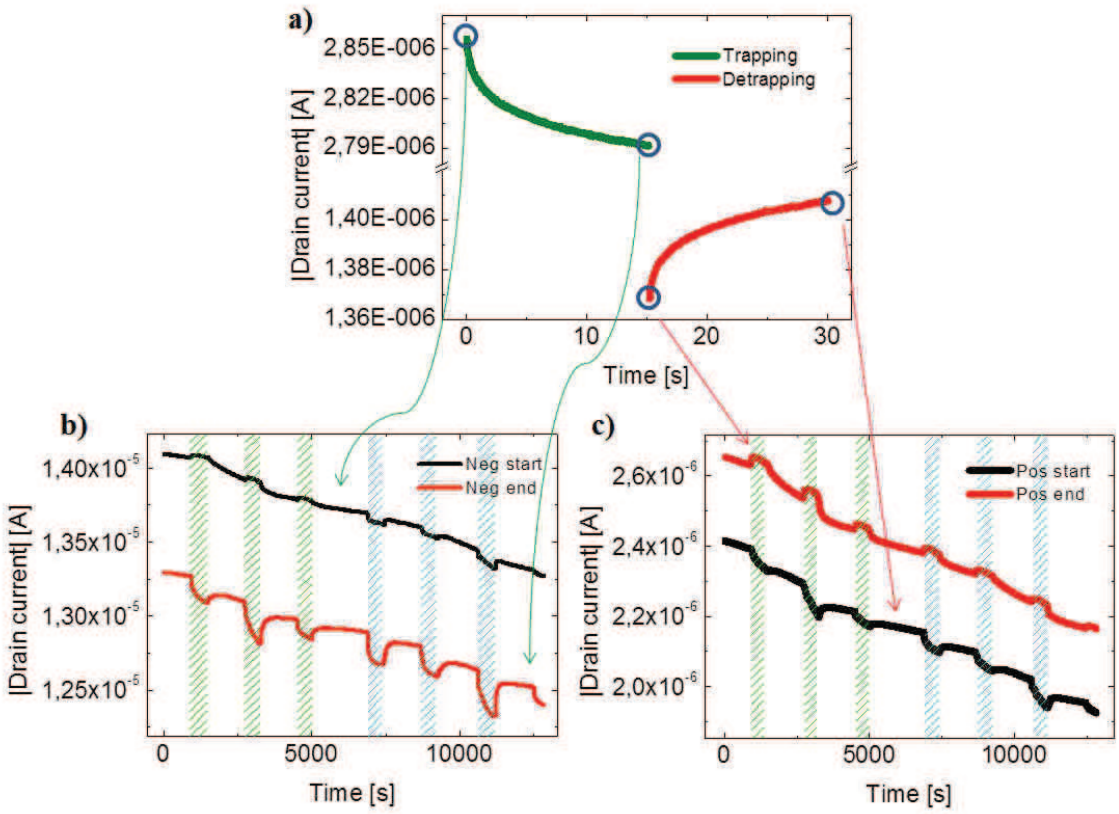

Figure 6.12: Transient current measurements during exposure to ethanol and acetone vapor. Behavior of the start and the end values of the transient current during the trapping (b)) and detrapping regime (c)). Green bars indicate exposure to ethanol, blue bars indicate acetone.

istics can be explained with different trapping and detrapping kinetics, figure 6.13 shows the percentual change of the drain current during exposure to ethanol and

acetone vapor in the forward and reverse current. The examples are those that have been shown in the previous section and were chosen so as to show comparable current changes in the forward sweep. In this way it can be seen that during acetone exposure the device shows smaller current changes in the reverse sweep compared to the changes during ethanol exposure. Fast filling and releasing traps are getting filled quickly during the forward sweep causing a decrease of the drain current and an increase of the drain current response. During the reverse sweep the traps which allow a fast release of the trapped charge carriers empty quickly. As a consequence more free charge carriers are present in the channel causing a higher drain current compared to the reverse sweep in ethanol vapor.

The assumption of a higher ratio of fast filling and emptying traps during exposure to acetone vapor consistently explains the peculiarities observed in the transfer characteristics and the transient current measurements. The different trapping kinetics in acetone and ethanol can not be distinguished by following only the forward sweep of the transfer characteristics. Instead, employing the relation of the reverse sweep to the forward sweep allows to distinguish the different trapping kinetics and improves the understanding of the ongoing mechanisms and the selectivity of the response. This section has shown that the area enclosed by the hysteresis of the transfer characteristics is a suitable parameter to follow the changes of the reverse current in respect to the forward current.

Even though a parameter extracted like the threshold voltage in the reverse sweep could also indicate the differences observed by the hysteresis, several publications show a rather noisy behavior of V_{th} [18] [38] [17]. For the exposures shown in figure 6.6 the voltage difference for similar currents in the reverse sweep in ethanol and acetone is below 0.1 V. As the slopes are virtually parallel, 0.1 V would correspond to the difference of V_{th}. The threshold voltage of the device depicted in 6.6 is approximately -25 V, resulting in a difference of V_{th} in acetone and ethanol of 0.4 %. For the same measurements the hysteresis shows a difference of 9.1 % between the response to ethanol and acetone vapor.

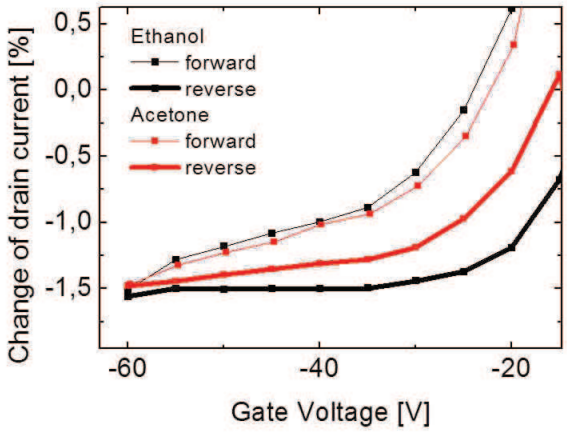

Figure 6.13: Relative variation of the drain current in the forward and reverse sweep during ethanol and acetone exposure. The examples shown here are the same that were used in 6.2.2

6.3 Transient response as parameter for gas detection

As it was shown in chapter 5.2.2 organic semiconductors suffer from a long term drift. Due to trapping the number of free charge carriers decreases over time and reduces also the response to analytes. While usage of the relative variation of current, hysteresis or mobility can be employed to reduce the impact of the drift and stabilize the responses of the transfer characteristics, transient measurement offer a more advanced possibility to improve the sensor robustness against long term drift.
The current of an organic field effect transistor varies as a function of the trapping and detrapping of free charge carriers if equilibrium is not reached. As it was shown in 5.2.2 the current can drift over several hours before eventually equilibrium is reached. The transient measurement method, introduced in the previous section, allows to normalize the amplitude of the trapping and detrapping by the measured current to reduce the long-term drift.

6.3.1 Normalization of the Amplitude

Figure 6.14 b) shows the behavior of the transient current, measured at the end of the trapping regime ("Neg end" in figure 6.12b), plotted over time and a) shows the

corresponding amplitude. The drain of the device was set to a potential of -50 V to the source while the gate was alternately biased at -47 and -53 V for 15 seconds each. Responses to ethanol vapor are shown to allow comparison of the response to 1400 ppm ethanol to the scale of the drift. Prior to the measurement the device was left grounded in the gas-test bench for more than 50 hours.

In the first 3000 seconds the end-current shows a strong decrease due to enhanced trapping, as it is indicated by the large amplitude in a). After approximately 4000 seconds the end-current stabilizes even though it still shows a small drift over time. At this point in time, also the amplitude of the trapping has almost reached equilibrium.

Graph a) in figure 6.15 plots the behavior of the amplitude of the transient current ($start - end$) divided by the end current, for the trapping regime. The resulting (rescaled) amplitude is a measure for the fraction of charge carriers trapped during each measurement compared to the absolute current:

$$Rescaled\ amplitude\ detrapping = \frac{Pos\ start - Pos\ end}{Pos\ end}$$

$$Rescaled\ amplitude\ trapping = \frac{Neg\ start - Neg\ end}{Neg\ end}$$

For the denotations please refer to graph 6.12.

At the onset of the measurement, when no traps are filled, the ratio of charge carriers which are getting trapped to free charge carriers is high, as all traps are empty. When most of the long lifetime traps are filled, the device settles to a more stable end current and also the fraction of trapped charges reduces to a value where it stays almost constant. Graph b) in the same figure shows the rescaled amplitude of the detrapping regime, which was extracted similar to the rescaled amplitude of the trapping regime. In nitrogen the ratio of released charge carriers to free charge carriers stays almost constant during the entire measurement. The increases of the rescaled amplitude in the graph are due to ethanol exposure.

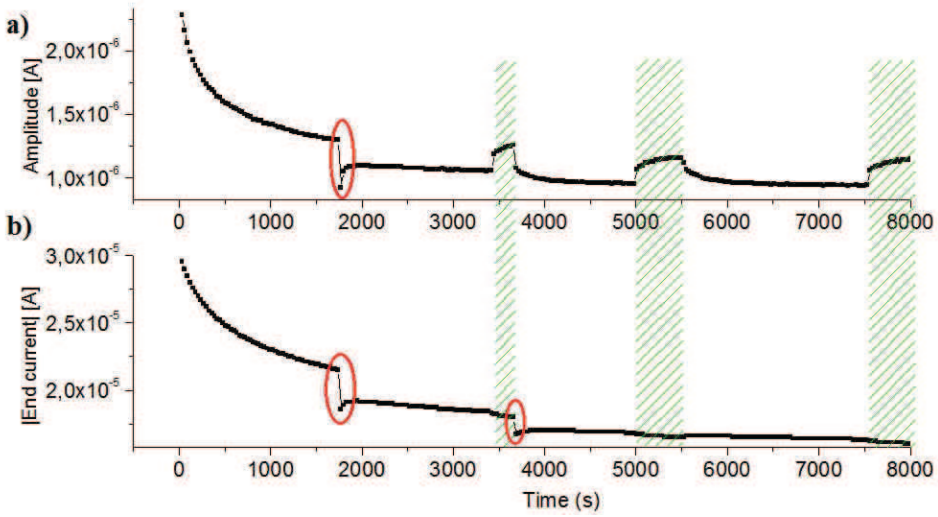

Figure 6.14: Transient measurements of 10 μm channel P3HT transistor during exposure to ethanol (indicated by green background). Red encircled artifacts are due to auto calibration of the measurement equipment which was switched off after second artifact. a) Trapping amplitude of the negative bias regime. b) Corresponding end current.

6.3.2 Performance of transient method versus transfer characteristics

Mori et al. investigated the baseline stability of organic field effect transistors for gas sensor applications [68]. On bare SiO_2 the drift of the threshold voltage influences

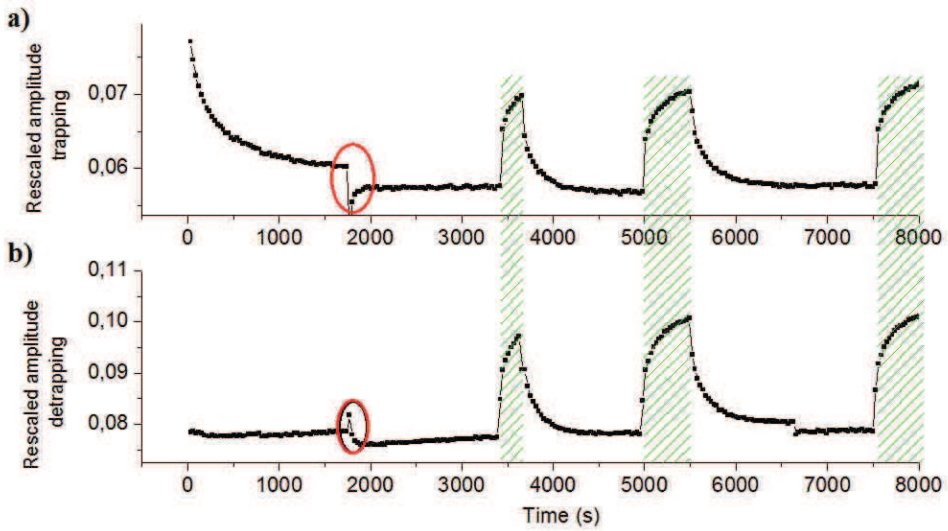

Figure 6.15: a) Rescaled amplitude of the measurement shown in figure 6.14. b) Rescaled amplitude of same measurement during detrapping at lower gate voltages

the on current of the device and causes a continuous decrease. The mobility on the other hand was found to remain constant over time and was suggested to be used as a more stable baseline. As it can be seen in figure 6.16 P3HT transistors made during this thesis, confirmed these observations. While the drain current shows a drift over several hours, the mobility stabilizes after an initial instability within a few minutes. The hysteresis is also susceptible to drift as it is based on the current behavior and magnifies ongoing changes. The sample measured for figure 6.16 is the same that

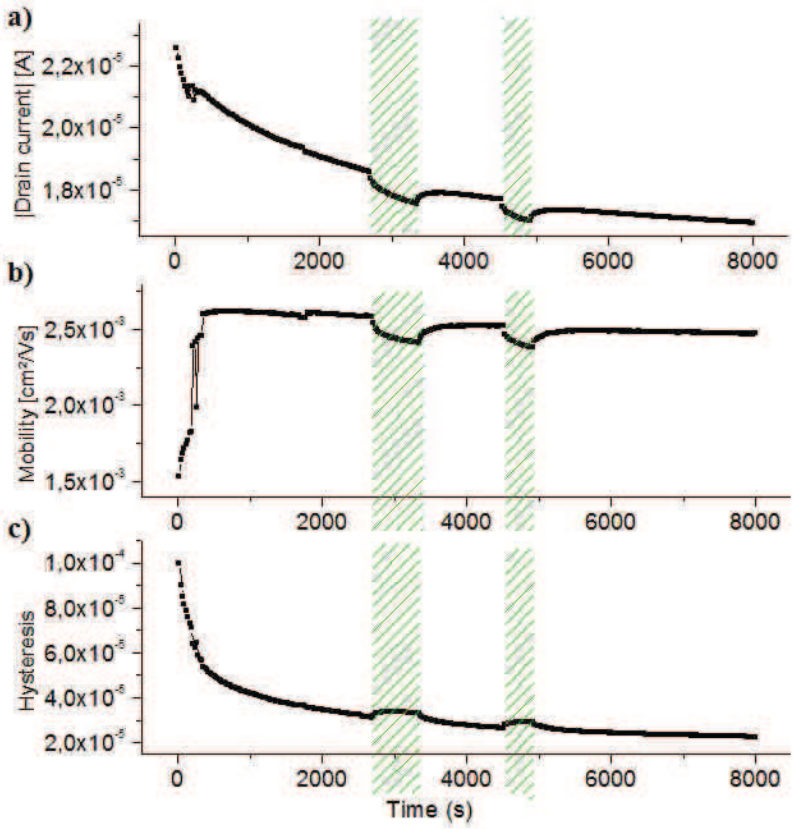

Figure 6.16: Behavior of a) drain current, b) mobility and c) hysteresis of the transfer characteristics of the device shown also in the previous section 6.3. Green bars indicate exposure to 800 ppm ethanol to compare drift to response magnitude.

was used for the transient measurements discussed in the previous section 6.3. In order to compare the sensitivity to ethanol vapor the device was exposed to several ethanol concentrations while the transfer characteristics were measured. After the device was left grounded for 50 hours to ensure no sustained effects influence the measurement, the transient current was measured while the device was exposed to the same concentrations again. For the transfer characteristics the drain voltage was

set to -15 V and the gate voltage was swept forward and backwards from 20 to -60 V in -5 V steps. For the transient measurement the conditions were given in 6.3.1. Figure 6.17 compares the obtained responses. The device was exposed twice to every ethanol concentration and the deviation of the responses are given as error bars in the graphs. The rescaled trapping and detrapping amplitude show a less linear dependence on the concentration than the other parameters. The measurement also reveals that the deviations of the responses to similar concentrations are slightly higher for the transient measurements. However, the measurement of the transient current has been introduced only lately during this work and the time spend for the optimization was very limited. Also the usage of three different instruments to bias and measure the devices during the transient measurements could be a source for noise, while the transfer characteristics were measured with a single instrument (see also the section about how the measurements were performed 4.2). Tuning the applied gate voltage and interval time can allow to improve the sensitivity.

Even though the transient measurements lag behind the transfer characteristics

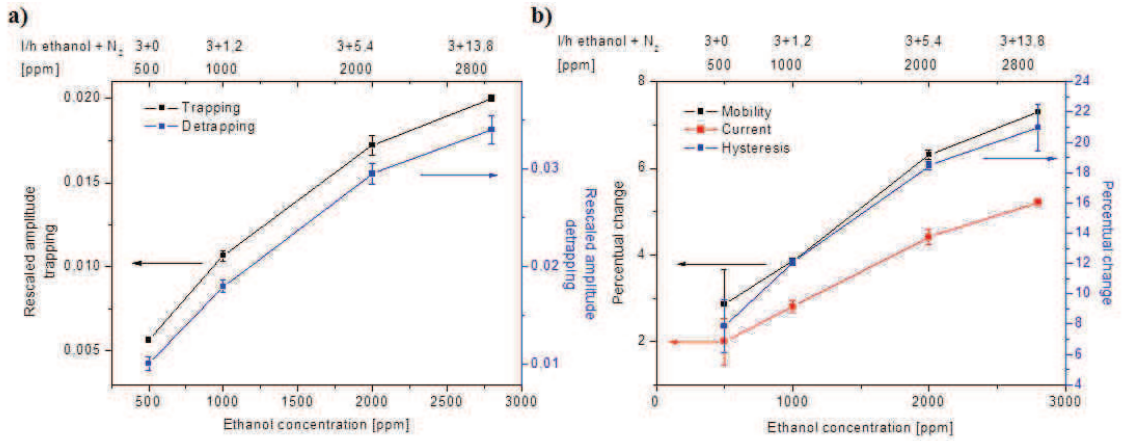

Figure 6.17: a) Response of rescaled transient current amplitude to ethanol exposure. b) Response of transfer characteristics for the same device. Outliers in b) at 500 ppm are perhaps due to incorrect ethanol concentration.

in terms of sensitivity and linearity a different advantage was observed. When the transfer characteristics are used P3HT based devices need up to several hours to settle. Measurements performed to soon show an excessive response as it was shown in section 5.2.2. Figure 6.18 shows the response of the rescaled amplitude in the

detrapping regime to ethanol. Though the first exposure to 900 ppm starts after only 26 minutes, the increase of the amplitude at the end of the exposure is similar to the second exposure to 900 ppm after almost two hours. b) Compares the responses of all three concentrations showing that the sensor has already reached a stable state where linear dependence of the response on the concentration is achieved. Even though no systematic studies on this behavior have been made yet, several measurements and samples support this observation.

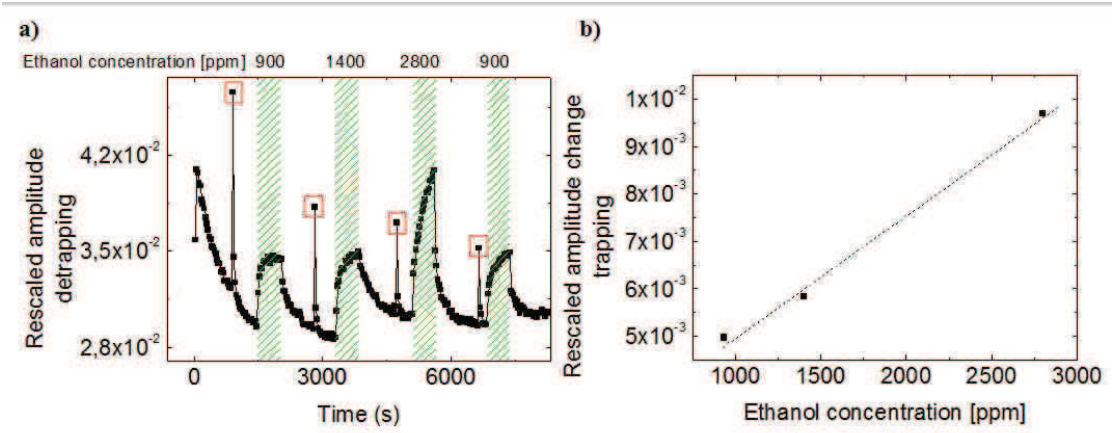

Figure 6.18: a) Response of rescaled amplitude in detrapping regime to ethanol vapor 26 minutes after onset of measurement. Red squares highlight artifacts induced by the autocalibration of the used analyzer. b) Change of rescaled amplitude versus ethanol concentration.

6.4 Conclusions

In this section the hysteresis of the transfer characteristics has been introduced as parameter for the detection of polar vapors. It has been shown that the hysteresis meets all demands as parameter for gas detection. Linearity has been shown for the response to ethanol vapor at concentrations between 500 and 2800 ppm. The sensitivity was found to be intermediate between the generally used on-current and mobility. Selectivity has been shown for the two analytes ethanol and acetone. While these two analytes can hardly be distinguished with the conventional transistor parameters used for the gas detection, the hysteresis shows a two times higher response to ethanol and enables the identification of the present analyte.

In the second part of this chapter a new method to measure the transient current was introduced and employed to probe the origin of the hysteresis. In agreement with published results, enhanced trapping in the presence of the analyte vapors was indicated as origin of the hysteresis increase. Even though the time resolution of the used equipment was insufficient to follow the entire behavior, the obtained results indicate a higher ratio of fast traps in presence of acetone as origin for the differences observed for the hysteresis response in ethanol and acetone.

The last section investigated the utilization of the transient current as parameter for the gas detection. Even though a good behavior in terms of sensitivity and linearity of the response has been observed, the performance lacks behind the performance of the transfer characteristics. Further studies are needed to investigate if improved measurement conditions can enhance the sensitivity. An interesting advantage of the transient current was found to be the decrease of the warm up time before a measurement shows a stable response. Further investigations on these aspects are needed.

7 Influences of the polymer chemical structure on the OFET response to polar vapors

One key advantage of organic semiconductors used as gas sensors, are the vast possibilities to tune the properties of the sensing layer by chemically tailoring the molecular structure. Hierlemann et al showed that the absorption of analyte molecules is an endothermic process which is mainly driven by the entropy of the system [32]. Different organic side chains attached to polysiloxanes did not significantly influence the mixing entropy, as the side chains had comparable sizes and therefore a comparable number of possible arrangements with the analyte molecules, but strongly influenced the mixing enthalpy and therefore the partition coefficient which determines the selectivity within a family of polymers to a particular analyte. Though these results obtained on quartz crystal microbalances can not be directly transferred to organic semiconductors, as electrical interactions between the analyte and the sensing layer are not taken into account, they have shown that side chain modifications are a viable approach to tune the selectivity of gas sensors based on organic molecules.

For OFETs Liao et al. showed that polythiophenes with different side chain lengths can be used in sensor arrays to discriminate amines by their size [64]. Torsi et al. showed that polythiophenes provided with alkoxy side-chains allow the detection of ethanol while the same backbone with long alkyl side chains was not responsive at all [98]. Even chiral detection was achieved by providing chiral recognizing side chains to alkoxyphenylene-thiophene oligomers [99].

To further the understanding of the analyte-semiconductor interaction this section examines the influences of different alkoxy side chains on the ethanol sensitivity of poly-bithiophene phenylene based sensors. Morphological studies and the affinity of the molecules to ethanol are combined with mass uptake studies to understand the

ongoing mechanism leading to the results obtained in OFET sensor configurations.

7.1 Interaction with ethanol vapor

The molecules used during this study were introduced in chapter 3.2. To understand the sensitivity of the different molecules to ethanol vapor we will first introduce quartz crystal microbalance experiments which were performed to measure the mass uptake of the films in presence of the analyte. To distinguish the contributions of absorption and adsorption to the mass uptake, the contact angle to ethanol is analyzed. Together with the morphological data shown in chapter 3.2 the obtained results are used to understand the responses induced by the different side chains in OFET sensors.

7.1.1 Ethanol mass uptake measured with a quartz crystal microbalance

To measure the mass uptake of the films in presence of the analyte, quartz crystal microbalance (QCM) measurements were performed in collaboration with Vincent Rouessac at the Institut Européen des Membranes in Montpellier. Measurements of the mass uptake directly reveal the amount of analyte which is adsorbed and absorbed by the semiconductor layer and help understanding the origin of the interaction between the analyte and the organic semiconductor.

7.1.1.1 Theory of quartz crystal microbalance measurements

A quartz crystal microbalance uses the frequency change of a quartz crystal to monitor changes of the mass of the crystal. Piezoelectric quartz crystals have a well known relation between the applied voltages and the mechanical deformations. For a QCM gold electrodes are evaporated onto both sides to electrically contact the quartz and engage it into shear vibrations by the application of an alternating voltage (see figure 7.1). The resonance frequency of the crystal is probed by variation of the exciting AC frequency. As the current through the piezoelectric quartz increases

with the amplitude of the oscillation, the resonance frequency is detected as a current maximum. This allows to measure the acoustic resonance of the quartz crystal by electrical means. The employed quartz crystals have a very narrow bandwidth which leads to very stable oscillations and allows to determine the resonance frequency very precisely. A resolution of less than 1 Hz at typical resonance frequencies around 6 MHz is possible.

Figure 7.1 a) depicts the formation of standing shear waves in a quartz crystal

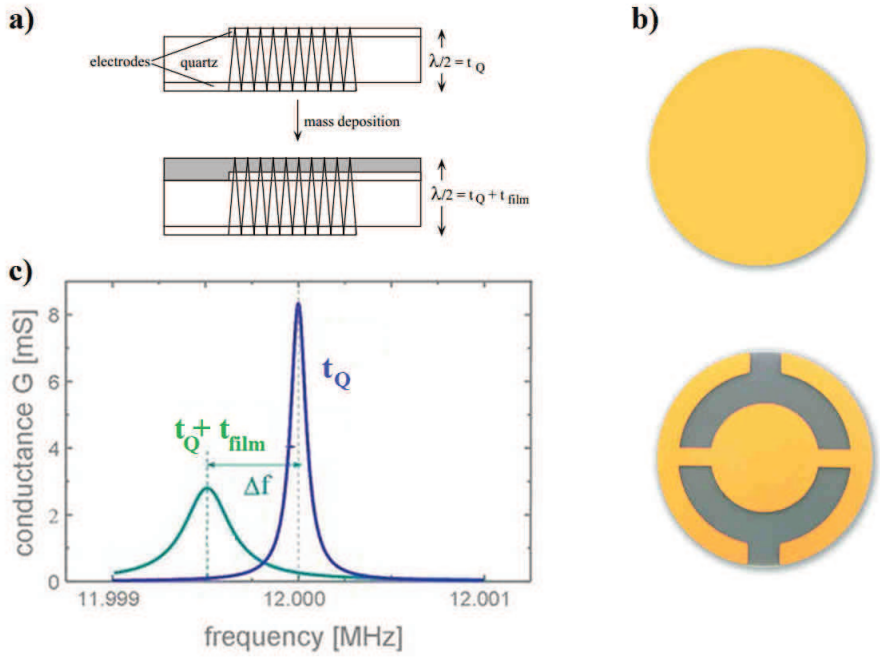

Figure 7.1: a) Shear vibrations in a uncoated quartz crystal and in a coated example. λ denotes the wavelength of the oscillation which increases with the thickness of the structure. b) Front (top) and rear view (bottom) of the employed quartz crystals. c) Example of the conductance dependence of a quartz crystal on the frequency for an empty and loaded quartz.

when it is excited with the resonance frequency. The wavelength of the overtone corresponds to twice the combined thickness of the quartz crystal, metal electrodes and material deposited on the quartz crystal surface. As the frequency is inversely proportional to the wavelength an increase of the thickness is reflected by a decrease of the resonance frequency which can be detected by measuring the current through the quartz crystal (7.1 c)). Sauerbrey showed that the change of the resonance

frequency $\Delta f/f$ induced by an increase of the quartz thickness by Δd corresponds to the change induced by any thin, rigid and homogeneous film deposited on the quartz surface with a similar mass [79]. This leads to the Sauerbrey equation describing the relation between a frequency change Δf and the corresponding mass change Δm (given in g):

$$\Delta f = -\frac{2f_0^2}{A\sqrt{p_q \mu_q}}\Delta m \tag{7.1}$$

where f_0 is the Resonance frequency of the quartz crystal in Hz before deposition of the film. A is the piezoelectrically active area in cm^2 which corresponds to the area covered by the film. p_q is the density of the quartz which corresponds to $2,65\ \frac{g}{cm^3}$ and μ_q is the shear modulus of the quartz ($\mu_q = 2,95 \times 10^{11}\ \frac{g}{cm \times s^2}$). As the Sauerbrey equation allows to directly translate a frequency change into a mass change, only the mass change will be considered onwards.

7.1.1.2 Experimental setup for quartz crystal microbalance measurements

Figure 7.2 shows a scheme of the custom made setup used for the quartz crystal microbalance measurements. This setup was established by Vincent Rouessac at IEM in Montpellier and kindly provided for the measurements discussed in this section. The quartz crystals used for this measurements have a diameter of 14 mm and a blank resonance frequency around 6 MHz. The cristals were mounted on a feedthrough which makes the electrical connection and stabilizes the temperature during the measurement. As the resonance frequency of a quartz is susceptible to drift with temperature a BIOBLOCK polystat thermostat was used with a waterbath to maintain the temperature of the quartz at 25°C. The frequency was monitored by a deposition monitor (Maxtek TM400) with a frequency resolution of 0,03 Hz at 6 MHz. The quartz was measured inside a 0,5 l custom made stainless steel chamber. To evacuate the air inside the chamber before the measurement and the vapor afterwards, an Alcatel Drytel 1025 pump was used which allows to pump down to 1×10^{-4} mbar. An analyte reservoir allows to generate vapors of various volatile compounds which can be introduced into the sample chamber by a Mass Flow Controller (Tylan 2900 series by BROOKS) which is controlled by a WKIA

pressure transmitter. This allows to automatically introduce vapors at various pressures up to the saturated vapor pressure of the respective analyte.

In order to measure the mass uptake by the PTPTs molecules, thin films of various

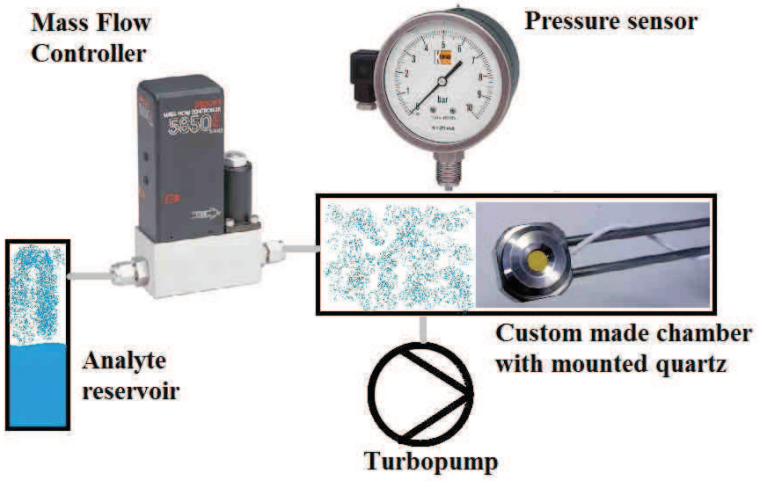

Figure 7.2: Scheme of the setup provided by Vincent Rouessac for the QCM measurements. The quartz is mounted inside a stainless stell chamber which can be evacuated by a turbopump. A mass flow controller in feeback with a pressure sensor provides the desired pressure of the volatile analyte.

thicknesses were deposited on the quartz crystals by spin coating from chloroform solution under a nitrogen atmosphere. The concentrations of the PTPTs in solution was 20 mg/ml, as films with thicknesses around 100 nm were envisaged to increase the mass uptake and therefore the reliability of the measurements. The different thicknesses were obtained by variation of the spin coating parameters. The roughness of the gold electrodes on the quartz crystals was in the range of μm and impeded direct measurements of the film thickness. To quantify the differences of the films the variations of the frequency of the quartz crystals before and after deposition were used. In order to reduce possible damages the crystals were not cleaned chemically and only a stream of nitrogen was used before deposition of the PTPT films. Testing the stability of the resonance frequency upon dismounting and remounting of the quartz crystals showed average variations in the order of 50 ng which is sufficiently lower than the masses of the deposited films which were between 15 to 60 μg. If an average density of 1 mg/cm^3 is assumed the corresponding thicknesses are around

100 to 300 nm. After the PTPT films were deposited the samples were left in the evaporator for 2 hours at 10^{-6} mbar to remove residual solvent traces from the film.

7.1.1.3 Time resolved mass uptake

The blue curve in figure 7.3 shows the time resolved mass uptake and loss of a thick EtHex-Me film with a mass of 58 μg during exposure to 37 mbar ethanol. The black curve indicates the pressure of the ethanol vapor inside the chamber. Before the measurements starts the chamber was evacuated by the turbo pump to a pressure below 1 mbar. This allowed to remove residual contamination from the chamber and the measured film. Once the frequency of the quartz stabilized under vacuum it showed no drift for a timescale of several minutes. Even though no systematic study about the stability of the baseline was performed, the average difference before and after an exposure was less than 2 Hz which corresponds to approximately 15 ng. The lowest differences used in this discussion are 10 ng which were obtained with the weakest absorbing molecule for pressure changes around 5 mbar.

Once the frequency of the quartz stabilized, the mass flow controller was opened until a desired pressure of the analyte in the chamber was reached. As it can be seen in figure 7.3 the mass uptake reaches saturation with some delay to the vapor pressure due to the time necessary for the analyte to diffuse inside the organic layer. When the mass uptake saturated, the vapor was first removed by a forepump before a turbopump was engaged to further remove analyte traces. Changing from the forpump to the turbopump is visible by a kink in the mass uptake around 630 seconds. EtHex-Me, which was chosen for the example in figure 7.3, was the molecule which showed the most pronounced time delay between changes of the pressure in the chamber and saturation of the corresponding mass uptake responses. This indicates a slow diffusion of the ethanol vapor inside the polymer. Despite the slow diffusion, the mass of the blank film before and after exposure changed only by 15 ng. Several exposures to similar concentrations revealed the reproducibility of the obtained results.

This type of time-dependent mass uptake measurements were performed with all

investigated films to measure the kinetics of absorption and desorption. These kinetics were important for the configuration of the delay time in a second type of measurements which shows the mass uptake or loss as a function of the vapor pressure. In the example in figure 7.3, more than 96 % of the final mass uptake are reached within the first minute after exposure. As the depicted sample shows the response of a thick film of the molecule with the slowest mass uptake, 1 minute was chosen as delay time to probe the pressure dependences of the ethanol mass uptake in the next section.

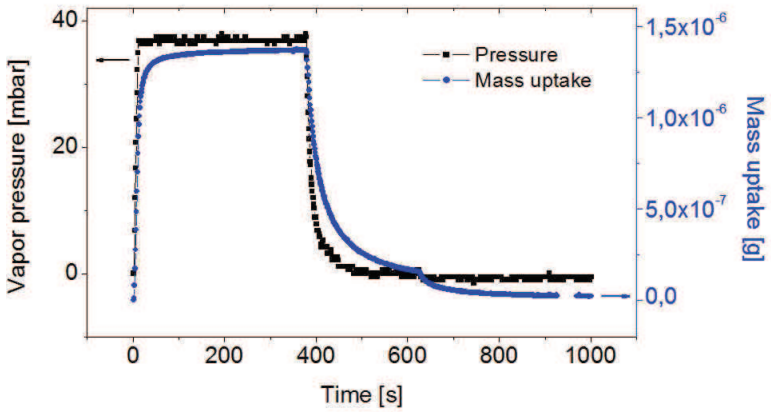

Figure 7.3: Ethanol mass uptake of EtHex-Me plotted over time for an ethanol pressure of 37 mbar. Black squares show the pressure inside the chamber. Blue circles indicate the mass change at the same time. Kink visible in the mass uptake around 630 seconds is caused by switching from forepump to turbopump.

7.1.1.4 Pressure dependent mass uptake

To measure the pressure dependence of absorption and desorption, the ethanol pressure was stepwise increased from 0 mbar to the saturated vapor pressure and then decreased back to 0 mbar. After each pressure step the system waited for the time chosen as delay time before the mass uptake was measured. To make the results comparable obtained for films with different thicknesses and different molecules, the mass uptake is divided by the mass of the films before exposure. This normalization enables direct comparison of the mass uptake for different materials.

Figure 7.4 a) shows the normalized absorption and desorption for all three PTPT

molecules obtained with at least two samples of different film-masses per molecule. The error bars indicate the variations of the normalized mass uptake for different thicknesses of the same molecule. As it can be seen the variation within one type of PTPTs, indicated by the error bars, is much smaller compared to the differences between the different types of molecules.

While EtHex and 3OBu show a similar behavior in absorption and desorption EtHex-Me shows a pronounced hysteresis. As the same delay time of 1 minute was used for all polymers, the higher mass during the desorption indicates a slower diffusion of the analyte into or out of the polymer compared to the other PTBTs. This was also indicated by the time dependent measurements in the last section. Over the entire pressure range EtHex shows the smallest normalized mass uptake for the PTPTs.

The variation of the mass of the polymer films in presence of the analyte vapor is caused by adsorption of the analyte molecules on the film surface and can be increased if the analyte is absorbed by the film. To figure out if ethanol is absorbed by EtHex, the molecule with the smallest mass uptake, the absolute mass uptake was compared to the mass uptake of a bare gold-covered quartz where the analyte only adsorbs on the surface. Contact angle measurements showed a strong affinity between the hydrophilic gold of the quartz and ethanol, as deposited drops spread out immediately over the whole surface while the rather hydrophobic PTPTs showed contact angles around 20° (see section 7.1.2) [85]. As the polymer films on SiO_2 showed no significant increase of the overall surface area (see AFM measurements in section 3.2) the amount of ethanol adsorbed on the polymers surface should be similar or even less than the amount on the more affine gold electrodes of the quartz. EtHex, which showed the lowest mass uptake of all PTPTs, showed a two times higher absolute mass uptake for the thin film and a more than six times higher mass uptake for the thick film compared to the bare quartz. Together with the almost constant mass uptake per film mass, these results indicate that ethanol not only accumulates on the surface of the film, but diffuses inside the layers of the PTBTs. These results are in accordance with Liao et al., who reported swelling of polythiophene films during exposure to butylamine vapor [64].

The concentrations used for the exposure of OFET sensors to ethanol were typically

less than 1000 ppm. If the pressure inside the gas test bench was close to 1 bar, 1000 ppm correspond to a partial pressure of 1 mbar. A zoom into the lower pressure region, which is more important for the OFET sensors, is shown in figure 7.4b).

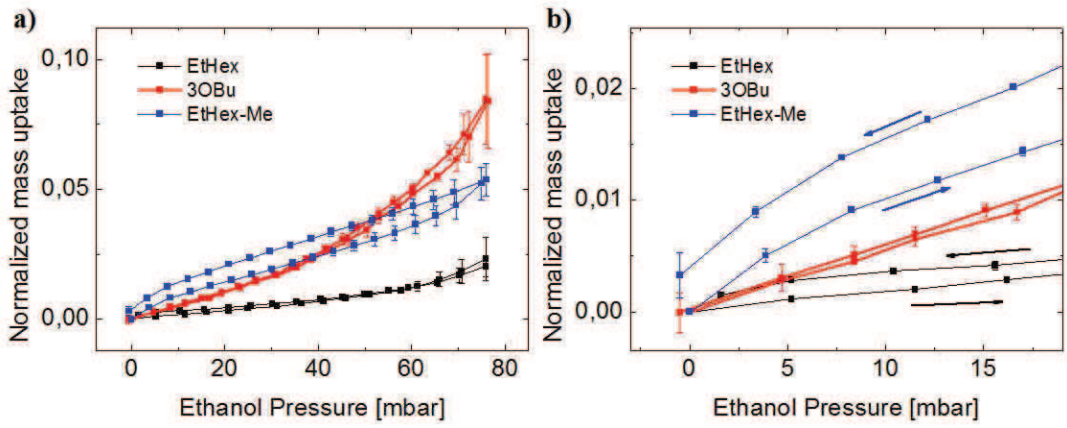

Figure 7.4: Ethanol mass uptake plotted over ethanol pressure for all three PTPT molecules. For EtHex-Me the lower curve corresponds to mass uptake and the higher to mass loss during pressure decrease. b) Shows a zoom into a) at low ethanol pressures.

7.1.2 Contact angle measurements

To further the understanding of the interaction between the PTBT molecules and ethanol, the contact angles were measured in collaboration with Stéphane Mery at the Institut de Physique et Chimie des Matériaux de Strasbourg.

Contact angle measurements probe the wettability of a solid surface by a liquid by measuring the tangent angle Θ at the base of the liquid (see figure 7.5). As it was described by Young, the contact angle is defined by the equilibrium between three interfacial tensions: solid-vapor γ_{sv}, liquid-vapor γ_{lv} and solid-liquid γ_{sl}. The liquid-vapor interaction is similar for all measurements and the solid-vapor interaction can also be assumed to be comparable for the polymers measured in this experiment. As a consequence the contact angle is mostly influenced by the liquid-solid interactions and indicates the intermolecular forces between the two components.

Films of the PTPT molecules were deposited by spin coating from 3 mg/ml solutions on glass substrates and on the same SiO_2 that was used for the OFET measurements.

Surface	Contact angle ethanol [°]	Contact angle H_2O[°]
EtHex	25	100
EtHex-Me	25	100
3OBu	15	85

Table 7.1: Contact angle of ethanol on PTPTs.

The higher concentrations of the solutions were used to increase the thickness of the films and reduce the influences of the substrates on the measurements. To investigate the influences of the different side chains on the interaction with ethanol, the static sessile drop method was used. The used goniometer provided an optical microscope with a back light where the contact angle was measured by manually aligning a turnable scale with the tangent at the base of the liquid, immediately after deposition of the liquid drop. No difference was found on SiO_2 or glass, indicating sufficient coverage by the polymers.

Table 7.1 summarizes the measured results for ethanol and distillated water. EtHex and EtHex-Me whose side chains have comparable polarities, show no difference within the resolution of the measurement, for ethanol and H_2O. 3OBu shows a more hydrophilic surface and also a slightly higher affinity to ethanol, most likely due to the very polar side chains. The higher affinity of all PTPTs to ethanol in comparison to H_2O can be explained by the higher amount of dispersive components and the weaker surface tension.

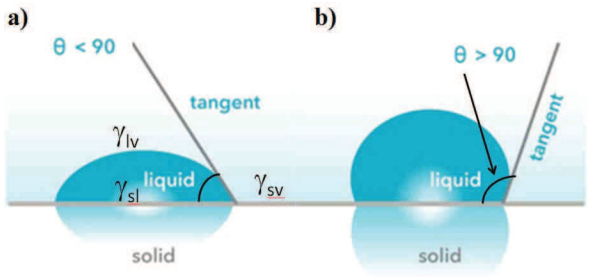

Figure 7.5: Contact angle between liquid and solid. a) High affinity b) Low affinity

7.1.3 Behavior of PTPT based OFET sensors

To measure the response of the PTPT molecules as OFET gas sensors, samples were prepared according to the procedure explained in chapter 5. First the long-term behavior of PTPT OFETs is shown during repeated measurements of the transfer characteristics. The second part presents the responses of the PTPTs to ethanol vapor. It is important to note that the OFET devices made of the different PTPT molecules compared in this chapter, were all measured simultaneously in the gas test bench to avoid errors due to inaccuracy of the ethanol concentrations

7.1.3.1 Electrical long-term behavior

Figure 7.6 shows the behavior of the transfer characteristic in the linear regime of PTPT OFETs during repeated measurements in nitrogen. All devices were freshly prepared with a channel length of 10 μm and thicknesses below 10 nm, as it was confirmed for the used production procedure by AFM 3.7. The drain voltage was set to -15 V while the gate was swept in 5 V steps from 20 to -60 V and back. Between adjacent measurements the devices were grounded for 60 seconds to reduce the bias stress.

The drain voltage of -15 V was chosen because the PTPT transistors still operate in the linear regime at this voltage and show a current sufficiently high to reduce the noise. In the linear regime the conductive channel extends over the whole distance between source and drain and creates a relatively homogeneous conductive channel without a pinched off region. As a consequence interactions between charge carriers and analyte vapor are homogeneous distributed over the entire channel. Though the threshold voltage is defined in the saturation regime, a similar concept will be used in this discussion to indicate differences related to the onset of the current.

The transfer characteristics of the OFETs composed of EtHex molecules is shown in a). In comparison to the other devices it shows a strong decrease of the current due to a shift of the threshold voltage V_{th} within the first 60 measurements. b) shows the corresponding mobility calculated at every gate voltage step. Though a small decrease is visible, the main change is induced by the threshold voltage shift. The decrease of the slope at higher gate voltages is most likely due to contact resis-

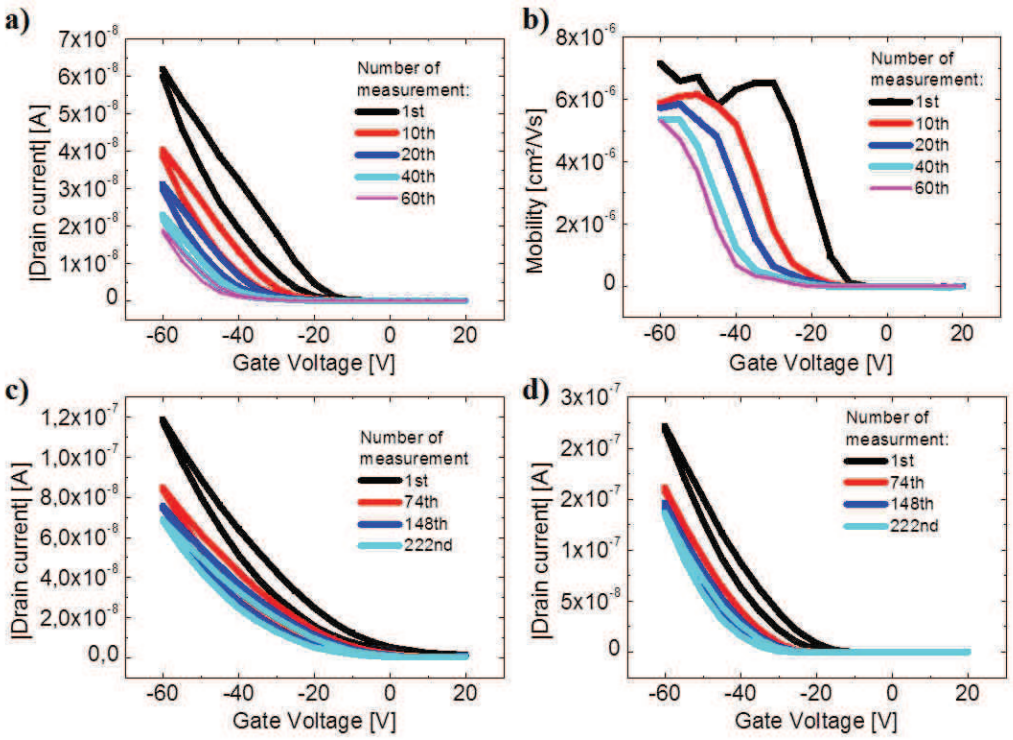

Figure 7.6: Transfer characteristics behavior of PTPTs during repeated measurements. a) Id-Vg of EtHex b) Corresponding mobility c) Id-Vg of 3OBu d) Id-Vg of EtHex-Me. Please note that for EtHex evolution is shown only for the first 60 measurements while 222 are shown for the other molecules

tance. c) And d) show the changes during the first 222nd measurements for 3OBu and EtHex-Me, respectively. Though the graphs show the behavior over a higher number of measurements the current reduction due to a shift of V_{th} is less significant compared to EtHex. However, 3OBu suffers also from a mobility decrease during the first measurements. This behavior is caused by bias stress effects which is caused by trapping of charge carriers in deep traps (see also 5.2.2).

The average mobilities of PTPT OFETs extracted from the first measurements are shown in table 7.2. Compared to alkyl substituted polythiophenes, like P3HT with mobilities around 10^{-2} and 10^{-3} cm^2/Vs, the alkoxy substituted PTPT molecules show a much lower performance. Though theoretical studies suggest a higher planarity and therefore a higher mobility for alkoxy substituted polythiophenes, experimental comparisons report a higher mobility for alkyl side chains [27] [97]. This difference was subscribed to the low degree of morphological and structural order

	Mobility [cm^2/Vs]
EtHex	$3.7 \pm 1.6 \times 10^{-6}$
EtHex-Me	$3.3 \pm 0.8 \times 10^{-5}$
3OBu	$1.8 \pm 0.3 \times 10^{-5}$

Table 7.2: Mobilities of PTPs extracted from fresh devices

in the alkoxy substituted polythiophenes. X-ray measurements, performed with the PTPT molecules revealed rather amorphous structures for all three molecules which can explain the low mobilities (see section 3.2). EtHex however, reveals the lowest mobility but the highest structural order. This can be understood as the X-ray measurements showed no π-π stacking and the ethyl-hexyl side chains are expected to show the strongest sterical hindrance for hopping charge transport.

7.1.3.2 OFET response to ethanol vapor

To compare the response of the PTPT molecules to ethanol vapor, the devices used to discuss the long-term behavior, were exposed to ethanol concentrations between 200 and 800 ppm in a nitrogen atmosphere. The drains were biased at -15 V while the gates were swept from 20 to -60 V and back in 1 V steps. Between measurements the devices were grounded for 10 seconds.

Though it would have been interesting to apply also the hysteresis as a parameter for gas detection on the PTPT films, the low currents inherent to these molecules made the current voltage characteristics more susceptible to noise. As the hysteresis amplifies ongoing changes between the forward and reverse sweep the noise decreased the applicability of the hysteresis and made the drain current the parameter of choice for the sensitivity comparison performed in this section.

Figure 7.7 a) - c) compare the transfer characteristics before exposure to 800 ppm ethanol and 5 minutes after the exposure started for EtHex, EtHex-Me and 3OBu, respectively. As it can be seen, all three polymers respond similarly to ethanol vapor. The decrease of the slopes in the on regime evidences a decrease of the mobility which causes a decrease of the drain current. Graph d) shows the evolution of the drain current for all PTPTs during four adjacent exposures to 800 ppm ethanol. The

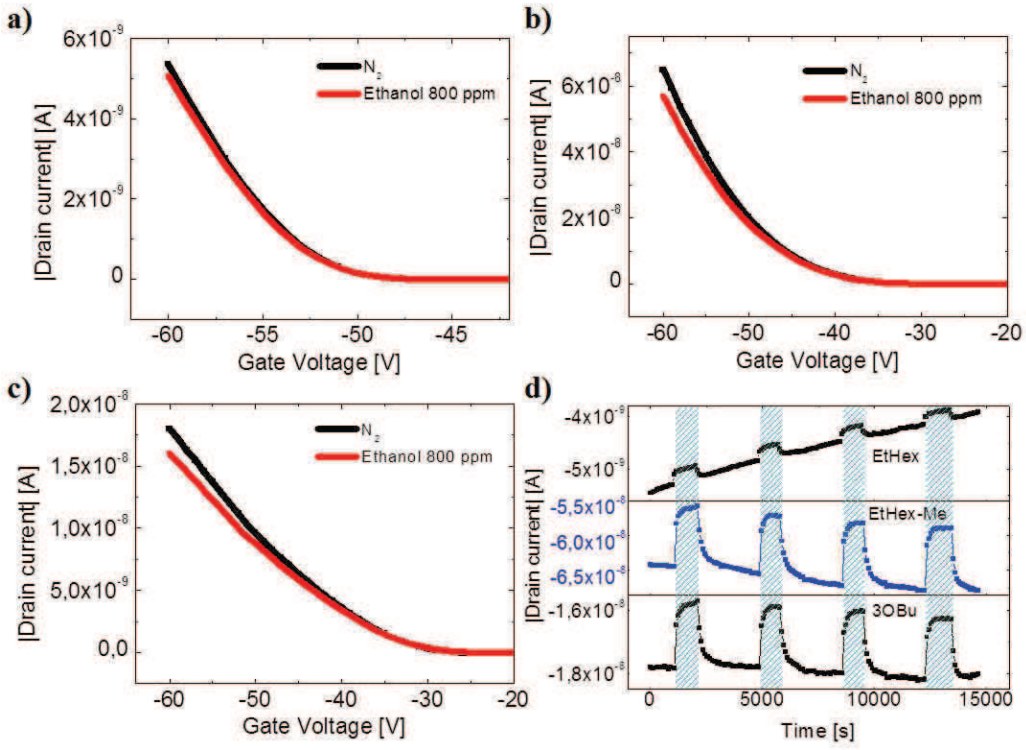

Figure 7.7: Responses of the transfer characteristics of PTPT based OFETS to 800 ppm ethanol vapor. Please note the different gate voltage ranges of the x-axis. a) EtHex, b) EtHex-Me c) 3OBu. d) Behavior of drain current at -60 Vg for all PTPTs during repeated exposure to 800 ppm ethanol.

devices show a comparable performance in terms of response speed and recovery, at the used timescales.

The only difference between the PTPT molecules in d) is the pronounced drift of the EtHex molecule. As it was discussed in the previous section, this is caused by the drift of the threshold voltage of the device. Figure 7.7 a) shows that the onset of the on regime of the EtHex device has moved to approximately -52 V at the time of the exposure. Tanese et al. showed that the response of polymers to analytes can be amplified by the gate voltage, if the device is used in a transistor configuration [91]. Though no explicit investigation was performed, it can be assumed that the amplification only works above the threshold voltage, so once the device is turned on. As a consequence of the differences in V_{th}, the amplification by the gate voltage should be more pronounced for the 3OBu and EtHex-Me devices with V_{th} around -35 and -45 V, respectively, than for the EtHex OFET.

In order to make the responses comparable, graph a) in figure 7.8 shows the averaged

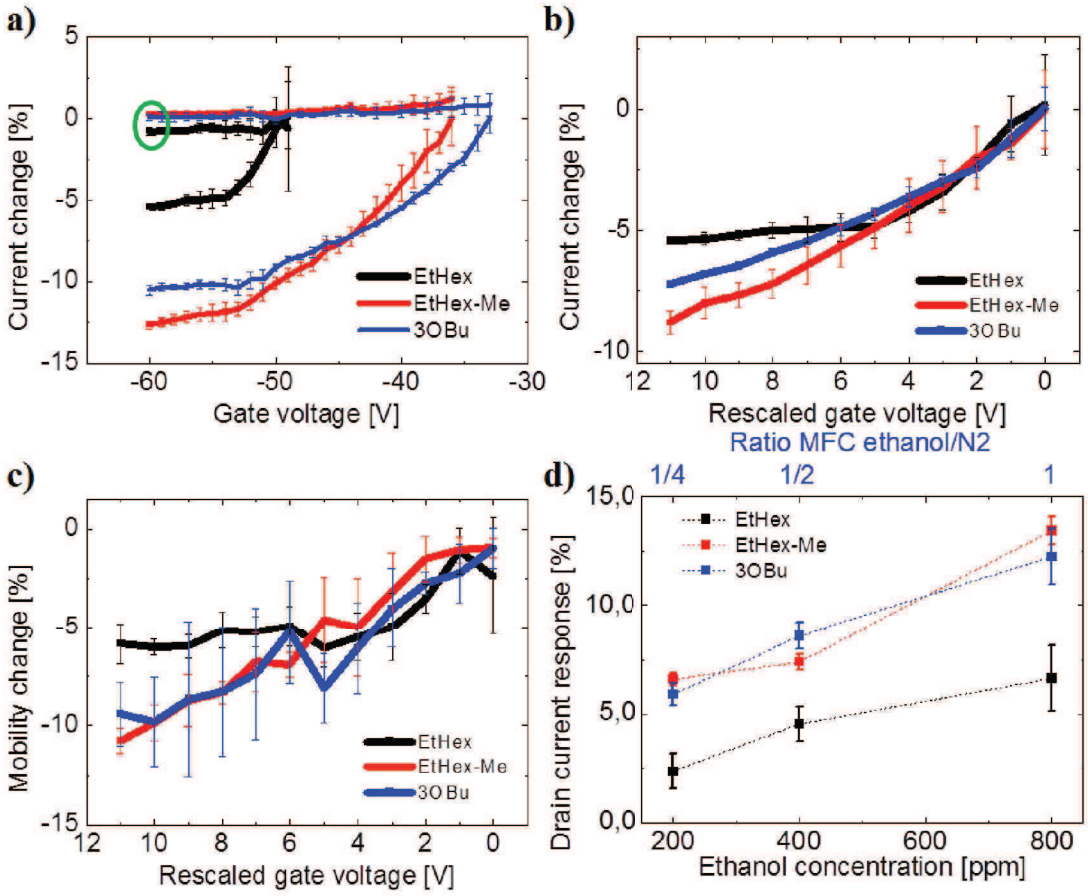

Figure 7.8: Responses of the PTPT molecules to ethanol vapor. a) averaged percentual current changes as a function of gate voltage during exposure to 800 ppm ethanol. Green encircled lines show the average change in N_2. To compare the amplification of the response by the gate voltage, the onsets of the current b) and mobility c) responses were shifted to a mutual gate voltage and limited to the gate voltage range available for the EtHex molecule. d) percentual current responses of PTPTs to ethanol at -60 V

responses of the current as a function of the gate voltage for all PTPTs during exposure to 800 ppm ethanol. The average changes of the currents between adjacent measurements in N_2 are also shown to serve as a baseline. The baseline is close to zero, except for the EtHex OFET, which is subjected to drift and therefore shows a constant deviation from zero. For every PTPT only that part is shown, where the current changes during the exposures deviate from the baseline in nitrogen. At gate voltages below the depicted ones no systematic changes were observed. As it can be seen, the response of EtHex-Me and 3OBu to ethanol starts already around -35 V.

While the gate voltage raises to -60 V the responses get amplified continuously. The response of EtHex starts only around -50 V and gets therefore less amplified by the gate voltage. Graph b) shifts the onset of the responses for all three PTPTs to the same value (0 V) and limits the responses to the gate voltage range that was available for the EtHex device. Though all PTPTs show a comparable response directly after the onset, EtHex saturates after 5 V and shows only a minor increase for higher gate voltages. EtHex-Me and 3OBu increase continuously and show a higher response 11 V after the onset of the response. Figure c) compares the relative responses of the mobilities derived similar to the current in b). 10 V after the onset the responses of EtHex-Me and 3OBu are 60 % higher compared to the EtHex device which saturates again approximately 5 V after the onset. While the graphs in 7.8 compare the responses to 800 ppm ethanol, saturation of the EtHex response was also observed at lower concentrations.

Though the origin of the weak gate voltage amplification for the EtHex molecules is not understood, these results corroborate the differences measured for the current responses at -60V which are shown in 7.8 d). While EtHex clearly shows a lower response EtHex-Me and 3OBu have a comparable sensitivity to ethanol.

7.2 Discussion of PTPT performance

The results shown in this chapter and the morphological studies in 3.2 allow to draw some conclusions about the influences of the side chain properties on the sensing performances of OFETs.

First of all, AFM images show that the PTPT films have a comparable morphology and thickness for the used OFET production procedure. This makes the results easier to compare, as all PTPTs have a comparable interface to the surrounding atmosphere. A second point that was revealed by the mass uptake measurements, is that the ethanol vapor does not only affect the bulk conductivity by interactions on the surface of the films, but also gets absorbed into the film where it can directly interfere with the charge transport in the conductive channel of the OFET.

The mass uptake experiments revealed that the EtHex molecule shows the weakest

absorption of ethanol into the film. EtHex also showed the weakest response as OFET sensor. EtHex-Me with a comparable side chain composition and therefore a similar affinity to ethanol, shows a higher mass uptake and response as OFET sensor. X-ray measurements revealed a more ordered structure for the EtHex molecule which has symmetrical side chains in comparison to EtHex-Me with asymmetrical ones. The interaction between polycrystalline semiconductors and analytes is expected to happen mostly at grain boundaries, as diffusion of the analyte into the crystalline parts seems to be unlikely [87]. In the case of the EtHex molecule, the higher crystallinity compared to EtHex-Me, can be expected to be a drawback for the sensing performance, as crystalline domains in an amorphous matrix can reduce the diffusion paths for the ethanol molecules to the semiconductor/dielectric interface. As a consequence some parts of the conductive channel of the EtHex OFET could be screened from the surrounding atmosphere by the crystalline domains and the area available for the interference of ethanol with the charge carriers at the semiconductor/dielectric interface could be reduced. As the interactions between ethanol and the EtHex molecules can be expected to be similar to the interactions of ethanol with EtHex-Me, the lower amount of analyte at the interface causes a lower response as OFET sensor.

For the 3OBu molecule with oxygen enriched side chains the most amorphous structure was revealed, but only an intermediate mass uptake. Nevertheless the sensor performance of the OFET device was comparable to EtHex-Me which showed a much higher mass uptake. For the contact angle measurements 3OBu showed a more hydrophilic character, and also a higher affinity to ethanol indicating stronger interactions between the two components. The additional oxygen atoms in the 3OBu side chains can be expected to give rise to stronger polar interactions with ethanol and for being responsible for the higher affinity. In OFET devices the amount of ethanol at the semiconductor/dielectric interface should be smaller for 3OBu in comparison to EtHex-Me due to the decreased absorption. In order to cause a comparable response strength, stronger interactions have to occur between the analyte and the 3OBu molecules. Though it is not understood yet, how the polar interactions between ethanol and the additional oxygen atoms in 3OBu side chains

contribute to the current response, the obtained results indicate an amplification of the individual analyte-semiconductor interaction by increasing the polarity of the side chains.

7.3 Performance comparison to standard materials

To compare the sensing performances of the PTPTs to standard materials that have also been reported in literature, this section first introduces the results derived from the P3HT OFETs that have been used during this thesis, before it compares the PTPT responses to ethanol sensitivities reported in literature.

The P3HT devices used for sensing were spin coated either from chloroform or ortho-dichlorobenzene solution without showing a significant difference in terms of response to ethanol vapor. The thicknesses measured by a Dektak profilometer were between 5 - 10 nm, comparable to the PTPT devices discussed before.

Figure 7.9 a) compares the OFET responses of P3HT and EtHex transistors to ethanol vapor. Even though EtHex shows the lowest response of all PTPTs it is higher than the response of P3HT. The larger error bars of the EtHex device are caused by noise which is higher for the low currents of the EtHex device. Graph b) compares the normalized ethanol mass uptake of P3HT and the PTPTs. At low ethanol pressures the mass uptake of P3HT is similar to EtHex.

Though the comparable mass uptake indicates a comparable absorption of ethanol

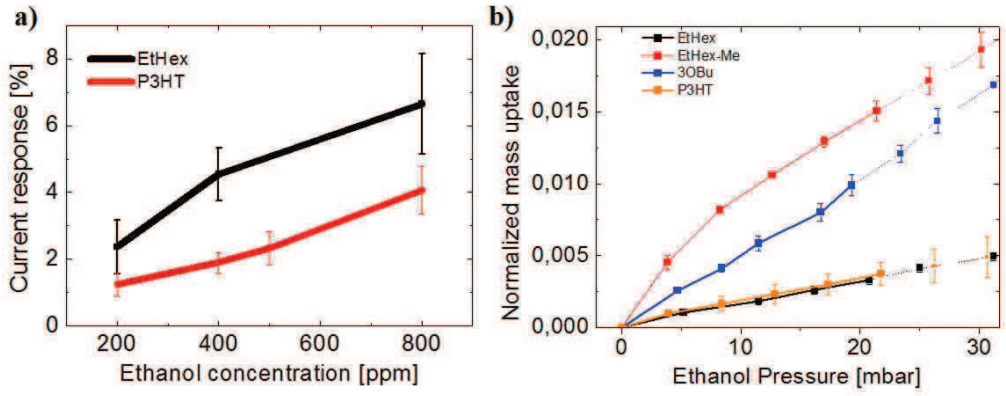

Figure 7.9: a) Comparison current response to ethanol for EtHex and P3HT devices. b) Normalized mass uptake.

into the P3HT and EtHex films, the electrical responses deviate from each other almost by a factor of 2. Contact angle measurements with distilled water have shown only minor differences of 105° and 100° for P3HT and EtHex, respectively. The small difference indicates that the oxygen of the alkoxy side chains is not completely screened by the nonpolar part of the side chains. Polar interactions between the OH group of the ethanol and the oxygen of the alkoxy chains were suggested in literature to account for the difference observed for alkyl and alkoxy substituted polythiophenes during exposure to ethanol vapor [98]. A similar mechanism can also be expected for the bithiophene-phenylene molecules.

In order to better understand the interactions between the PTPTs and ethanol, simulations of the behavior of a single PTPT molecule in presence of an ethanol molecule, were performed at the Institut Charles Gerhardt in Montpellier by Jean-Marc. For the simulations, both molecules, the ethanol and the PTPT, were supposed to be in vapor phase. As it was explained in section 3.2 the oxygen of the alkoxy side chains stabilizes the molecular structure by weak interactions with the sulfur of the neighboring thiophenes. As the simulations revealed, this weak interaction is disturbed in presence of ethanol. The oxygen atom in the alkoxy side chains favors the stronger hydrogen bond with the H of the OH group in ethanol. As the S-O interaction is lost, the planarity of the molecule decreases and reduces the conjugation length and mobility. For the 3OBu molecule the simulations showed that the ethanol molecule can hardly access the oxygen close to the backbone and therefore this type of interaction may not explain the high response to ethanol. However, it has to be taken into account that the PTPT molecules and the ethanol were modeled as gases. In condensed films the spatial arrangement of the backbone and the side chains can deviate from the modeled behavior and enhance the accessibility for the ethanol molecules.

The formation of a hydrogen bond between polar analytes and the side chains of the semiconductor, is an interaction unique to alkoxy side chains which enhances the interference of the analyte with the conductive channel of the organic semiconductor. This interaction would additionally contribute to the dipole induced increase of the energetic disorder, which is present in molecules with alkyl side chains, and amplify

the electrical response. Interactions between the sensing layer and the analyte with a high binding strength are favorable for sensor applications as an increased response strength is expected to help improving the selectivity [86].

Comparing alkyl and alkoxy substituted polythiophenes in OFET structures, Torsi et al. reported no response for the alkyl side chains and responses around 0,4 % for the alkoxy side chains during exposure to 700 ppm ethanol [98]. The response was expected to arise from the higher dipole moment of the alkoxy side chains. Li reported an increase of the response of P3HT based chemiresistors from 0,2 to 2 % for 400 ppm ethanol by changing the nanostructure of the film [57]. Though it has a nonpolar structure, pentacene is one of the most investigated materials for OFET gas sensors. Due to the high order, pentacene films are very sensitive to the energetic disorder induced by polar vapors resulting in a very high sensitivity [5]. Reported responses to 100 ppm ethanol vary between 0,3 and 10 %, probably due to differences in purity and film quality [67] [86]. A new benchmark in terms of sensitivity was set by Zhao et al. by investigating single crystalline nanoribbons composed of a pentacene analogue [117]. Upon exposure to 500 ppm ethanol the drain current decreased by almost 50 %. However, the examples with a higher sensitivity than the PTPTs employ more elaborated deposition techniques like evaporation or physical vapor transport. The facile fabrication in combination with a fairly high sensitivity due to the alkoxy side chains make the bithiophene-phenylene based semiconductors interesting materials for the detection of polar vapors.

7.4 Conclusions

In this section it has been shown that tuning of the side chains strongly affects the sensitivity of bithiophene-phenylene based organic semiconductors (PTPTs) to ethanol vapor. The polymers shared the same backbone but the side chains varied in terms of sterical hindrance and polarity.

First of all, comparison to P3HT, which is provided with alkyl side chains, revealed higher responses for the alkoxy substituted PTPTs. Though mass uptake and affinity to ethanol were comparable for the EtHex molecule and P3HT, the electrical

responses to ethanol vapor were still higher for EtHex based OFETs. Simulations, performed by the chemistry group of the project TRANSFILSEN, indicated the disturbance of planarizing interactions between the oxygen of the alkoxy side chains and the sulfur of neighboring thiophenes, by the polar moment of ethanol. This can be suggested as a possible additional sensing mechanism which can explain the higher sensitivity of alkoxy substituted molecules to ethanol. Though P3HT and EtHex do not share the same backbone, the obtained results are supported by the findings of Torsi, who compared the sensitivity of alkyl and alkoxy substituted polythiophenes and also reported an increase of the response for the alkoxy side chains [98].

Comparison of the sensitivity to ethanol among the different PTPT molecules, also revealed differences induced by the side chains. While EtHex showed a higher response to ethanol than P3HT, it still showed the lowest sensitivity in comparison to 3OBu and EtHex-Me. A lower absorption, which is expected to be caused by the higher crystallinity of the EtHex molecule, results in a lower amount of ethanol molecules interfering with the charge transport at the semiconductor/dielectric interface.

Comparing EtHex-Me and 3OBu, the latter showed a lower absorption. As a consequence the amount of ethanol which can directly influence the charge transport at the dielectric/semiconductor interface is lower in 3OBu in comparison to EtHex-Me. However, the responses of the OFET devices were comparable for both molecules. Contact angle measurements showed that 3OBu is more hydrophilic due to the more polar side chains. Though the underlying mechanism is unclear, it can be assumed that the stronger interactions between the more polar 3OBu side chains and the polar ethanol molecules enhance the response of the OFET. As a consequence of the stronger interactions between the polar 3OBu side chains and ethanol, the drain current response to a lower amount of ethanol present at the conductive channel is comparable to the response of EtHex-Me where a higher amount of ethanol diffuses to the channel.

The results derived in this sections show that the response of polymers in OFET devices to ethanol can be strongly influenced by the choice of the side chains. Polarity

and sterical hindrance determine the affinity and the structure of the sensing layer and can be tuned to increase diffusion of the analyte into the semiconductor or to amplify the analyte-semiconductor interactions. Though this was already reported before, the current responses of PTPT based OFETs during exposure to ethanol is among the highest published for spin coated polymers, so far, provided the approximated analyte concentrations are reliable. The results of Mori for pentacene indicate that even further enhancement of the sensitivity can be achieved by the application of a HMDS interface layer [67].

For future studies, special interest should be spent on the enhanced response of the strongly polar side chains of 3OBu. The potentially higher sensitivity, on a molecular scale, could be harvested in more porous films to further increase the response strength. As it was shown in literature, variation of the solvent could be a promising means to improve the structure of the films [57].

For the OFET devices, thickness dependent measurements can be a possibility to enhance the contribution of the individual side chains to the sensing performance and to improve the understanding of the influences of the different side chains. Additionally, the verification of the observed responses with calibrated gases would be an interesting mean to ensure the exceptionally high sensitivity.

8 Downscaling the channel length of bottom-contact OFETs

Miniaturization of gas sensing OFETs offers a variety of practical advantages, like improved integration into portable devices and a lower power consumption due to the lower driving voltages needed to operate the devices. Rather progressive reasons to reduce device dimensions were suggested by Wang et al. [110]. In large-area devices, the number of interactions needed between analyte molecules and the organic semiconductor to produce an observable current change is rather high. The conductive channel of a nanoscale device incorporates a smaller number of semiconducting molecules. As a consequence, a similar number of analyte-semiconductor interactions causes a higher relative change of the current voltage characteristics, which is expected to give rise to a more defined response. The investigations of Dodabalapur on pentacene and P3HT OFETs with long and short channels revealed fundamental differences in the sensor response to 1-pentanol as a function of the channel length [110] [109]. In long-channel devices analyte-induced trapping of charge carriers at the grain boundaries decreases the source-drain current, as it was also shown by Duarte et al. [20]. When the channel length decreases and the number of grain boundaries between source and drain becomes less important, the devices responses to the analyte change their polarity and show a current increase. Though two mechanisms were suggested as origin of the current increase, the generation of excess charges due to analyte-semiconductor interactions or the reduction of the injection barrier at the contacts, detailed investigations are still outstanding.

The investigation and exploitation of these effects occurring at low channel lengths, is not only fundamental to the understanding of sensing mechanisms, but can also help to improve the basic sensor characteristics: the sensitivity and selectivity to analytes. In order to allow the investigation of these fundamental properties and to work towards the nanoscale platform envisaged by the project TRANSFILSEN to enable enhanced gas sensor sensitivity and the investigation of intramolecular charge transport, this chapter focuses on the elaboration of short-channel OFETs. To en-

sure proper transistor-like behavior at short channel lengths the transverse electric field induced by the gate voltage at the semiconductor/dielectric interface has to be much larger than the longitudinal electric field caused by source and drain [31]. This becomes especially important at low dimensions, as the longitudinal electric field increases inversely with the channel length and leads to the so called short-channel effects.

In this chapter, the first section will briefly explain the effects decreasing the electrical performance of short channel devices and show how these effects can be overcome. As all devices used in this thesis incorporate SiO_2 as dielectric, Si_xN_y will be introduced as high-k alternative and the performance will be discussed in comparison to SiO_2. The last section shows the results obtained on Si_xN_y at channel lengths of 350 and 500 nm.

8.1 Short-channel effects

The long channel behavior of organic and inorganic field effect transistors is described by the equations 2.2 and 2.3 in the linear and saturation regime, respectively. These equations are valid if the transverse electric field between the source and gate electrodes is much larger than the longitudinal field between source and drain. When the length of the channel is decreased without adaption of the other device parameters, this so called gradual channel approximation is no longer valid and the behavior deviates from the long channel behavior [31].

The first short channel effect that can be observed as the channel length decreases, is the inability of the drain current to saturate at drain voltages higher than the pinch-off voltage. Instead, a continuous increase can be observed which is caused by channel length modulation. In an OFET the applied gate voltage attracts charge carriers to the interface between the semiconductor and the dielectric where they establish a conductive channel between source and drain. When the source-drain voltage increases at a fixed gate voltage, the lateral electric field reduces the transverse field in vicinity to the drain electrode. In the linear regime of a transistor the source drain voltage V_{DS} is smaller than the effective source gate voltage V_{GS}-V_{th}

and the conductive channel is continuous between source and drain. At the pinch-off voltage, the longitudinal electric field compensates the transverse field in vicinity to the drain electrode, i.e. V_{DS}=V_{GS}-V_{th}, and the accumulated charge carriers which generated the conductive channel, get extracted from the channel in vicinity to the drain electrode. This creates a depleted region which interrupts the conductive channel between source and drain. For higher drain voltages the current becomes independent of the applied drain voltage and saturates, according to equation 2.3. Though a further increase of the drain voltage enlarges the depleted part of the channel, the fraction remains negligible for long channel devices. However, in an inappropriately build short channel device, the depleted part of the channel spreads over an important fraction of the channel and reduces the effective channel length significantly. As the drain current in the saturated regime 2.3 is inversely proportional to the effective channel length, a continuous current increase can be observed. If the channel length of a transistor decreases, the contribution of the channel resistance to the total resistance reduces while the importance of a possible contact resistance increases. A deterioration of the device performance by an increased contact resistance can be recognized by a superlinear increase of the output characteristics at low drain voltages.

If the channel length is further reduced, the transverse and longitudinal electric fields become comparable and the depleted region occupies a large fraction of the channel. This reduces the gate voltage which is required to establish a conductive channel and therefore decreases the threshold voltage as a function of the applied drain voltage. If the same dielectric is used for several channel lengths which show short channel effects, the resulting threshold voltage shift, or threshold voltage roll-off, is inversely proportional to the channel length. At sufficiently short channel lengths the threshold voltage roll-off can turn a normally off into a normally on device [48] [31].

Another short channel effect is drain induced barrier lowering (DIBL). At gate voltages below the threshold voltage, the potential barrier in the channel is constant for most of the channel length, for transistors with long channel behavior. If the transistor shows DIBL the depleted region at the drain extends far into the channel

and lowers the potential barrier, charge carriers have to overcome in the off state, thus leading to a higher off current (see also figure 8.1) [54].

In addition to the threshold voltage roll-off and DIBL, residual impurities and

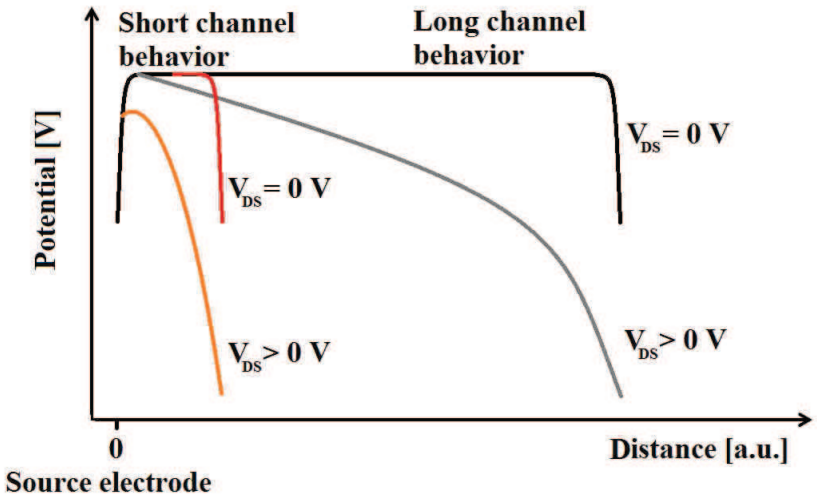

Figure 8.1: Scheme of potential profiles for two different drain voltages ($V_{GS} < V_{th}$). Device with short channel behavior shows drain induced barrier lowering.

doping by moisture cause extrinsical doping of the bulk and increase the off-current in comparison to long channel devices.

When the depleted region finally extends over the whole channel and the conductive channel vanishes, a space charge limited current (SCLC) occurs between source and drain. This is also referred to as non destructive punch-through current and was shown by Hirose et al. [33] to account for organic semiconductors which have an ohmic contact to source and drain electrodes. For similar dielectric thicknesses (200 nm) and channel lengths (30 nm) contact limited devices still showed saturation as the contact limitation suppressed the SCLC. However, contact limited devices give rise to other drawbacks, like superlinear current increase in the linear regime of the output characteristics and underestimation of the mobility in the transfer characteristics.

While several techniques, like incorporation of a mesa structure or asymmetric work functions of the electrodes, have been employed to suppress short-channel effects, an increase of the capacitance of the dielectric is the easiest way to ensure that the transverse electric field stays superior to the longitudinal field. [14] [108] [55]. Due

to the higher capacitance the gate voltage needed to accumulate charge carriers in the channel and to surpass V_{th} reduces. As a consequence V_{DS} needed to fulfill $V_{GS} - V_{th} = V_D$ decreases too and saturation can be reached at lower transverse and longitudinal fields. Lower applied voltages also reduce deteriorating effects like DIBL or off current increase due to impurities.

Equation 8.1 defines the capacity of a capacitor with the surface A, the thickness d and the relative dielectric constant ϵ_r. ϵ_0 is the vacuum permittivity.

$$C = \epsilon_0 \epsilon_r \frac{A}{d} \tag{8.1}$$

While the thickness d can be changed by the fabrication process, ϵ_r is a material constant. In order to enhance the effect, both parameters will be used in this work to tune the device behavior.

8.2 High k dielectrics as alternative to SiO_2

Silicon dioxide is the most frequently used dielectric layer for OFET devices. Wet or dry oxidation of silicon wafers provides smooth and homogeneous dielectric layers which effectively reduce leakage current and provide a high breakdown voltage. The only shortcoming of SiO_2 is the small dielectric constant ϵ_r, which is around 3.4 - 3.9. Alternatives to SiO_2 with very high dielectric constants are called high-k dielectrics and are typically employed in modern electronics. Materials like $SrTiO_2$ showed dielectric constants above 100 and are potential candidates for future application in inorganic semiconductors [46].

In organic semiconductors the interaction of the high-k dielectrics with the semiconducting layer is less well understood, yet. While some groups report significant decreases of the charge carrier mobility for higher dielectric constants [90] [103], other groups found a conservation of the mobility for similar changes of ϵ_r [50] [113]. As a trade off between an increase of the dielectric constant and a possible reduction of the mobility, silicon nitride with a dielectric constant of 7, was chosen as substitute for SiO_2. OFETs with silicon nitride as dielectric have been reported in literature without showing a significant decrease in mobility in comparison to SiO_2

[50]. A further advantage of silicon nitride is the absence of hydroxyl groups on the surface which are present in form of silanol in SiO_2 and are expected to act as trap centers [15].

8.2.1 Dielectric deposition

Plasma enhanced chemical vapor deposited (PECVD) silicon nitride offers important advantages for dielectric layers, like a relatively low deposition temperature and good dielectric strength [59]. The used silicon nitride films were deposited at the ICube laboratory by using an electron-cyclotron resonance PECVD system (ECR-PECVD), fabricated by Roth&Rau (see figure 8.2).

The system comprises a load-lock and a process chamber divided in 2 zones. The first is the resonance zone (ECR) and the second is the deposition zone where the polarized substrate is located. In the first zone the reactive gas is subjected to a strong magnetic field and excited by a 2.45 GHz microwave antenna. This excitation increases the kinetic energy of the electrons and ionizes the gases. Near the substrate holder a plasma is generated by a radio frequency source. Ionized atoms or molecules which come to the borders of the plasma are accelerated towards the neighboring surface, and therefore also towards the substrate. The film growth is dominated by surface reactions of the impinging ions and depends on the sticking probability, the probability of recombination and subsequent evaporation, surface diffusion and mean energy per deposited atom [69]. Before inlet of the gases and generation of a plasma, the system is pumped down to a pressure of 10^{-7} mbar.

The silicon nitride films were deposited on highly n-doped silicon wafers. To remove the native oxide and possible contaminations, RCA cleaning was performed in the class 10000 clean room at ICube. If the wafers were not entered into the PECVD system immediately after the RCA cleaning, the last oxide, grown to remove ionic contaminants, was kept as protective layer during storage.

As almost every PECVD system has its particular structure and dimensions, recipes published in literature could not be simply adapted to our system. Instead the knowledge of the MaCEPV group of Abdelilah Slaoui was consulted and several

recipes used for the deposition of silicon nitride were tested. In order to measure leakage currents and dielectric constants of the films metal-insulator-semiconductor structures with 1×1 mm metal electrodes were fabricated and tested in collaboration with the Master-I internship student Hugo Faure. The most appropriate recipe found, was based on the experience of Bhabani Shankar Sahu, a former post-doc of the MaCEPV group (Growth conditions are shown in the Appendix 10.1). Results obtained by Bhabani showed that the obtained silicon nitride deviates from stoichiometric Si_3N_4 only by 2% towards a higher nitrogen content. As this does not exactly correspond to Si_3N_4 this particular silicon nitride will be abbreviated by Si_xN_y in this manuscript.

The relative dielectric constant of the Si_xN_y was measured to be 6.9±0.2. Fig-

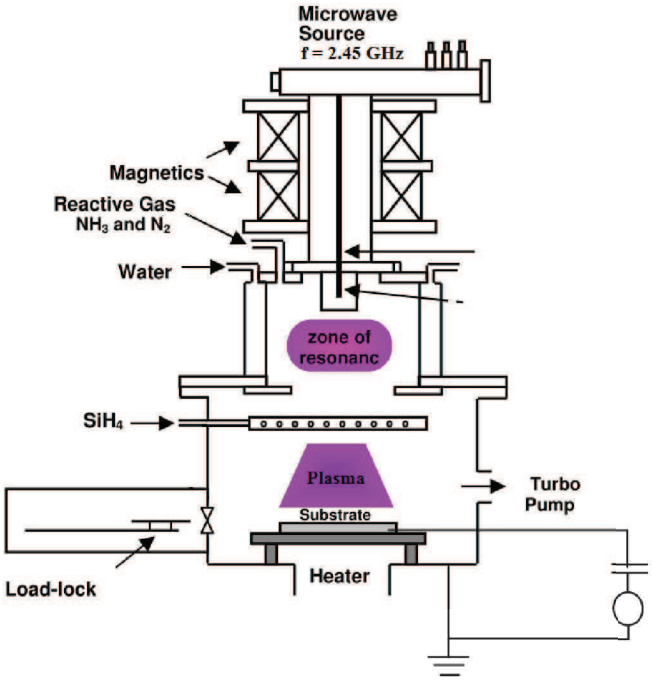

Figure 8.2: Scheme of RF-ECR PECVD at ICube used for silicon nitride deposition

ure 8.3 compares the leakage currents of 100 nm thick PECVD deposited Si_xN_y to commercially available SiO_2 of the same thickness. Though the Si_xN_y shows a much higher leakage current it has to be taken into account that the corresponding equivalent oxide thickness is only 57 nm. The equivalent oxide thickness (t_{EOT}) is a measure for the thickness of silicon oxide needed to achieve the same capacitance

as a different material with the dielectric constant ϵ_r and the thickness t_1:

$$t_{EOT} = t_1 \times \frac{\epsilon_{SiO_2}}{\epsilon_r} \tag{8.2}$$

Comparison of the leakage current in Si_xN_y with PECVD deposited silicon nitride layers reported in literature, showed a comparable performance [60] [74] [59].

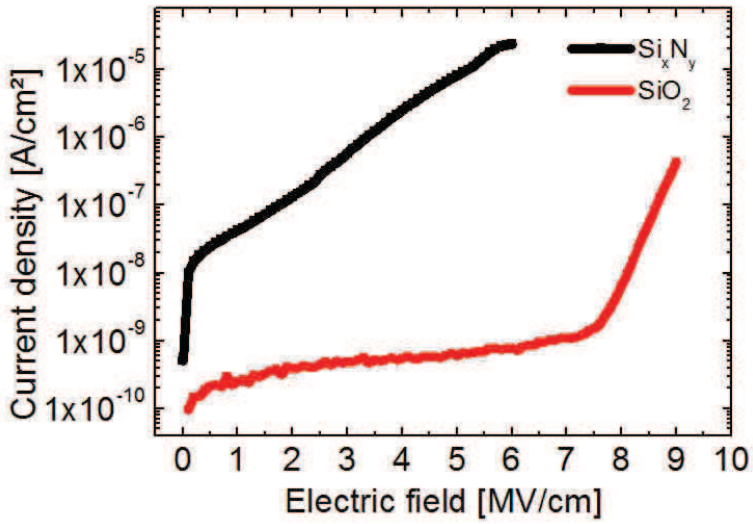

Figure 8.3: Comparison of leakage current density obtained for 100 nm thick commercially available SiO_2 and PECVD-deposited Si_xN_y

8.2.2 Elaboration of devices

Source and drain of the bottom gate-bottom contact transistor structures were elaborated by electron beam lithography (EBL) with a Raith-140-2 EBL system by the group of Michel Hehn at the Institut Jean Lamour in Nancy. The advantages of EBL are the high resolution which allows to draw patterns with less than 10 nm resolution and the versatility, as the pattern can easily be changed without the need for masks. The latter point was of special interest as a stepwise decrease of the channel length was envisaged for the downscaling.

The software LayoutEditor was used to design the structure of the electrodes. Two different types of source and drain electrodes were used as schemed in figure 8.4. The structure in a) shows interdigitated source and drain electrodes with a high width-to-length ratio allowing a high current. The 265 μm long channel between

each pair of digits was repeated 117 times and resulted in a channel length of approximately 31 mm. The depicted example shows the structure for a channel length of 3,5 μm. For shorter channel lengths the distance between the digits was reduced while the total number of digits, and therefore the channel width, stayed constant. A second electrode design used a smaller width of only 50 μm and is depicted in b). The design of the contact pads was changed in b) to reduce spreading current between the pads which becomes more important when the width to length ratio decreases.

In order to pattern the electrode structure a positive, electron sensitive resist was

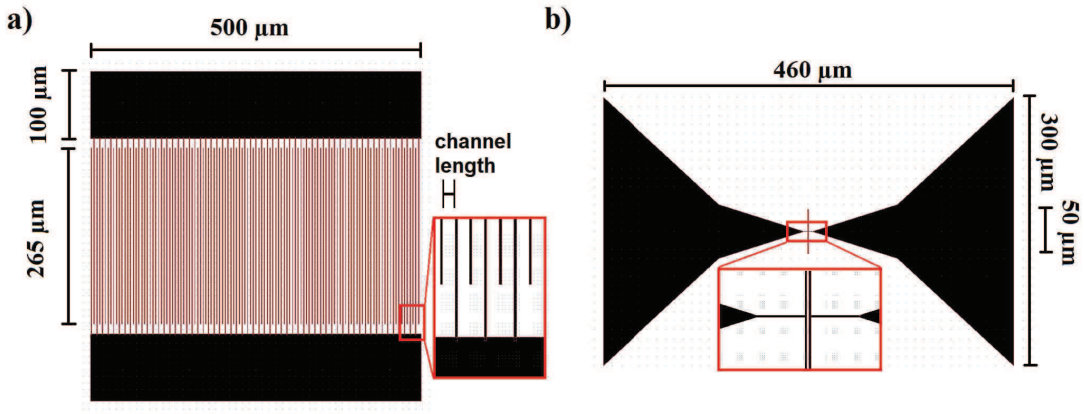

Figure 8.4: Structure of source and drain electrodes patterned by electron beam lithography. Red framed images show magnifications of the actual source and drain electrodes. The interdigitated structure in a) enables high width to length ratios. The total number of digits was 117, resulting in a width of 31 mm. For different channel lengths the width remained constant while the distance between the digits was adjusted. The structure in b) was used for small width to length ratios. The width of the channel was 50 μm.

spin coated on the dielectric which was subsequently exposed to the electron beam to draw the designed structures. Exposure of the positive resist to the electron beam changes the solubility and enables the removal of the exposed area with the appropriate developer. After removing the exposed parts, a 2 nm thick Cr and 20 nm thick Au film were evaporated on the surface. Lift off of the remaining resist in an acetone bath removed the gold layer on the resist and left the structure drawn with the electron beam, i.e. the source and drain electrodes.

In contrast to the standard procedure described in chapter 5.1.1, the substrates were

only rinsed with acetone and isopropanol before spin coating P3HT from 5 mg/ml solution prepared with o-DCB. Though UV ozone cleaning was shown to successfully remove contaminants like, oil, grease, fluxes and contamination absorbed during prolonged exposure to air [104], it was not used for the Si_xN_y substrates prepared in this thesis, as an increase of the leakage current between source and drain by three orders of magnitude was observed after blank substrate underwent a 15 minutes UV ozone treatment. Korowicz et al. reported on charging of the Si_3N_4 after UV-ozone and suggested UV-induced hot electrons from the silicon substrate as underlying mechanism [52].

Similar to the standard production procedure, the samples were dried in a vacuum of less than 10^{-6} mbar for 2 hours after deposition of the semiconductor, to evaporate residual traces of the solvent.

8.3 Performance comparison of Si_xN_y to SiO_2

In order to compare the effect of the higher dielectric constant of Si_xN_y to the performance on SiO_2, samples with 3.5 μm channel lengths were fabricated on 100 nm thick dielectrics. The design of the electrodes used for both type of substrates is shown in figure 8.4 a). After manufacturing the devices were characterized in a glove box in the dark without air exposure.

Figure 8.5 shows the resulting output and transfer characteristics. SiO_2 is depicted in the left column and Si_xN_y in the right one. First of all, the gate leakage of the Si_xN_y device was less than 3 % of the drain current for the on-part of the transfer characteristics in the linear regime (See graph f) in 8.5). In the saturated regime the leakage current was below 0.1 %. SiO_2 showed an even lower gate leakage below 0.1 %. As a consequence of the low fraction of leakage current observed for both substrates, the corruption of the current voltage characteristics by this factor can be neglected.

Before discussing the performance of the devices, it needs to be mentioned that the threshold voltage will not be employed for the comparison of short channel effects. As it was pointed out in several publications, the concept of the threshold voltage

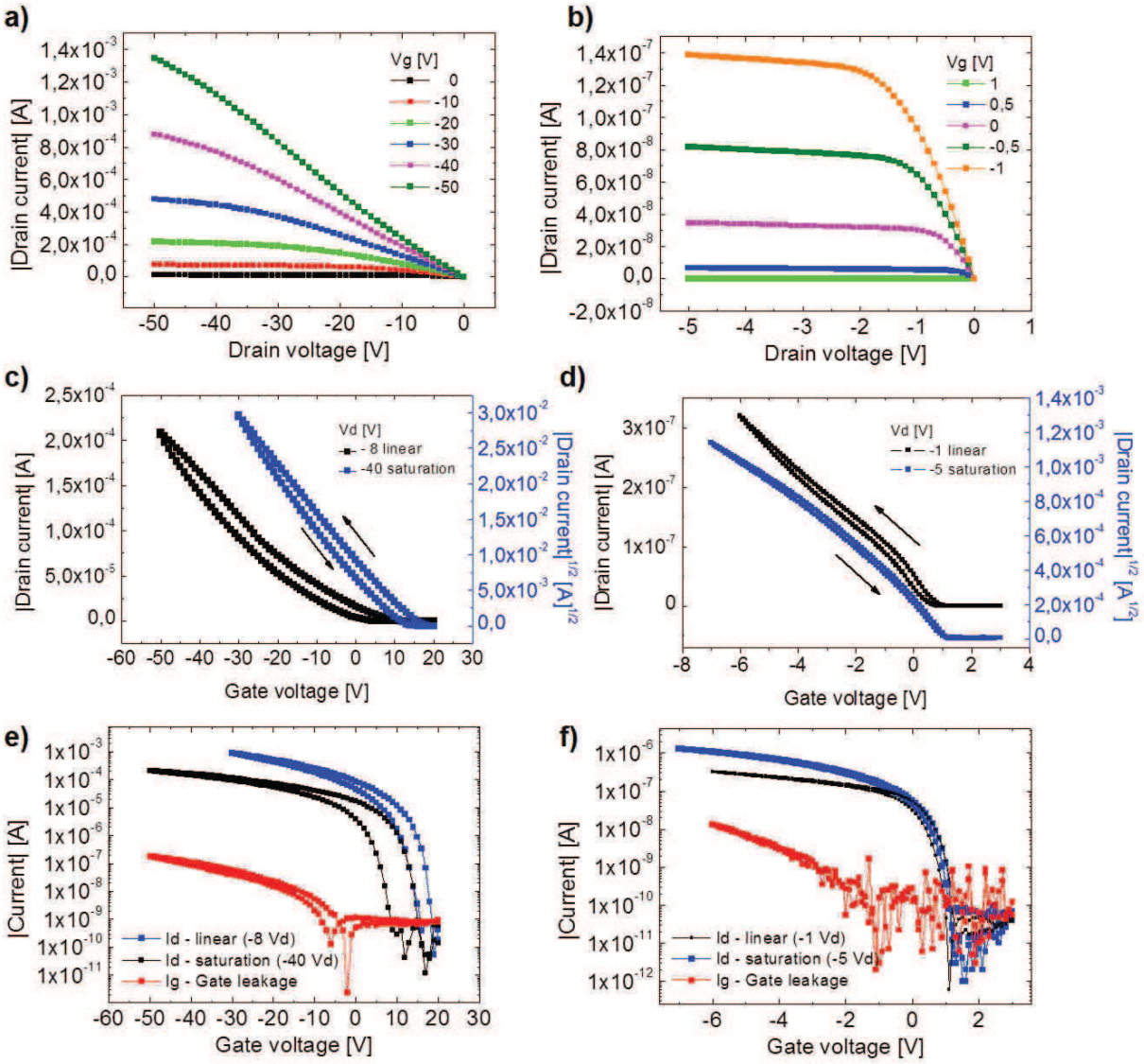

Figure 8.5: Current voltage characteristics of 3,5 μm channel length transistors on SiO_2 a), c), e) and Si_xN_y b), d), f). Output characteristics: a) and b). Transfer characteristics in linear regime refer to the left y-axis. Square root of the drain current is plotted for the saturation regime, referring to the y-axis on the right side c) and d). Arrows indicate direction of hysteresis which is similar for all devices. e) and f) show semilogarithmic plot of transfer characteristics. Red plotted data shows leakage current from the gate for comparison.

seems to be inappropriate for organic semiconductors as gate voltage dependent mobility and contact resistance lead to strong variations of the results [75] [36]. Instead of being an intrinsic property, describing traps states and energy level alignment, de-

vice and measurement parameters strongly influence the obtained result. To replace the threshold voltage the turn on voltage, also known as onset of the subthreshold slope, will be used as it describes the gate voltage at which charge carriers begin to populate the channel and is expected to be an intrinsic property for a given device. The onset of the subthreshold slope is independent of the drain voltage for long channel devices but also shows a drain-voltage dependent shift for short channel devices, similar to what is expected for the threshold voltage (see also [31]). Furthermore the onset of the subthreshold slope allows to treat transfer characteristics, like the ones obtained in 8.5 on Si_xN_y, unambiguously.

In the output characteristics, depicted in a) and b), the transition to saturation is around -30 V drain voltage for SiO_2 and even higher for gate voltages above -40 V. On Si_xN_y saturation of the drain current occurs already at drain voltages below -3 V. Additionally, the device on the Si_xN_y dielectric shows a linear current increase at low drain voltages, while the superlinear increase on SiO_2 indicates device degradation by enhanced contact resistance.

On the other hand, the device on Si_xN_y shows drawbacks, too. Though a clear difference between the linear and saturation regime can be observed, the device still shows a continuous increase in the saturation regime. Additionally a positive gate voltage is necessary to turn the device off. However, the positive turn-off voltage can not be subscribed to short channel effects, as it was also observed for 50 μm channel length devices on 100 nm Si_xN_y and has also been reported in literature for transistors showing long channel behavior [58]. Additionally a threshold voltage roll-off would be indicated by a drain voltage dependence of the onset of the subthreshold slope, which can not be observed in the semilogarithmic plot of the transfer characteristics in f). Instead the onset of the subthreshold slope on SiO_2 shifts from -16 to -19 V for drain voltages of -8 and -40 V, respectively, indicating short channel behavior.

Comparing graphs e) and f) Si_xN_y shows a very low subthreshold slope of 150 mV/decade compared to 1 V/decade on SiO_2. Though the lower subthreshold slope on Si_xN_y decreases the voltage necessary to turn the device on or off, the on/off current ratio of 10^4 is 2 decades lower than on SiO_2. The underlying reason was found

to be the mobility, which is around 3×10^{-3} on SiO_2 but only 5-20$\times10^{-5}$ cm^2/Vs on Si_xN_y. The variation of the mobility on Si_xN_y is caused by the inconstancy of the slope of the transfer characteristics, which is steeper at low gate voltages and flatter at higher voltages (see graph d) in figure 8.5). Though this can be an indication for contact resistance, the linear current increase of the output characteristics indicates a different origin for this behavior. Also a mobility decrease due to an increase of the dielectric constant, as it was reported in several publications, seems to be unlikely because no difference was observed for pentacene on silicon oxide and nitride dielectrics and the long alkyl chains of P3HT have shown to rather decrease this phenomenon [50] [113].

A different possible reason for the mobility decrease was indicated by attempts to characterize the Si_xN_y surface by AFM. The obtained images showed only self-similar triangular artifacts. If the tip is not broken, this indicates that the tip radius is too big to enter depressions on the samples surface and therefore images its own triangular shape. As it was ensured for the AFM tip to not be broken, surface structures with small lateral, but large vertical dimensions, are the most possible reason for this artifact. Surface roughness was shown by several publications to be responsible for a decrease in mobility. Several publications suggest enhanced trapping, induced by a higher number of grains or misaligned grains, to be responsible for the mobility decrease in OFETs based on oligomers [9] [106]. Comparing pentacene on PECVD deposited silicon nitrides with different roughnesses, Knipp et al. did not observe significant differences for the grain size, but almost one order of magnitude difference in mobility. Temperature dependent measurements did neither reveal differences in activation energy, indicating no increase of trapping on the rough dielectric. Instead surface scattering effects were suggested as origin for the mobility decrease on rough surfaces [51]. Steudel et al. reasoned that surface scattering effects do not seem to be likely either, in organic semiconductors, as the wave functions of charge carriers are localized and the mean free path length is only in the order of the conjugation length, i.e. a few nm. Instead, it was suggested that charge carriers are getting trapped locally, in depressions on the surface where they can not be removed by the longitudinal field between source and drain as a movement perpendicular to the

longitudinal field is needed. Additionally in the on regime, the applied gate voltage opposes the movement of the charge carriers away from the surface [88]. The immobilized charge carriers would screen the electric field from the gate and decrease the extracted mobility.

Comparing the transfer characteristics in the saturated regime obtained on Si_xN_y from figure 8.5 d) with the ones depicted by Steudel, shows a similar deviation from the linear behavior to increasingly concave curvature for increasing roughnesses. Though not discussed in the report of Steudel, the decrease of the drain current at higher gate voltages can be an additional support for the filling of depressions in the dielectric with immobilized charge carriers, as an increasing gate voltage decreases the probability for trapped charge carriers to escape and enhances the adverse effect of an irregular dielectric topography on free charge carriers. Furthermore, trapping of charge carriers by trap states in the band gap is known to increase the subthreshold slope of the transfer characteristics [80]. For the device on Si_xN_y the subthreshold slope was 150 mV/decade compared to 1 V/decade on SiO_2, indicating only low contribution of trapping in the band gap of P3HT to the deterioration of the charge transport on silicon nitride.

Summarizing the performance on both substrates, Si_xN_y suffers from a, probably roughness induced, low mobility and a higher leakage than SiO_2, but shows almost no short channel effects at 3.5 μm channel length. Surprisingly, the decrease of the voltages needed to reach saturation and the improvement of the subthreshold slope are superior to the values expected by the differences of the dielectric constants of Si_xN_y and SiO_2 only. It is known for charge transport in OFETs with an SiO_2 dielectric to suffer from the hydroxyl groups on the surface of the oxide which act as trap centers [15]. As nothing similar was reported for Si_xN_y, it can be assumed that these trapping centers decrease the performance of the SiO_2 to a level, worse than what would be expected from the higher dielectric constant, only. As the surface morphology of Si_xN_y can be improved by finding more appropriate deposition conditions it was continued to employ Si_xN_y as dielectric for short channel devices, despite the low charge carrier mobility.

8.4 Preliminary results on short channel length devices

To the moment no general relation exists for OFETs to describe the minimum channel length for long channel behavior for a given dielectric constant and thickness. Depending on the used semiconductor and device configuration, long channel length behavior has already been reported for channel length-to-dielectric thickness ratios of 1 [116] while it has been absent on the other hand, for ratios of 14 [2]. In the absence of general guidelines, the presence of short channel effects has to be confirmed experimentally for the particular semiconductor/dielectric/electrodes material combination.

To follow this task, the performance of P3HT OFETs on Si_xN_y was studied at small channel lengths. The shortest channel lengths investigated are 500 and 350 nm which were prepared on 60 nm thick Si_xN_y. The devices were prepared with both source and drain electrodes designs shown in 8.4. The interdigitated design in a) showed a very low yield of only 1 out of 10 for the 350 nm channels and 4 out of 10 for the 500 nm channels. Shorts between source and drain were responsible for most of the failed devices and are most likely caused by the large width of the interdigitated electrodes on the relatively rough dielectric surface. In order to reduce the risk of shorts between source and drain, devices were produced with the design shown in 8.4 b) with the same channel lengths and channel widths of only 50 μm. Furthermore this also allowed to verify the scaling behavior of the transistors at smaller widths, as the high width-to-length ratio of the interdigitated design can not be preserved at very low channel lengths.

All samples were prepared according to the procedure described in 8.2.2.

8.4.1 Performance of high width-to-length ratio devices

Figure 8.6 compares the current voltage characteristics of 500 and 350 nm long channels with a width of 31 mm. As it can be seen in the graphs e) and f) the leakage currents from the gate are still less than one percent of the drain currents in the on regime, despite the thinner Si_xN_y. Comparing the leakage currents for the

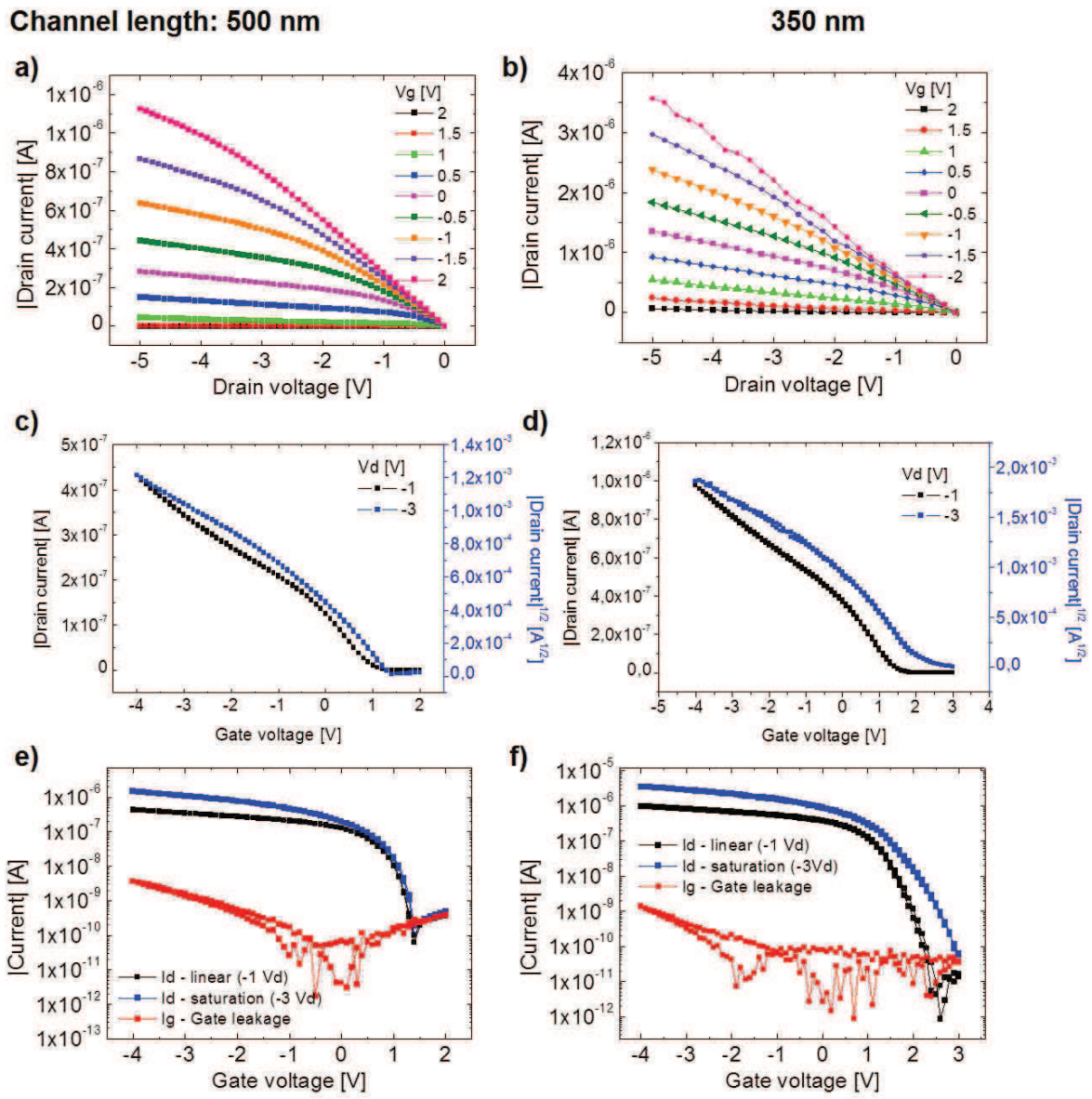

Figure 8.6: Current voltage characteristics of 500 and 350 nm channel length transistors with 31 mm width on 60 nm thick Si_xN_y. Output characteristics: a) and b). Transfer characteristics in c) and d) at -1 V refer to the left y-axis. For -3 V the square root of the drain currents are plotted, referring to the y-axis on the right side. e) and f) show semilogarithmic plots of transfer characteristics. Red plotted data show leakage currents from the gate for comparison.

depicted devices, e) shows an almost one oder of magnitude higher leakage current than the device in f). As both transistors are located on the same substrate, this indicates strong local variations of the quality of the dielectric leading to variations

of the on/off current ratio.

For the transistors with 500 nm channel length, the output characteristics in a) still show a transition to the saturation regime, but the steeper slopes of the curves indicate pronounced channel length modulation. The transfer characteristics show no drain voltage dependence for the onset of the subthreshold slope at 1.5±0.2 V , but minor dependences for the slope with 180±40 and 200±55 mV/decade at -1 and -3 V drain voltage respectively. These values are close to the results obtained on 3.5 μm channels in 8.5, indicating only minor affection of the device performance by short channel effects at a channel length of 500 nm.

For the 350 nm channels only one transistor was not shorted between source and drain. The output characteristics in b) show hardly a transition to saturation and in the semilogarithmic plot of the transfer characteristics in f), threshold voltage roll-off can be observed. At -1 V drain voltage, the onset of the subthreshold slope is at 2.6 V and increases beyond 3 V for -3 V drain voltage. Also the subthreshold slope shows a more pronounced drain voltage dependence with 210 and 280 mV/decade at -1 and -3 V drain voltage, respectively, indicating enhanced short channel effects. The transfer characteristics depicted in c) and d) show again a concave curvature which is identical for both channel lengths and expected to be indicative for the mobility decrease due to high dielectric roughness.

8.4.2 Performance of low width-to-length ratio devices

The design with a short width-to-length ratio shown in figure 8.4 b) effectively reduced the risk of source-drain shorts. Out of 23 transistors produced with each length, 19 were working for the 350 nm channels and 10 for the 500 nm channels. The higher failure rate for the 500 nm channels was due to gate leakage, which is caused by the variations of the quality of the Si_xN_y, as the transistors with high gate leakage accumulated on certain spots on the substrate.

The current voltage characteristics of representative 500 and 350 nm channels with 50 μm width are shown in figure 8.7. As it can be seen in the graphs c) and d) the gate leakage current in the on regime of the linear transfer characteristics has increased up to 25 % for these examples. Current leakage occurs mostly between the

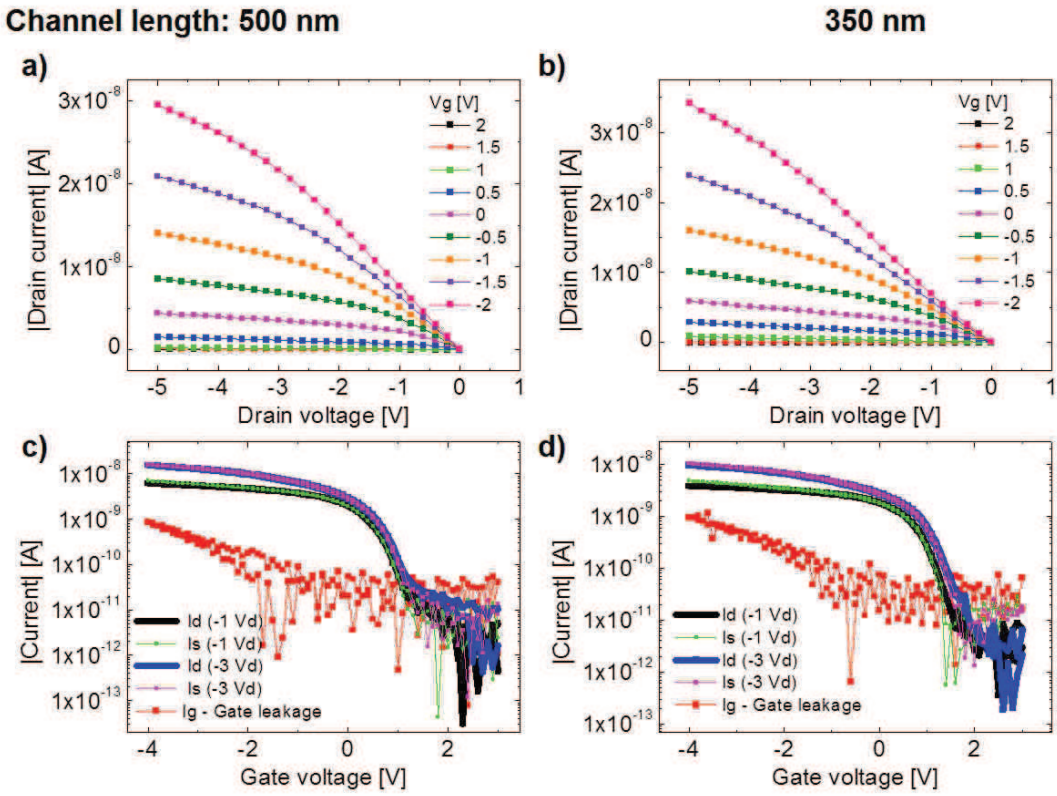

Figure 8.7: Current voltage characteristics of 500 and 350 nm channel length transistors with 50 μm width on Si_xN_y. Output characteristics in a) and b). Semilogarithmic plots of transfer characteristics in c) and d). Source and drain current are shown for low and high drain voltages. Red plotted data show leakage currents from the gate for comparison.

source and drain electrodes on top of the dielectric and the gate below. The area covered by the electrodes decreased by approximately 50 % by changing from the interdigitated electrodes design to the short width design. On the other hand, the width of the source-drain channel decreased by more than 99.8 %. As the current in a transistor is proportional to the width, as described by the equations 2.3 and 2.2, this leads to a strong decrease of the source-drain current which is not balanced by a sufficient decrease of the gate leakage current. As a consequence for 17 out of 46 devices the gate leakage was superior to the source-drain current. Despite the strong reduction of the channel width, the on/off ratio of the working transistors can still reach the range of 10^3.

The output characteristics in a) and b) show virtually no differences. Both indicate a transition to saturation but suffer from a channel length modulation induced lack

	onset [V]		Subthreshold slope [mV/decade]	
Drain voltage	-1	-3	-1	-3
500 nm	1.4±0.2	1.6±0.3	265±75	293±95
350 nm	1.6±0.1	1.9±0.2	295±110	385±110

Table 8.1: Onset voltage and subthreshold slope of 500 and 350 nm channels with small channel width.

of saturation. Onset and slope of the subthreshold current are displayed in table 8.1. These statistically more reliable values show also the onset of short channel effects for the 500 nm channels as it is also indicated by the output characteristics and the higher subthreshold slope compared to the 3.5 μm device. The drain voltage dependence of the onset of the subthreshold slope is smaller compared to the 350 nm channels, but still obvious for some devices.

The mobilities extracted from the small and high width transistors were 1.5±0.5 and 2.5±0.5×10^{-5} cm^2/Vs, respectively, indicating good agreement of the current scaling behavior with the theoretical expectations 2.2. Within the course of this study several batches Si_xN_y were deposited but all consistently showed mobilities in the order of 10^{-5} cm^2/Vs. Also the utilization of P3HT with higher mobilities of 10^{-2} cm^2/Vs, measured on SiO_2, did not increase the mobility on Si_xN_y, indicating that the roughness and therefore the low mobility are inherent to the used recipe for the silicon nitride deposition.

8.5 Conclusions

In this chapter the elaboration of P3HT based transistors with short channel lengths has been described. Though the length envisaged for the TRANSFILSEN project of only 10 nm was not reached, only minor short channel effects were observed for 500 nm channels on PECVD deposited silicon nitride as dielectric layer.

Silicon nitride showed interesting properties in comparison to SiO_2, like decreased hysteresis, superior subthreshold slope and operating voltages far below the values

expected due to the higher dielectric constant. The origin of this enhanced device performance is expected to be caused by the absence of hydroxyl groups in silicon nitride, which are known to act as trap centers on SiO_2 dielectrics [15]. Despite these advantages of the PECVD deposited silicon nitride, P3HT-based OFETs showed an up to three orders of magnitude smaller mobility compared to the performance on SiO_2. AFM images and the behavior of the transfer characteristics indicate increased surface roughness as origin of this drawback. As the roughness is inherent to the silicon nitride deposited with the used recipe in the PECVD system, but not a general feature of silicon nitride, investigations are ongoing, in collaboration with Nancy, to examine commercially available Si_3N_4 dielectrics for their application in OFETs.

9 Conclusions

Though the goal of the TRANSFILSEN project, which is ambitioned in various aspects, was not reached yet, this work helps to improve the understanding of organic semiconductors in gas sensor applications.

To enable the characterization of organic semiconductors under the influence of gases, a gas test bench has been established that allows to generate gas samples of various volatile compounds. No parasitic responses were obtained from the used procedures. LabVIEW and MATLAB programs have been written to control the instrument used for the electrical characterization and to extract automatically important device parameters.

The hysteresis of the transfer characteristics has been demonstrated as a new parameter that allows to improve the selectivity of OFET based sensors. For P3HT and ethanol vapor, the hysteresis has shown a behavior comparable to the reported parameters on-current and mobility in terms of sensitivity and linearity of the response. Additional benefit for the selectivity has been shown for the simultaneous utilization of the hysteresis with the on-current or the mobility. By using the conventional transistor parameters it is hardly possible to distinguish ethanol and acetone vapor, while the simultaneously monitored hysteresis shows a two times higher response to ethanol vapor and therefore allows a clear discrimination of the analytes.

To investigate the origin of the hysteresis, measurements of the transient drain current have been performed, which indicate enhanced trapping in presence of ethanol vapor. This result is also in agreement with the findings of Duarte et al who indicated trapping as origin of the on-current decrease in presence of ethanol [20]. Though the time resolution of the used instrument was not sufficient to show it directly, the transient measurements indicate different kinetics of the trapping and detrapping as origin of the hysteresis difference in presence of ethanol and acetone vapor.

Furthermore the suitability of the transient drain current as a parameter for the ethanol detection was tested. Though the response lacks behind the transfer characteristics in terms of sensitivity and linearity, this measurement procedure allows to

reduce the drift of the sensor due to bias stress effects. As the drift of the baseline is an issue for many sensors, particularly for organic based sensors, further experiments are needed to investigate if this technique could also be advantageous in comparison to pulsed measurements, which are employed to reduce the bias stress effects.

The dependence of the sensor response on the side chains of the used molecules has been investigated for ethanol vapor. Polymers based on the same backbone were provided with side chains varying in terms of sterical hindrance and polarity. Mass uptake and contact angle measurements were performed to improve the understanding. First of all, the alkoxy side chains showed a more pronounced response to ethanol vapor in comparison to P3HT with alkyl side chains. While this is in agreement with Torsi et al, mass uptake measurements revealed that the higher response is not caused by a higher absorption into the film [98]. Instead additional interactions occuring between the alkoxy substituted polymers and the ethanol vapor are expected to be responsible for the higher response. Simulations performed by the chemistry group of the project TRANSFILSEN indicate the formation of hydrogen-bonds and a subsequent decrease of the planarity of the molecules as additional interaction mechanism for the alkoxy side chains.

For side chains with similarly low polarities, the response followed the mass uptake which was influenced by the crystallinity of the film.

Oxygen-enriched side chains showed an intermediate mass uptake at low vapor pressures but a high response as OFET sensor. As the mass uptake indicates a rather low fraction of ethanol in vicinity to the conductive channel of the OFET sensor, an enhanced interaction mechanism is expected to be responsible for the high response obtained in OFET sensors. Though the underlying mechanism remains unclear, the results indicate oxygen enriched side chains as a promising way to increase the interaction strength and improve the sensitivity of OFET sensors to polar vapors.

To enable the elaboration of nanoscale transistors with long channel behavior, silicon nitride deposited by PECVD was tested for its suitability as a high-k dielectric. Comparing the behavior of 3.5 μm channels on 100 nm thick silicon oxide and silicon nitride showed pronounced differences that could not be explained only by the two times higher dielectric constant. In addition to the higher capacitance, the absence

of hydroxyl groups in silicon nitride was suggested as origin of the reduced driving voltages, the improved subthreshold slope and the decreased hysteresis of the transfer characteristics. However, the silicon nitride showed an up to three orders of magnitude smaller mobility in comparison to SiO_2. AFM images indicated a high surface roughness as origin of the reduced mobility.

The shortest channel lengths achieved were 350 and 500 nm on silicon nitride layers of 60 nm thickness. The devices showed short channel effects at this length scale, though they did not affect the charge transport severely. For transistors with a small width to length ratio the leakage current form the gate started to deteriorated the device performances as it increased up to 25 % of the source drain current. As it can be expected that the mobility increases for a smoother surface, and the contribution of the leakage current therefore decreases, commercially available silicon nitride will be tested for its application in OFETs.

Bibliography

[1] a.L. Kukla, Yu.M. Shirshov, and S.a. Piletsky. Ammonia sensors based on sensitive polyaniline films. *Sensors and Actuators B: Chemical*, 37(3):135–140, December 1996.

[2] Michael D. Austin and Stephen Y. Chou. Fabrication of 70 nm channel length polymer organic thin-film transistors using nanoimprint lithography. *Applied Physics Letters*, 81(23):4431, 2002.

[3] Hua Bai and Gaoquan Shi. Gas sensors based on conducting polymers. *Sensors*, pages 267–307, 2007.

[4] Zhenan Bao, Ananth Dodabalapur, and Andrew J. Lovinger. Soluble and processable regioregular poly(3-hexylthiophene) for thin film field-effect transistor applications with high mobility. *Applied Physics Letters*, 69(26):4108, 1996.

[5] M Bora, D Schut, and M a Baldo. Combinatorial detection of volatile organic compounds using metal-phthalocyanine field effect transistors. *Analytical chemistry*, 79(9):3298–303, May 2007.

[6] J.L. Bredas, J.C. Scott, K. Yakushi, and G B Street. Polarons and bipolarons on polypyrrole: Evolution of the band structure and optical spectrum upon doping. *Physical Review B*, 30(2):1023–1025, 1984.

[7] M. Brinkmann and J.-C. Wittmann. Orientation of Regioregular Poly(3-hexylthiophene) by Directional Solidification: A Simple Method to Reveal the Semicrystalline Structure of a Conjugated Polymer. *Advanced Materials*, 18(7):860–863, April 2006.

[8] Bronkhorst. Fluidat on the Net, 2013.

[9] Michael L. Chabinyc, Rene Lujan, Fred Endicott, Michael F. Toney, Iain McCulloch, and Martin Heeney. Effects of the surface roughness of plastic-compatible inorganic dielectrics on polymeric thin film transistors. *Applied Physics Letters*, 90(23):233508, 2007.

[10] Josephine B. Chang, Vincent Liu, Vivek Subramanian, Kevin Sivula, Christine Luscombe, Amanda Murphy, Jinsong Liu, and Jean M. J. FreÌĄchet. Printable polythiophene gas sensor array for low-cost electronic noses. *Journal of Applied Physics*, 100(1):014506, 2006.

[11] Josephine B. Chang and Vivek Subramanian. Effect of active layer thickness on bias stress effect in pentacene thin-film transistors. *Applied Physics Letters*, 88(23):233513, 2006.

[12] Sang-Mok Chang, Hiroshi Muramatsu, Chikashi Nakamura, and Jun Miyake. The principle and applications of piezoelectric crystal sensors. *Materials Science and Engineering: C*, 12(1-2):111–123, August 2000.

[13] Hang Chen, Mira Josowicz, Jiri Janata, and Karin Potje-Kamloth. Chemical Effects in Organic Electronics. *Chemistry of Materials*, 16(23):4728–4735, November 2004.

[14] Wei-Yang Chou, Shih-Ting Lin, Horng-Long Cheng, Fu-Ching Tang, Yow-Jon Lin, Chang-Feng You, and Yu-Wu Wang. Excimer laser irradiation induced suppression of off-state leakage current in organic transistors. *Applied Physics Letters*, 90(22):222103, 2007.

[15] Lay-lay Chua, Jana Zaumseil, Jui-fen Chang, and Eric C Ou. General observation of n-type field-effect behaviour in organic semiconductors. *Nature*, 434(March):194–199, 2005.

[16] a. Das, R. Dost, T. Richardson, M. Grell, J.âĂĽJ. Morrison, and M.âĂĽL. Turner. A Nitrogen Dioxide Sensor Based on an Organic Transistor Constructed from Amorphous Semiconducting Polymers. *Advanced Materials*, 19(22):4018–4023, November 2007.

[17] A. Das, R. Dost, T.H. Richardson, M. Grell, D.C. Wedge, D.B. Kell, J.J. Morrison, and M.L. Turner. Low cost, portable, fast multiparameter data acquisition system for organic transistor odour sensors. *Sensors and Actuators B: Chemical*, 137(2):586–591, April 2009.

[18] A. Das, A.K. Tyagi, M. Grell, T.H. Richardson, and M.L. Turner. Multiparameter OFET Sensor At Low Power. In *International Conference on Nanoscience, Engineering and Technology (ICONSET 2011)*, number L, pages 500–504, 2011.

[19] DDBST GmbH Center for Applied Thermodynamics. Dortmund Data Bank, 2013.

[20] Davianne Duarte, Deepak Sharma, Brian Cobb, and Ananth Dodabalapur. Charge transport and trapping in organic field effect transistors exposed to polar analytes. *Applied Physics Letters*, 98(13):133302, 2011.

[21] Ravishankar S. Dudhe, Jasmine Sinha, Anil Kumar, and V. Ramgopal Rao. Polymer composite-based OFET sensor with improved sensitivity towards nitro based explosive vapors. *Sensors and Actuators B: Chemical*, 148(1):158–165, June 2010.

[22] Martin Egginger, Siegfried Bauer, Reinhard Schwödiauer, Helmut Neugebauer, and Niyazi Serdar Sariciftci. Current versus gate voltage hysteresis in organic field effect transistors. *Monatshefte für Chemie - Chemical Monthly*, 140(7):735–750, April 2009.

[23] H J Fell, E J Samuelsen, J Als-Nielsen, G Grübel, and J Må rdalen. Unexpected orientational effects in spin-cast, sub-micron layers of poly(alkylthiophene)s: A diffraction study with synchrotron radiation. *Solid State Communications*, 94(10):843–846, 1995.

[24] Ausschuss fuer Gefahrenstoffe. TRGS 900. Technical Report 47, 2006.

[25] M C Gallazzi, L Tassoni, C Bertarelli, and G Pioggia. Poly(alkoxybithiophenes) sensors for organic vapours. *Sensors and Actuators B : Chemical*, 88:178–189, 2003.

[26] D. Gamota and P. Brazis. IEEE Standard for Test Methods for the Characterization of Organic Transistors and Materials. 2008.

[27] Gregorio García, Vicente Timón, Alfonso Hernández-Laguna, Amparo Navarro, and Manuel Fernández-Gómez. Influence of the alkyl and alkoxy side chains on the electronic structure and charge-transport properties of polythiophene derivatives. *Physical chemistry chemical physics : PCCP*, 13(21):10091–9, June 2011.

[28] H. L. Gomes, P. Stallinga, F. Dinelli, M. Murgia, F. Biscarini, D. M. de Leeuw, T. Muck, J. Geurts, L. W. Molenkamp, and V. Wagner. Bias-induced threshold voltages shifts in thin-film organic transistors. *Applied Physics Letters*, 84(16):3184, 2004.

[29] Gong Gu and Michael G. Kane. Moisture induced electron traps and hysteresis in pentacene-based organic thin-film transistors. *Applied Physics Letters*, 92(5):053305, 2008.

[30] A Guadarrama, M L Rodr, and C Sanz. Electronic nose based on conducting polymers for the quality control of the olive oil aroma Discrimination of quality , variety of olive and geographic origin. *Analytica chimica acta*, 432:283–292, 2001.

[31] J Haddock, X Zhang, S Zheng, Q Zhang, S Marder, and B Kippelen. A comprehensive study of short channel effects in organic field-effect transistors. *Organic Electronics*, 7(1):45–54, February 2006.

[32] a Hierlemann, Aj Ricco, K Bodenhofer, a Dominik, and W Gopel. Conferring selectivity to chemical sensors via polymer side-chain selection: thermodynamics of vapor sorption by a set of polysiloxanes on thickness-shear mode resonators. *Analytical chemistry*, 72(16):3696–708, August 2000.

[33] Takeshi Hirose, Takashi Nagase, Takashi Kobayashi, Rieko Ueda, Akira Otomo, and Hiroyoshi Naito. Device characteristics of short-channel polymer field-effect transistors. *Applied Physics Letters*, 97(8):083301, 2010.

[34] G. Horowitz. Organic thin film transistors: From theory to real devices. *Journal of Materials Research*, 19(07):1946–1962, 2004.

[35] Gilles Horowitz, Mohsen E. Hajlaoui, and Riadh Hajlaoui. Temperature and gate voltage dependence of hole mobility in polycrystalline oligothiophene thin film transistors. *Journal of Applied Physics*, 87(9):4456, 2000.

[36] Gilles Horowitz, Riadh Hajlaoui, Habib Bouchriha, Ramzi Bourguiga, and Mohcen Hajlaoui. The Concept of âĂIJThreshold VoltageâĂİ in Organic Field-Effect Transistors. *Advanced Materials*, 10(12):923–927, August 1998.

[37] J. Huang, T. J. Dawidczyk, B. J. Jung, J. Sun, a. F. Mason, and H. E. Katz. Response diversity and dual response mechanism of organic field-effect transistors with dinitrotoluene vapor. *Journal of Materials Chemistry*, 20(13):2644, 2010.

[38] J. Huang, T. J. Dawidczyk, B. J. Jung, J. Sun, a. F. Mason, and H. E. Katz. Response diversity and dual response mechanism of organic field-effect transistors with dinitrotoluene vapor. *Journal of Materials Chemistry*, 20(13):2644, 2010.

[39] Jia Huang, Joseph Miragliotta, Alan Becknell, and Howard E Katz. Hydroxy-terminated organic semiconductor-based field-effect transistors for phosphonate vapor detection. *Journal of the American Chemical Society*, 129(30):9366–76, August 2007.

[40] B J Hwang, J Y Yang, and C W Lin. Recognition of alcohol vapor molecules by simultaneous measurements of resistance changes on polypyrrole-based composite thin films and mass changes on a piezoelectric crystal. *Sensors and Actuators B : Chemical*, 75:67–75, 2001.

[41] ICx Technologies. Fido Explosives Detectors, 2013.

[42] J. Joseph and M. Brown. *Introduction to Biomedical Equipment Technology, Third Edition*. 1998.

[43] Oana D. Jurchescu, Jacob Baas, and Thomas T. M. Palstra. Effect of impurities on the mobility of single crystal pentacene. *Applied Physics Letters*, 84(16):3061, 2004.

[44] D Khodagholy, G G Malliaras, R M Owens, and Ecole Nationale. Polymer-Based Sensors. *Polymer Science:A Comprehensive Reference*, 8:101–128, 2012.

[45] Se Hyun Kim, Hoichang Yang, Sang Yoon Yang, Kipyo Hong, Danbi Choi, Chanwoo Yang, Dae Sung Chung, and Chan Eon Park. Effect of water in ambient air on hysteresis in pentacene field-effect transistors containing gate dielectrics coated with polymers with different functional groups. *Organic Electronics*, 9(5):673–677, October 2008.

[46] Seong Keun Kim, Sang Woon Lee, Jeong Hwan Han, Bora Lee, Seungwu Han, and Cheol Seong Hwang. Capacitors with an Equivalent Oxide Thickness of $<$0.5 nm for Nanoscale Electronic Semiconductor Memory. *Advanced Functional Materials*, 20(18):2989–3003, September 2010.

[47] Hagen Klauk. Organic thin-film transistors. *Chemical Society reviews*, 39(7):2643–66, July 2010.

[48] Hagen Klauk, Günter Schmid, Wolfgang Radlik, Werner Weber, Lisong Zhou, Chris D Sheraw, Jonathan a Nichols, and Thomas N Jackson. Contact resistance in organic thin film transistors. *Solid-State Electronics*, 47(2):297–301, February 2003.

[49] R.J. Kline, M.D. McGehee, E.N. Kadnikova, J. Liu, and J.M.J. Frechet. Controlling the Field-Effect Mobility of Regioregular Polythiophene by Changing the Molecular Weight. *Advanced Materials*, 15(18):1519–1522, September 2003.

[50] D. Knipp, R. a. Street, A. Völkel, and J. Ho. Pentacene thin film transistors on inorganic dielectrics: Morphology, structural properties, and electronic transport. *Journal of Applied Physics*, 93(1):347, 2003.

[51] D. Knipp, R. A. Street, and A. R. Völkel. Morphology and electronic transport of polycrystalline pentacene thin-film transistors. *Applied Physics Letters*, 82(22):3907, 2003.

[52] DH Korowicz, PV Kelly, KF Mongey, and GM Crean. Surface charge analysis characterisation of ultraviolet-induced damage in silicon nitride dielectrics. *Applied surface science*, 168:304–306, 2000.

[53] H. Laurs and G. Heiland. Electrical and optical properties of phthalocyanine films. *Thin Solid Films*, 149(2):129–142, 1987.

[54] J.B. Lee, P. Chang, J.a. Liddle, and V. Subramanian. 10-nm Channel Length Pentacene Transistors. *IEEE Transactions on Electron Devices*, 52(8):1874–1879, August 2005.

[55] M. Leufgen, U. Bass, T. Muck, T. Borzenko, G. Schmidt, J. Geurts, V. Wagner, and L.W. Molenkamp. Optimized sub-micron organic thin-film transistors: the influence of contacts and oxide thickness. *Synthetic Metals*, 146(3):341–345, November 2004.

[56] Bo Li, Genevieve Sauvé, Mihaela C Iovu, Malika Jeffries-El, Rui Zhang, Jessica Cooper, Suresh Santhanam, Lawrence Schultz, Joseph C Revelli, Aaron G Kusne, Tomasz Kowalewski, Jay L Snyder, Lee E Weiss, Gary K Fedder, Richard D McCullough, and David N Lambeth. Volatile organic compound detection using nanostructured copolymers. *Nano letters*, 6(8):1598–602, August 2006.

[57] Bo Li, R Zhang, G Sauve, J Cooper, M C Iovu, S Santhanam, Lawrence Schultz, Jay L Snyder, L E Weiss, T Kowalewski, and G K Fedder. Nanostructure Dependence of Conductive Polymer Chemical Sensors. *IEEE Sensors*, pages 843–846, 2006.

[58] Flora M. Li, Arokia Nathan, Yiliang Wu, and Beng S. Ong. Organic thin-film transistor integration using silicon nitride gate dielectric. *Applied Physics Letters*, 90(13):133514, 2007.

[59] Flora M. Li, Arokia Nathan, Yiliang Wu, and Beng S. Ong. A comparative study of plasma-enhanced chemical vapor gate dielectrics for solution-processed polymer thin-film transistor circuit integration. *Journal of Applied Physics*, 104(12):124504, 2008.

[60] Jun Li, Xiao-Wen Zhang, Liang Zhang, Hao Zhang, Xue-Yin Jiang, Wen-Qing Zhu, and Zhi-Lin Zhang. Effect of a SiN x insulator on device properties of pentacene-TFTs with a low-cost copper source/drain electrode. *Semiconductor Science and Technology*, 25(4):045027, April 2010.

[61] Liqiang Li, Peng Gao, Martin Baumgarten, Klaus Müllen, Nan Lu, Harald Fuchs, and Lifeng Chi. High Performance Field-Effect Ammonia Sensors Based on a Structured Ultrathin Organic Semiconductor Film. *Advanced Materials*, 25:3419–3425, May 2013.

[62] F Liao, C Chen, and V Subramanian. Organic TFTs as gas sensors for electronic nose applications. *Sensors and Actuators B: Chemical*, 107(2):849–855, 2005.

[63] F. Liao, M.F. Toney, and V. Subramanian. Thickness changes in polythiophene gas sensors exposed to vapor. *Sensors and Actuators B: Chemical*, 148(1):74–80, June 2010.

[64] F. Liao, S. Yin, M.F. Toney, and V. Subramanian. Physical discrimination of amine vapor mixtures using polythiophene gas sensor arrays. *Sensors and Actuators B: Chemical*, 150(1):254–263, September 2010.

[65] Liang Luo, Seong Ho Choi, and C. Daniel Frisbie. Probing Hopping Conduction in Conjugated Molecular Wires Connected to Metal Electrodes. *Chemistry of Materials*, 23(3):631–645, February 2011.

[66] Iain McCulloch, Martin Heeney, Clare Bailey, Kristijonas Genevicius, Iain Macdonald, Maxim Shkunov, David Sparrowe, Steve Tierney, Robert Wagner, Weimin Zhang, Michael L Chabinyc, R Joseph Kline, Michael D McGehee, and Michael F Toney. Liquid-crystalline semiconducting polymers with high charge-carrier mobility. *Nature materials*, 5(4):328–33, April 2006.

[67] Tomohiko Mori, Yoshihiro Kikuzawa, and Koji Noda. Improving the sensitivity and selectivity of alcohol sensors based on organic thin-film transistors by using chemically-modified dielectric interfaces. *2009 IEEE Sensors*, pages 1951–1954, October 2009.

[68] Tomohiko Mori, Yoshihiro Kikuzawa, and Koji Noda. Improving baseline stability of gas sensors based on organic field-effect transistors by monitoring carrier mobility. *2011 IEEE SENSORS Proceedings*, pages 1002–1005, October 2011.

[69] S A Moshkalyov, J A Diniz, J W Swart, P J Tatsch, M Machida, and I Introduction. Deposition of silicon nitride by low-pressure electron cyclotron resonance plasma enhanced chemical vapor deposition in N 2 / Ar / SiH 4. *Journal of Vacuum Science & Technology B*, 15(6):2682–2687, 1997.

[70] C. Nguyen Van and K. Potje-Kamloth. Electrical and NOx gas sensing properties of metallophthalocyanine-doped polypyrrole/silicon heterojunctions. *Thin Solid Films*, 392(1):113–121, July 2001.

[71] Kiyomi Nigorikawa, Yoshihito Kunugi, Yutaka Harima, and Kazuo Yamashita. A selective gas sensor using a polypyrrole thin film as a sensitive matrix on a piezoelectric crystal. *Journal of Electroanalytical Chemistry*, 396(1-2):563–567, October 1995.

[72] F. Opekar and K. Stulik. Electrochemical sensors with solid polymer electrolytes. *Analytica chimica acta*, 385:151–162, 1999.

[73] Alessandra Operamolla and Gianluca M. Farinola. Molecular and Supramolecular Architectures of Organic Semiconductors for Field-Effect Transistor Devices and Sensors: A Synthetic Chemical Perspective. *European Journal of Organic Chemistry*, 2011(3):423–450, January 2011.

[74] Kie Jin Park and Gregory N. Parsons. Bulk and interface charge in low temperature silicon nitride for thin film transistors on plastic substrates. *Journal of Vacuum Science & Technology A: Vacuum, Surfaces, and Films*, 22(6):2256, 2004.

[75] Colin Reese and Zhenan Bao. Detailed Characterization of Contact Resistance, Gate-Bias-Dependent Field-Effect Mobility, and Short-Channel Effects with Microscale Elastomeric Single-Crystal Field-Effect Transistors. *Advanced Functional Materials*, 19(5):763–771, March 2009.

[76] Ladawan Ruangchuay, Anuvat Sirivat, and Johannes Schwank. Polypyrrole/poly(methylmethacrylate) blend as selective sensor for acetone in lacquer. *Talanta*, 60(1):25–30, May 2003.

[77] Ladawan Ruangchuay, Anuvat Sirivat, and Johannes Schwank. Electrical conductivity response of polypyrrole to acetone vapor: effect of dopant anions and interaction mechanisms. *Synthetic Metals*, 140(1):15–21, January 2004.

[78] a. Salleo, T. W. Chen, a. R. Völkel, and R. a. Street. Intrinsic hole mobility and trapping in a regioregular poly(thiophene). *Physical Review B*, 70(11):115311, September 2004.

[79] Gunter Sauerbrey. Verwendung von Schwingquarzen zur Wägung dünner Schichten und zur Mikrowägung. *Zeitschrift für Physik*, 155:206–222, 1959.

[80] S. Scheinert and G. Paasch. Fabrication and analysis of polymer field-effect transistors. *Physica Status Solidi (a)*, 201(6):1263–1301, May 2004.

[81] M. Schwoerer and H.C. Wolf. *Organische Molekulare Festkörper - Einführung in die Physik von pi-Systemen*. Wiley-VCH, Berlin, 2005.

[82] Tsuyoshi Sekitani, Shingo Iba, Yusaku Kato, Yoshiaki Noguchi, Takao Someya, and Takayasu Sakurai. Suppression of DC bias stress-induced degradation of organic field-effect transistors using postannealing effects. *Applied Physics Letters*, 87(7):073505, 2005.

[83] H. Shirakawa, E.J. Louis, A.G. Macdiarmid, C.K. Chiang, and A. Heeger. Synthesis of Electrically Conducting Organic Polymers: Halogen Derivattives of Polyacetylene. *Journal of the Chemical Society, Chemical Communications*, (16):578–580, 1977.

[84] H Sirringhaus, P J Brown, R H Friend, M M Nielsen, K Bechgaard, and A J H Spiering. Two-dimensional charge transport in self-organized, high mobility conjugated polymers. *Nature*, 401:685–688, 1999.

[85] Tennyson Smith. The hydrophilic nature of a clean gold surface. *Journal of Colloid and Interface Science*, 75(1):51–55, 1980.

[86] Takao Someya, Ananth Dodabalapur, Jia Huang, Kevin C See, and Howard E Katz. Chemical and physical sensing by organic field-effect transistors and related devices. *Advanced materials (Deerfield Beach, Fla.)*, 22(34):3799–811, September 2010.

[87] Takao Someya, Howard E. Katz, Alan Gelperin, Andrew J. Lovinger, and Ananth Dodabalapur. Vapor sensing with α,ω-dihexylquarterthiophene field-effect transistors: The role of grain boundaries. *Applied Physics Letters*, 81(16):3079, 2002.

[88] Soeren Steudel, Stijn De Vusser, Stijn De Jonge, Dimitri Janssen, Stijn Verlaak, Jan Genoe, and Paul Heremans. Influence of the dielectric roughness on the performance of pentacene transistors. *Applied Physics Letters*, 85(19):4400, 2004.

[89] C.K. Tan and D.J. Blackwood. Interactions between polyaniline and methanol vapour. *Sensors and Actuators B : Chemical*, 71(June):184–191, 2000.

[90] H. S. Tan, N. Mathews, T. Cahyadi, F. R. Zhu, and S. G. Mhaisalkar. The effect of dielectric constant on device mobilities of high-performance, flexible organic field effect transistors. *Applied Physics Letters*, 94(26):263303, 2009.

[91] Maria Cristina Tanese, Daniel Fine, Ananth Dodabalapur, and Luisa Torsi. Interface and gate bias dependence responses of sensing organic thin-film transistors. *Biosensors & bioelectronics*, 21(5):782–8, November 2005.

[92] Guoqiang Tang, Simon S. Y. Chen, Kwan H. Lee, Almantas Pivrikas, Muhsen Aljada, Paul L. Burn, Paul Meredith, and Paul E. Shaw. The nature and role of trap states in a dendrimer-based organic field-effect transistor explosive sensor. *Applied Physics Letters*, 102(24):243301, 2013.

[93] N. Tessler and Y. Roichman. Two-dimensional simulation of polymer field-effect transistor. *Applied Physics Letters*, 79(18):2987, 2001.

[94] Nir Tessler, Yevgeni Preezant, Noam Rappaport, and Yohai Roichman. Charge

Transport in Disordered Organic Materials and Its Relevance to Thin-Film Devices: A Tutorial Review. *Advanced Materials*, 21(27):2741–2761, July 2009.

[95] L Torsi, a Dodabalapur, L Sabbatini, and P.G Zambonin. Multi-parameter gas sensors based on organic thin-film-transistors. *Sensors and Actuators B: Chemical*, 67(3):312–316, September 2000.

[96] L Torsi, A J Lovinger, B Crone, T Someya, A Dodabalapur, H E Katz, Bell Laboratories, Lucent Technologies, Murray Hill, Dipartimento Chimica, and Via Orabona I. Correltation between Oligothiophene Thin Film Transistor Morphology and Vapor responses. *The Journal of Physical Chemistry B*, 106:12563–12568, 2002.

[97] L Torsi, M. C. Tanese, N. Cioffi, M. C. Gallazzi, L. Sabbatini, and P. G. Zambonin. Alkoxy-substituted polyterthiophene thin-film-transistors as alcohol sensors. *Sensors and Actuators B: Chemical*, 98(2-3):204–207, 2004.

[98] L. Torsi, M. C. Tanese, N. Cioffi, M. C. Gallazzi, L. Sabbatini, P. G. Zambonin, G. Raos, S. V. Meille, and M. M. Giangregorio. Side-Chain Role in Chemically Sensing Conducting Polymer Field-Effect Transistors. *The Journal of Physical Chemistry B*, 107(31):7589–7594, August 2003.

[99] Luisa Torsi, Gianluca M Farinola, Francesco Marinelli, M Cristina Tanese, Omar Hassan Omar, Ludovico Valli, Francesco Babudri, Francesco Palmisano, P Giorgio Zambonin, and Francesco Naso. A sensitivity-enhanced field-effect chiral sensor. *Nature materials*, 7(5):412–417, May 2008.

[100] C. Ucurum, H. Goebel, F. a. Yildirim, W. Bauhofer, and W. Krautschneider. Hole trap related hysteresis in pentacene field-effect transistors. *Journal of Applied Physics*, 104(8):084501, 2008.

[101] C. Ucurum, H. Siemund, and H. Göbel. Impact of electrical measurement parameters on the hysteresis behavior of pentacene-based organic thin-film transistors. *Organic Electronics*, 11(9):1523–1528, September 2010.

[102] B. Vercelli, S. Zecchin, N. Comisso, G. Zotti, A. Berlin, E. Dalcanale, and L.B. Groenendaal. Solvoconductivity of Polyconjugated Polymers: The Roles of Polymer Oxidation Degree and Solvent Electrical Permittivity. *Chemistry of Materials*, 14(11):4768–4774, November 2002.

[103] J. Veres, S.D. Ogier, S.W. Leeming, D.C. Cupertino, and S. Mohialdin Khaffaf. Low-k Insulators as the Choice of Dielectrics in Organic Field-Effect Transistors. *Advanced Functional Materials*, 13(3):199–204, March 2003.

[104] J.R. Vig. UV/Ozone cleaning of Surfaces. *Parts, Hybrids, and Packaging, IEEE Transactions on*, 12(4):365–370, 1976.

[105] M C J M Vissenberg and M Matters. Theory of the field-effect mobility in amorphous organic transistors. *Physical Review B*, 57(20):964–967, 1998.

[106] A. Völkel, R. Street, and D. Knipp. Carrier transport and density of state distributions in pentacene transistors. *Physical Review B*, 66(19):195336, November 2002.

[107] Guangming Wang, James Swensen, Daniel Moses, and Alan J. Heeger. Increased mobility from regioregular poly(3-hexylthiophene) field-effect transistors. *Journal of Applied Physics*, 93(10):6137, 2003.

[108] J. Z. Wang, Z. H. Zheng, and H. Sirringhaus. Suppression of short-channel effects in organic thin-film transistors. *Applied Physics Letters*, 89(8):083513, 2006.

[109] L Wang, D Fine, S Khondaker, T Jung, and a Dodabalapur. Sub 10nm conjugated polymer transistors for chemical sensing. *Sensors and Actuators B: Chemical*, 113(1):539–544, January 2006.

[110] Liang Wang, Daniel Fine, and Ananth Dodabalapur. Nanoscale chemical sensor based on organic thin-film transistors. *Applied Physics Letters*, 85(26):6386, 2004.

[111] David C. Wedge, Arindam Das, René Dost, Jeff Kettle, Marie-Beatrice Madec, John J. Morrison, Martin Grell, Douglas B. Kell, Tim H. Richard-

son, and Stephen Yeates. Real-time vapour sensing using an OFET-based electronic nose and genetic programming. *Sensors and Actuators B: Chemical*, 143(1):365–372, December 2009.

[112] J. Wöllenstein and K. Schmitt. Lecture on gassensors, 2011.

[113] He Yan, Zhihua Chen, Yan Zheng, Christopher Newman, Jordan R Quinn, Florian Dötz, Marcel Kastler, and Antonio Facchetti. A high-mobility electron-transporting polymer for printed transistors. *Nature*, 457(7230):679–86, February 2009.

[114] Jye-shane Yang and Timothy M Swager. Fluorescent Porous Polymer Films as TNT Chemosensors : Electronic and Structural Effects. *Journal of the American Chemical Society*, 120:11864–11873, 1998.

[115] Jana Zaumseil and Henning Sirringhaus. Electron and ambipolar transport in organic field-effect transistors. *Chemical reviews*, 107(4):1296–323, April 2007.

[116] Y. Zhang, J.R. Petta, S. Ambily, Y. Shen, D.C. Ralph, and G.G. Malliaras. 30 nm Channel Length Pentacene Transistors. *Advanced Materials*, 15(19):1632–1635, October 2003.

[117] G Zhao, Huanli Dong, Lang Jiang, and Huaping Zhao. Single crystal field-effect transistors containing a pentacene analogue and their application in ethanol vapor detection. *Applied Physics Letters*, 101:103302, 2012.

[118] Erjun Zhou, Qingshuo Wei, Shimpei Yamakawa, Yue Zhang, Keisuke Tajima, Chunhe Yang, and Kazuhito Hashimoto. Diketopyrrolopyrrole-Based Semiconducting Polymer for Photovoltaic Device with Photocurrent Response Wavelengths up to 1.1 μm. *Macromolecules*, 43(2):821–826, January 2010.

10 Appendix

Parameter	Value
Temperature ramp [C, min]	320°, 5
Used gases [sccm]	SiH_4: 5, N_2: 30
Deposition time [min, s]	8:30
Pressure [mbar] - before deposition	4×10^{-7}
Pressure [mbar] - during deposition	1×10^{-2}
MW power [W] -configured	500
MW power [W] -actual value	502
MW reflected power [%]	7
Magnet current [A] -configured	5
Magnet current [A] - actual value	5.2
RF power [W] - configured	100
RF power [W] - actual value	28
Rf reflected power [%]	7
DC bias voltage [V] -configured	150
DC bias voltage [V] - actual value	148
Tune position	493
Load position	464

Table 10.1: Growth conditions used for a 100 nm thick Si_xN_y layer. "actual values" were read out during the deposition. MW = Microwave, RF = Radio frequency

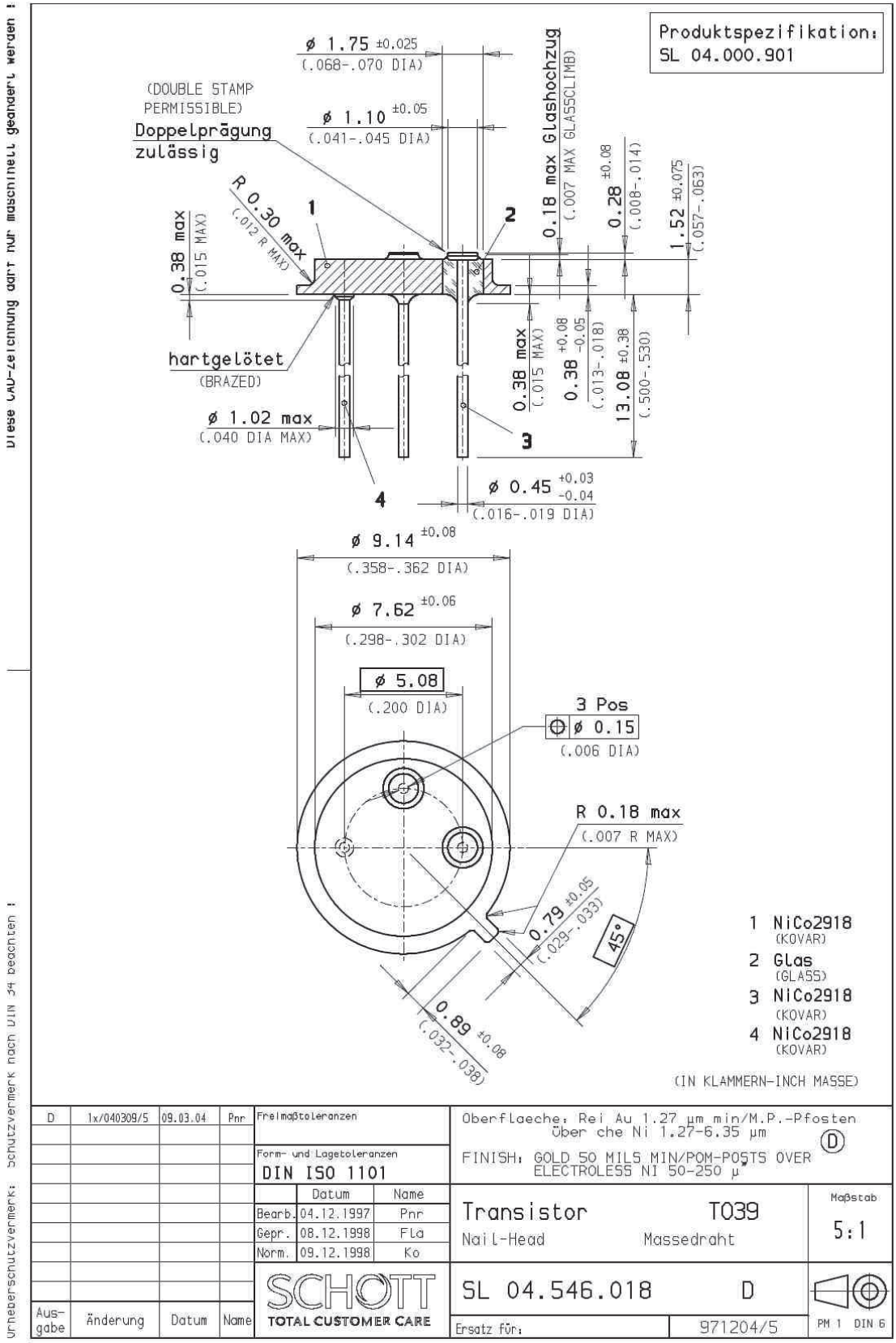

Figure 10.1: Datasheet To39 supports

11 Acknowledgments

On these last pages of the manuscript I would like to express my gratitude to the people who helped me to finish this work.

I would like to thank Professor Daniel Mathiot for giving me the opportunity to perform my thesis in his laboratory. A very special thanks goes also to all members of this lab who, even if they are not mentioned individually here, helped to provide very good experimental conditions by supporting my work with their knowledge and/or equipment.

I am very happy to thank my jury members Françoise Serein-Spirau, Bernard Doudin, George Malliaras and Klaus Leifer for participating in my defense committee and for creating a pleasant atmosphere during my presentation and in the following question time. I want to emphasize especially my admiration for my referees George Malliaras and Klaus Leifer, who I first met during conferences, and who are not only extraordinary people in their research fields, but also very pleasant and open-minded conversational partners.

The person without whom the accomplishment of this thesis would not have been possible, is my supervisor Thomas Heiser. He made a very good impression on me during our first meeting and I'm glad this impression has even improved over the years. In his collegial manner he helped me to improve my scientific skills without making me forget that "There are more things in Heaven and Earth... Than are dream't of in your Philosophy".

I am also very grateful to my Co-advisor Patrick Lévêque. He was not only a reliable source of informations, but his eloquent and gentle use of the English language reminded me of the nice British courtesy that I forgot since I left school.

Nicolas Leclerc was always a good contact for everything concerning chemistry and I enjoyed, especially in the beginning of my thesis, the ambiance at the former LIPHT laboratory.

This nice ambiance was of course created by the nice colleagues who were often around: Véronique, Laure and Sadiara. Though I mostly danced with Samba, the

times I've spend with anyone of you were always a pleasure.
Though the LIPHT, and now, ECPEES laboratory is blended with nice people, I would like to mention especially Patricia, as she was one of the few, who told me that the remaining two months can be sufficient to write my thesis. Thank you very much for this encouragement! I'm not really sure I could have made it without your motivation.
Coming back to InESS/ICube, a cordial thanks goes to my office-mates, Youssef who helped me a lot in the first days by acquainting me with the campus, lots of coffee, tea, terrific Moroccan sweets and with his little daughter in the end, and to Azhar, for tons of food, entertaining tinkering with the car and bike and many pleasant hours. Also to Thomas R. even if I can't find the article I wanted to send you...
Thanks to Rony and Olzhas for discussions, football and support.
Thanks to Caroline Eckert for organization, assistance and contributions to the organic group in various ways.
Support in various ways I experienced also by the technical staff of the laboratory: Stéphane Roques, Nicolas Zimmermann, Sebastian Schmitt, Nicolas Colin, Jérémy Bartringer, Pascal Leindecker, und natürlich Florent Dietrich. Thanks a lot to all of you for coffee, bolts and holes and tubes and all the hours you've supported me during the installation of the test-bench and during the rest of my thesis.
Thanks to the stagaires, Yoann, Yoann, Thibault, Lucas and Hugo who pushed this work and the TRANSFILSEN project forward and made some participants even soar in the Vosges.
Though we didn't see often I would like to thank Jérôme Heitz for helping me to develop the hysteresis as sensing parameter and for writing the first Matlab skripts that initiated the automatization of the data acquisition and analysis.
I am also very grateful to Abdelilah Slaoui, Gérald Ferblantier and Bhabani who supported me with their equipment, knowledge and especially their kindness.
Thanks to Stéphane Méry, Hicham Majjad, Sabine Siegwald and Céline Etrillard, from the IPCMS institute who supported this work in various ways.
I am very grateful to the project partners of the TRANSFILSEN projects: To the

chemist at the Institute Charles Gerhardt in Montpelier: Françoise Serein-Spirau, Jean-Pierre Lere-Porte and Thibaut Jarrosson, for long and short molecules and nice meetings near the sea. Also thank you very much for initiating the collaboration with Vincent Rouessac at the Institute Européen des Membranes, which helped a lot to find an interpretation for the gas sensing properties of the polymers. At the Institute de Science des Matériaux de Mulhouse: Laurent Simon, Jean-Luc Bubendorff, Dominique Aubel, François Vonau and Wael Hourani. Thank you very much for many nice AFM images and the hospitality during various visits. At the Institute Jean Lamour in Nancy I am very grateful to Michel Hehn, François Montaigne, Daniel Lacour and Stefan Mc Murtry for the patterned structures and invitations in Nancy and Strasbourg.

Last but not least I want to thank the people who this thesis is dedicated to: my family and Annette. Thank you for all the good times we shared and your love and support throughout the years.